Proposal to Continue the Study of Hyperon CP Violation in FY99

The HyperCP Collaboration

May 15, 1998

A. Chan, Y.C. Chen, J. Sheng, P.K. Teng, C. Yu, and Z. Yu
Academia Sinica, Nankang, Taipei 11529, Taiwan, Republic of China

W.S. Choong, G. Gidal, K.B. Luk[1], and P. Zyla
Lawrence Berkeley Laboratory and University of California, Berkeley, CA 94720, USA

M. Crisler, C. James and J. Volk
Fermilab, Batavia, IL 60510, USA

J. Felix, G. Lopez
Universidad de Guanajuato, León, Mexico

R.A. Burnstein, A. Chakravorty, D.M. Kaplan, L.M. Lederman, W. Luebke, D. Rajaram, H.A. Rubin, C.G. White, and S.L. White
Illinois Institute of Technology, Chicago, IL 60616, USA

N. Leros and J.-P. Perroud
Université de Lausanne, Lausanne, Switzerland

H.R. Gustafson, M.J. Longo, and F. Lopez
University of Michigan, Ann Arbor, MI 48109, USA

B V. Papavassiliou
New Mexico State University, Las Cruces, NM 88003, USA

M. Jenkins and K. Clark
University of South Alabama, Mobile, AL 36688, USA

M. Carmack, E.C. Dukes[2], C. Durandet, T. Holmstrom, M. Huang, Z. Kou, and K.S. Nelson
University of Virginia, Charlottesville, VA 22901, USA

[1]Spokesperson: LUK@CSA.LBL.GOV, (510)486-7054
[2]Spokesperson: DUKES@UVAHEP.PHYS.VIRGINIA.EDU, (804)982-5364

HyperCP Physics Goals

- Perform a sensitive search for CP violation by comparing the decay process $\Xi^- \to \Lambda\pi^-$, $\Lambda \to p\pi^-$ with its anti-process $\overline{\Xi}^+ \to \overline{\Lambda}\pi^+$, $\overline{\Lambda} \to \bar{p}\pi^+$. A positive result would be:
  - The first evidence of CP violation outside of the decay of the K_L.
  - Unambiguous evidence of direct CP violation.
- Search for CP violation in $K^\pm \to 3\pi$ decays.
- Search for rare and forbidden hyperon and charged kaon decays.
- Test CPT using hyperons.
- Measure various hyperon parameters, including: polarization, production cross sections, and decay parameters.

The HyperCP Spectrometer

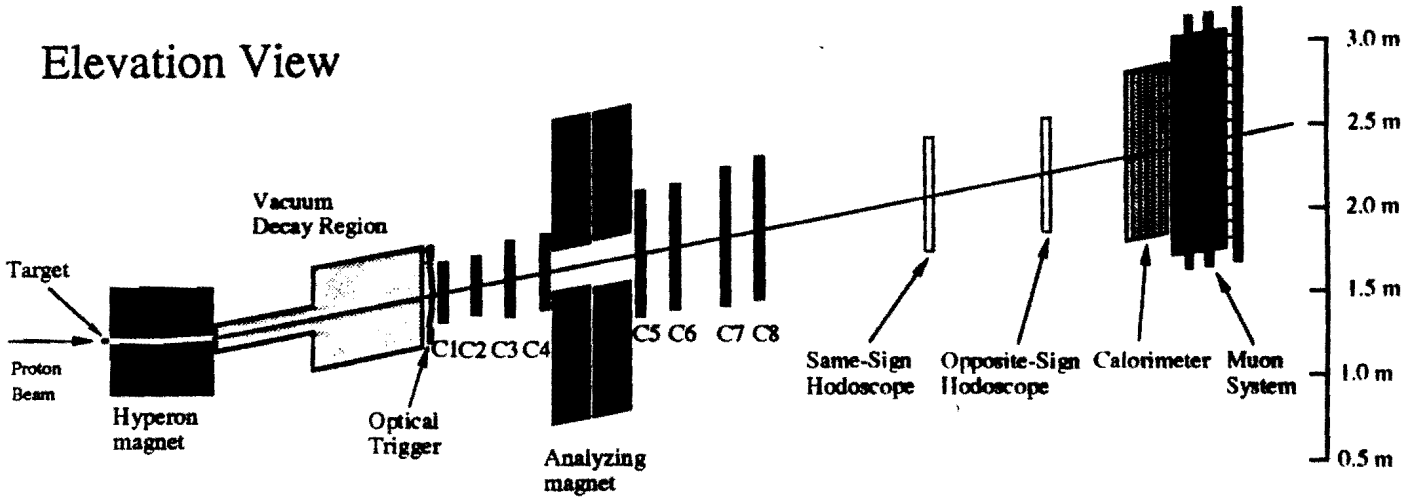

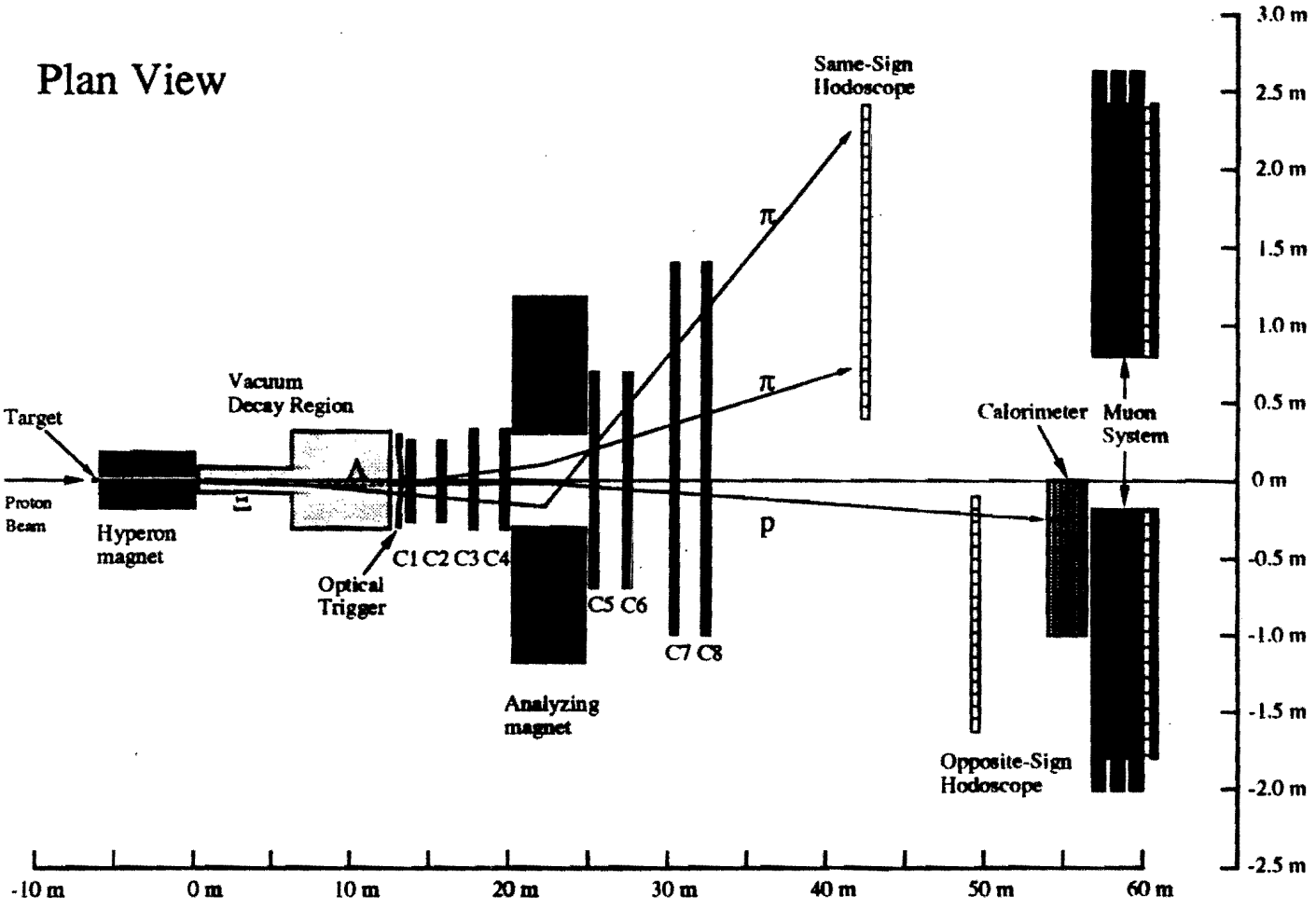

Summary of the 1997 Run

* Between April 1997 and September 1997, collected

$$\sim 75 \times 10^9 \text{ triggers}$$

of which,

$$\sim 39 \times 10^9 \ \Xi \text{ triggers}$$

on ~10,000 Exabyte 5-Gb tapes (~33 Tb).

* This should yield roughly

$$1.2 \times 10^9 \text{ reconstructed } \Xi^- \text{ events}$$

and

$$0.3 \times 10^9 \text{ reconstructed } \bar{\Xi}^+ \text{ decays}$$

* This results in an overall sensitivity of

$$\delta A_{\Lambda\Xi} \approx 2 \times 10^{-4}$$

Spectrometer Improvements for the 1999 Run

* Increase the DAQ throughput to 40 Mb/s by:
  - using faster Exabyte 8705 drives
  - improving software

* Improve the collimator design to reduce the rate of secondary interactions at the exit.

* Various minor improvements to the spectrometer and the beam line.

Expectation:

	1997 Run	1999 Run	Increase
Intensity (protons/s)	7.5×10^9	1.0×10^{10}	1.3
Spill duty factor	18s/60s	40s/80s	1.7
Calender time (weeks)	16	16	1.0
Mean efficiency (%)	28	50	1.8
Total number of protons	6×10^{15}	2.4×10^{16}	4.0

Here we assumed a 20 week run with 4 weeks of tune-up. Every additional month of running will increase the data sample by an amount equal to the total accumulated in 1997.

Fermilab

Fermi National Accelerator Laboratory
P.O.Box 500 • Batavia, Illinois • 60510
630-840-3211 Fax 630-840-2939

Director's Office

January 14, 1998

Prof. Kam-Biu Luk
Department of Physics
University of California
Berkeley, California 94720

Prof. E. C. Dukes
Jesse W. Beams Lab. of Physics
University of Virginia
Mc Cormick Road
Charlottesville, Virginia 22901

Dear Craig and Bill,

Thank you for your presentation to the Physics Advisory Committee (PAC) on the status of E-871 and its proposed extension in a 1999 fixed-target run. The Committee's recommendation and comments follow:

The HyperCP experiment (E-871) is designed to measure a CP-violating asymmetry between the process $\Xi^- \to \Lambda\pi^-$, $\Lambda \to p\pi^-$ and its conjugate, with a sensitivity of 1×10^{-4}. This sensitivity may be sufficient to observe an asymmetry due to standard model physics, and the measurement could provide the first evidence for direct CP violation.

The Committee was pleased to learn that the detector performed well during the 1996-1997 fixed-target run. Initial physics distributions based on a small fraction of the data look very encouraging, and the Committee commends the collaboration for its work. Because of a late start, however, the experiment collected data for only about five months and will not achieve its goal of a precision of 1×10^{-4}.

The Committee would like to see results of an analysis of 10% of the 1997 data sample, including a full Monte Carlo simulation, to be presented at the May 1998 PAC meeting. The collaboration should also present a more refined study of systematic errors to help evaluate the physics reach of the experiment.

The Committee recommends approval of a run for HyperCP in 1999, conditional on successful analysis of the data subsample discussed above.

I have accepted the PAC's advice, and ask that you plan on making a presention at their May 15-17 meeting. I also hope that your collaboration will be able to provide some results which can be shown at the DOE Annual Program Review which will be held March 31-April 2.

HyperCP Progress

The past several months we have been working on:

- Pushing the farm analysis forward.
  - Verifying the data integrity and studying cuts for track finding, event reconstruction, and event selection.
  - Implementing a space point track reconstruction program.
- Refining and validating constants files.
  - Chamber residuals, magnetic field map, etc.
- Refining and validating the Monte Carlo.
- Investigating biases.
  - Using 10% of the data that has been processed and reprocessed.
  - Using Monte Carlo simulations.

Status of the Farm Analysis

- The primary event reconstruction started at the end of November, 1997, with about 3,000 MIPs on three Fermilab farms.
- By the middle of February, 1998, we were ramped up to 6,770 MIPs.

HyperCP Production Farms							
System	Start Date	Model	Workers	CPU	MIPs	ms/Event	Tapes/Day
fnsfh a	15-Nov-97	SGI 4D/35	32	R4000	2200	80	4
b	15-Jan-98		10	R4400		30	4
c	15-Jan-98		10	R4400		30	4
fnsfo	25-Nov-97	SGI 180	13	R10000	1576	15	10
fnckm	01-Dec-97	IBM 43P	10	PowerPC	1150	16	4
fncke	20-Jan-98	IBM 320	16	RS/6000	400	100	1.3
fnckh	20-Jan-98	IBM 320H	16	RS/6000	480	80	1.3
fnckf	12-Feb-98	IBM 320	12	RS/6000	360	100	1.3
fncki	12-Feb-98	IBM 320H	20	RS/6000	600	80	3

- There were lots of startup problems: software, hardware, and operator. Things seem to be going much better now.
- By March 11 we had processed 1036 tapes, or about 10% of our raw data sample.

Totals as of 11-Mar-98				
	Ξ^-	$\overline{\Xi}^+$	Polarized	Total
Total Tapes Processed	262	594	180	1036
Raw Triggers	1.9 Billion	4.3 Billion	1.3 Billion	7.5 Billion
Events Reconstructed	105 Million	98 Million	58 Million	261 Million
Bytes to Stream 2	94 GB	88 GB	43 GB	225 GB
Bytes to Stream 5	36 GB	32 GB	14 GB	82 GB

- Since March 11 we have been: 1) putting the space-point tracker on the farm, 2) splitting the data to produce micro-DST tapes, and 3) reprocessing all 10% of the data for systematic studies.
- The reprocessing started April 25, and ended today.
- We expect reconstruction of the entire sample will take 10 months.

Mass comparison

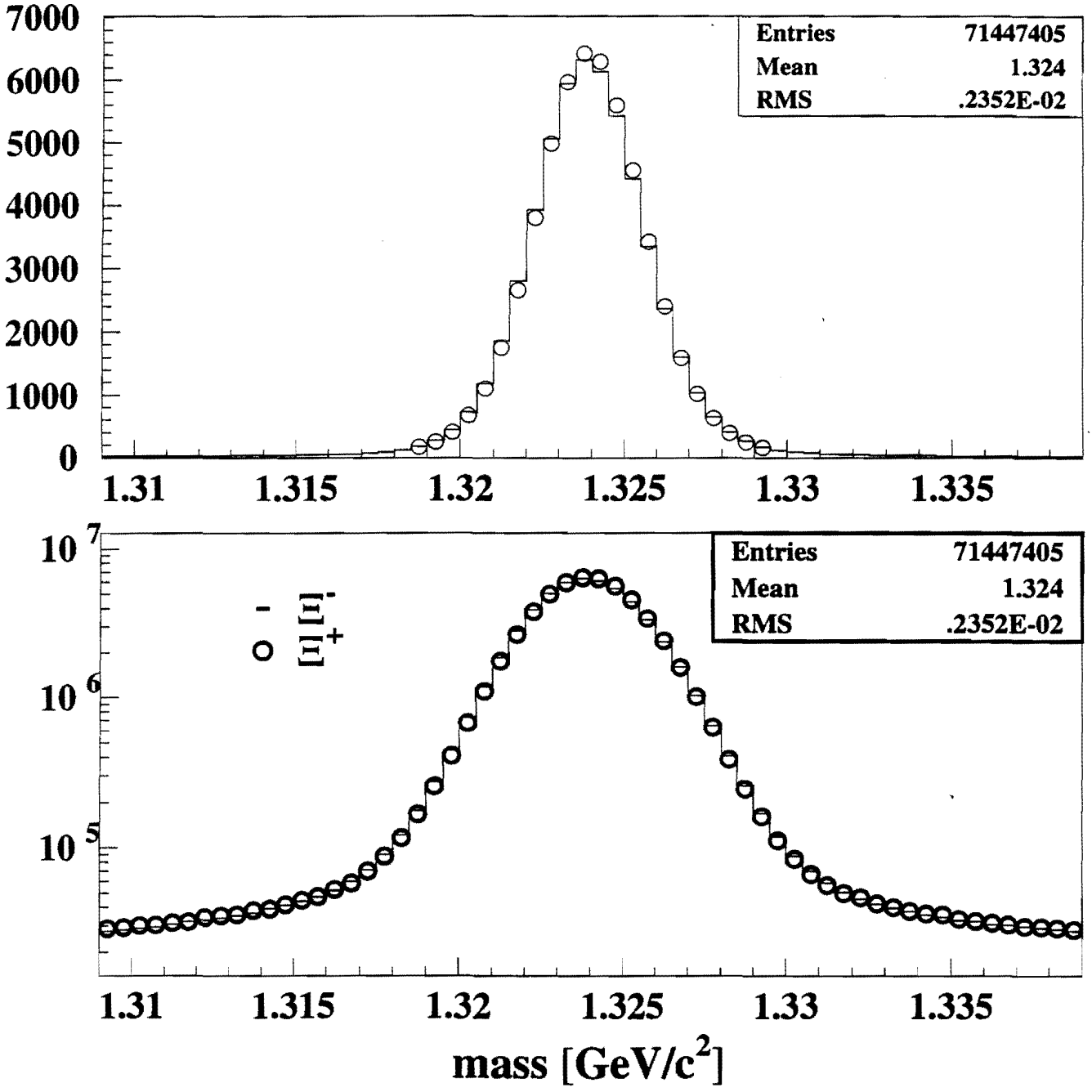

Mass comparison

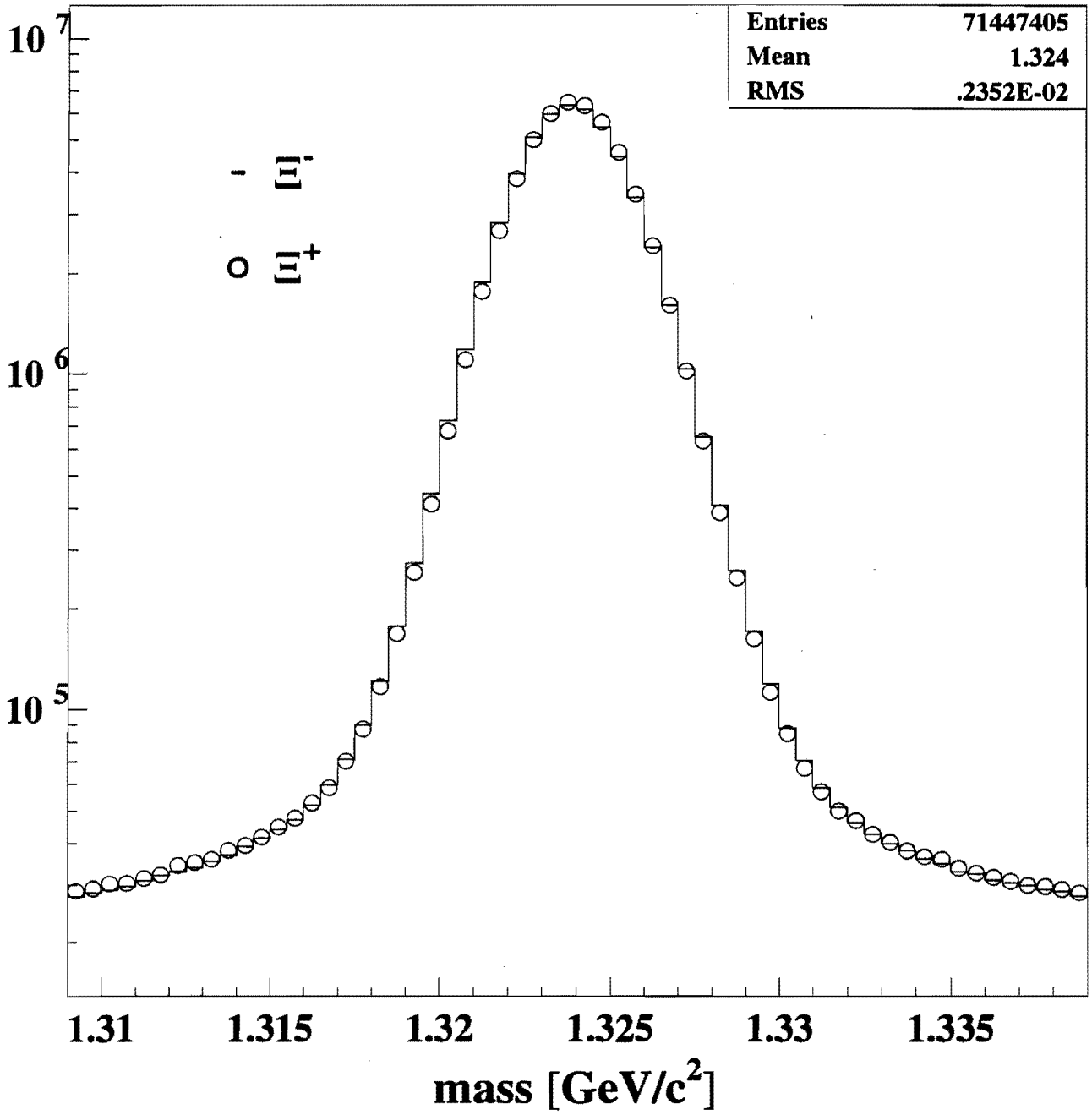

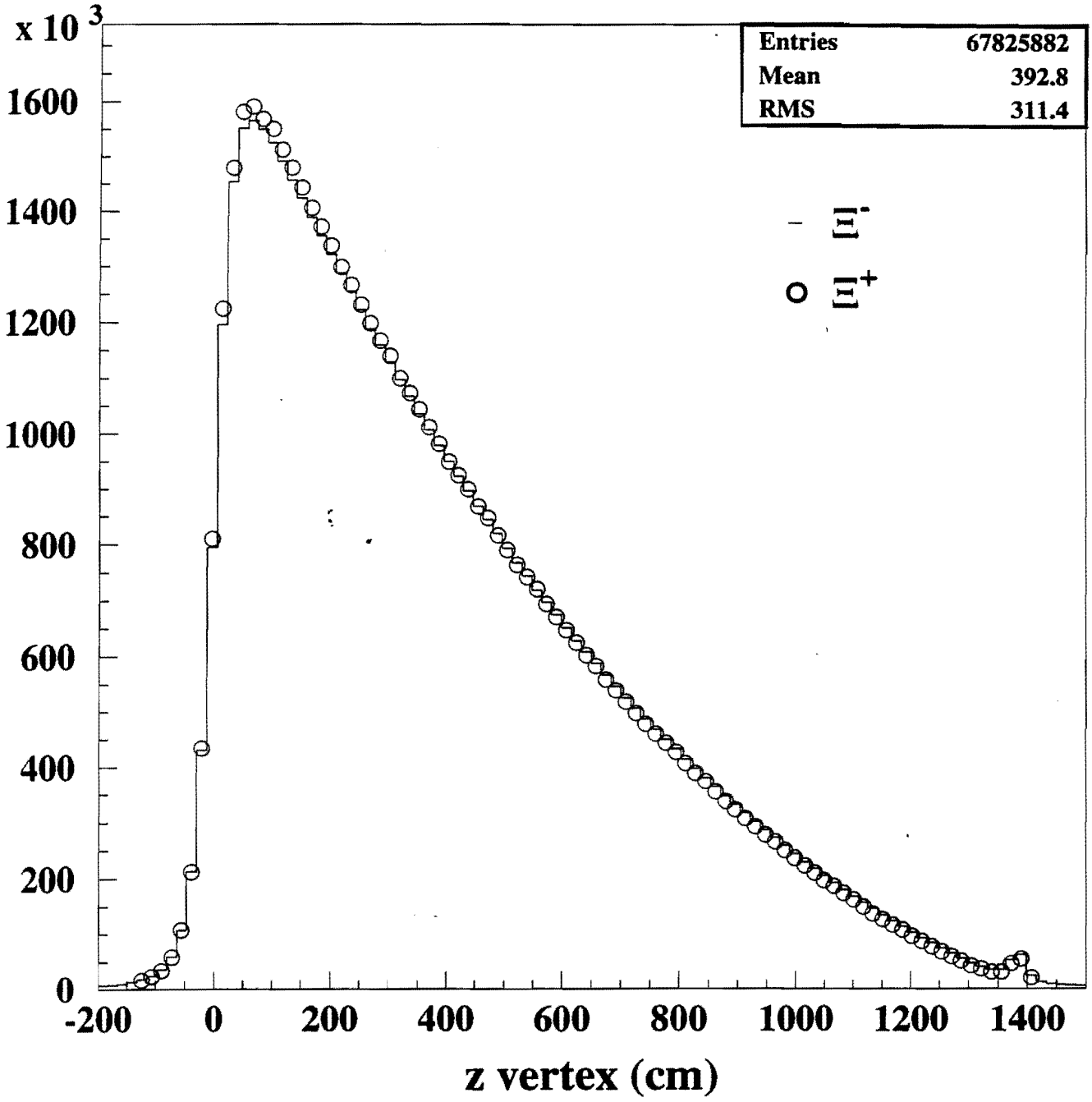
x 10 3
1600
1400
1200
1000
800
600
400
200
0
-200
0
200
400
600
800
1000
1200
1400
z vertex (cm)
Entries 67825882
Mean 392.8
RMS 311.4
Ξ^-
Ξ^+

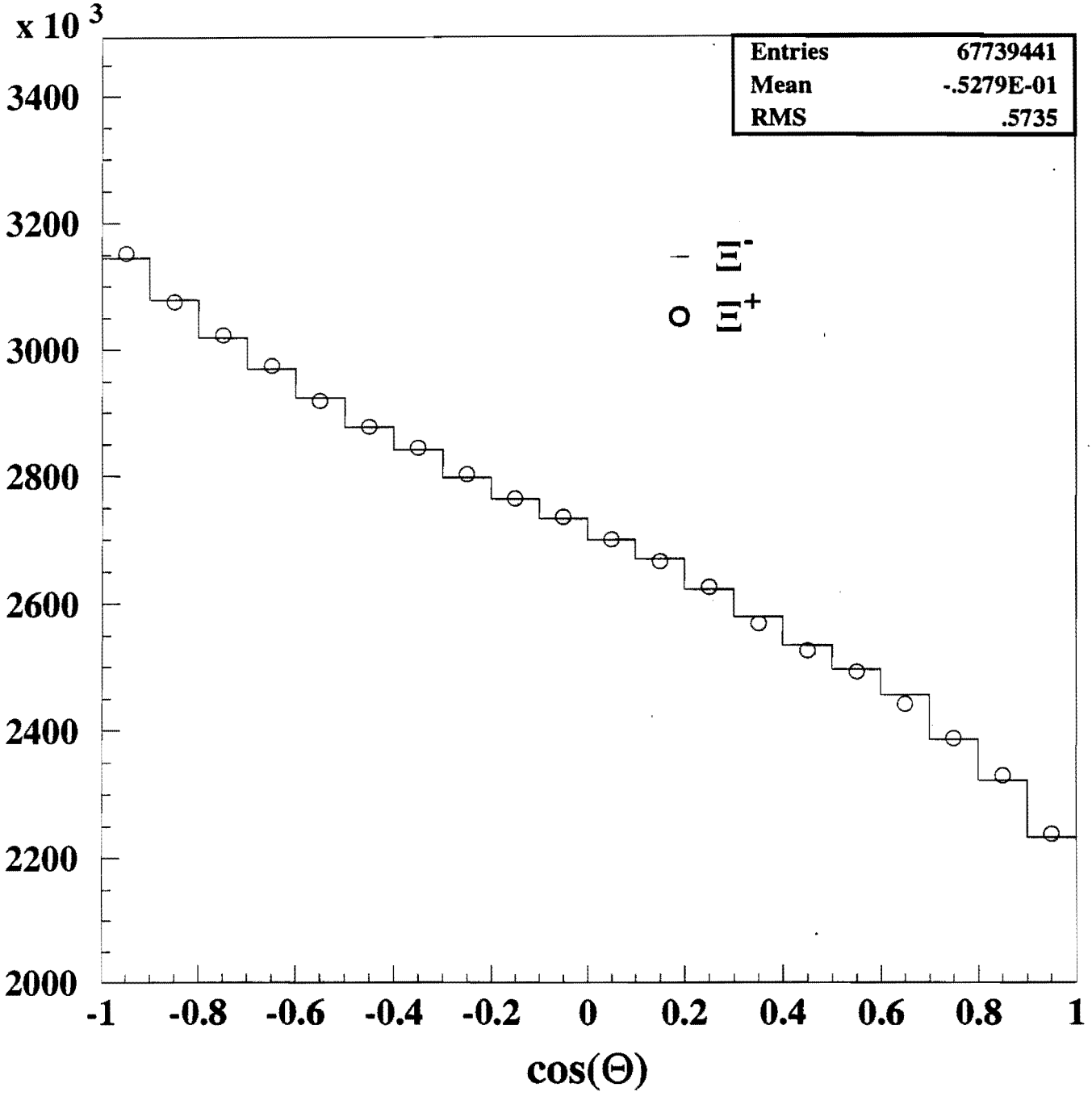
x 10 3
3400
3200
3000
2800
2600
2400
2200
2000
Entries 67739441
Mean -.5279E-01
RMS .5735
Ξ-
Ξ+
-1
-0.8
-0.6
-0.4
-0.2
0
0.2
0.4
0.6
0.8
1
cos(Θ)

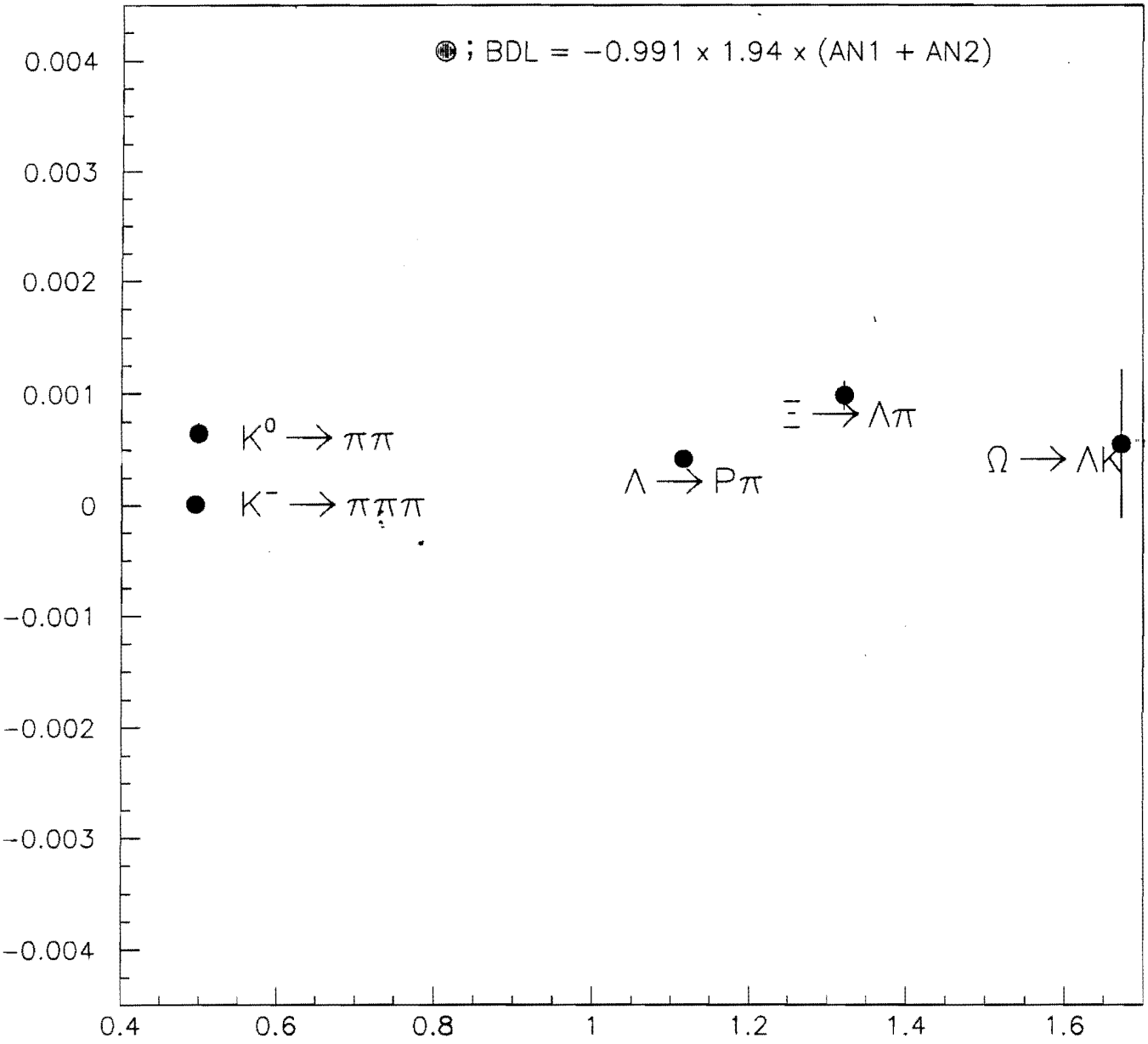
● ; BDL = −0.991 x 1.94 x (AN1 + AN2)
0.004
0.003
0.002
0.001
0
−0.001
−0.002
−0.003
−0.004
0.4
0.6
0.8
1
1.2
1.4
1.6
K⁰ → ππ
K⁻ → πππ
Λ → Pπ
Ξ → Λπ
Ω → ΛK

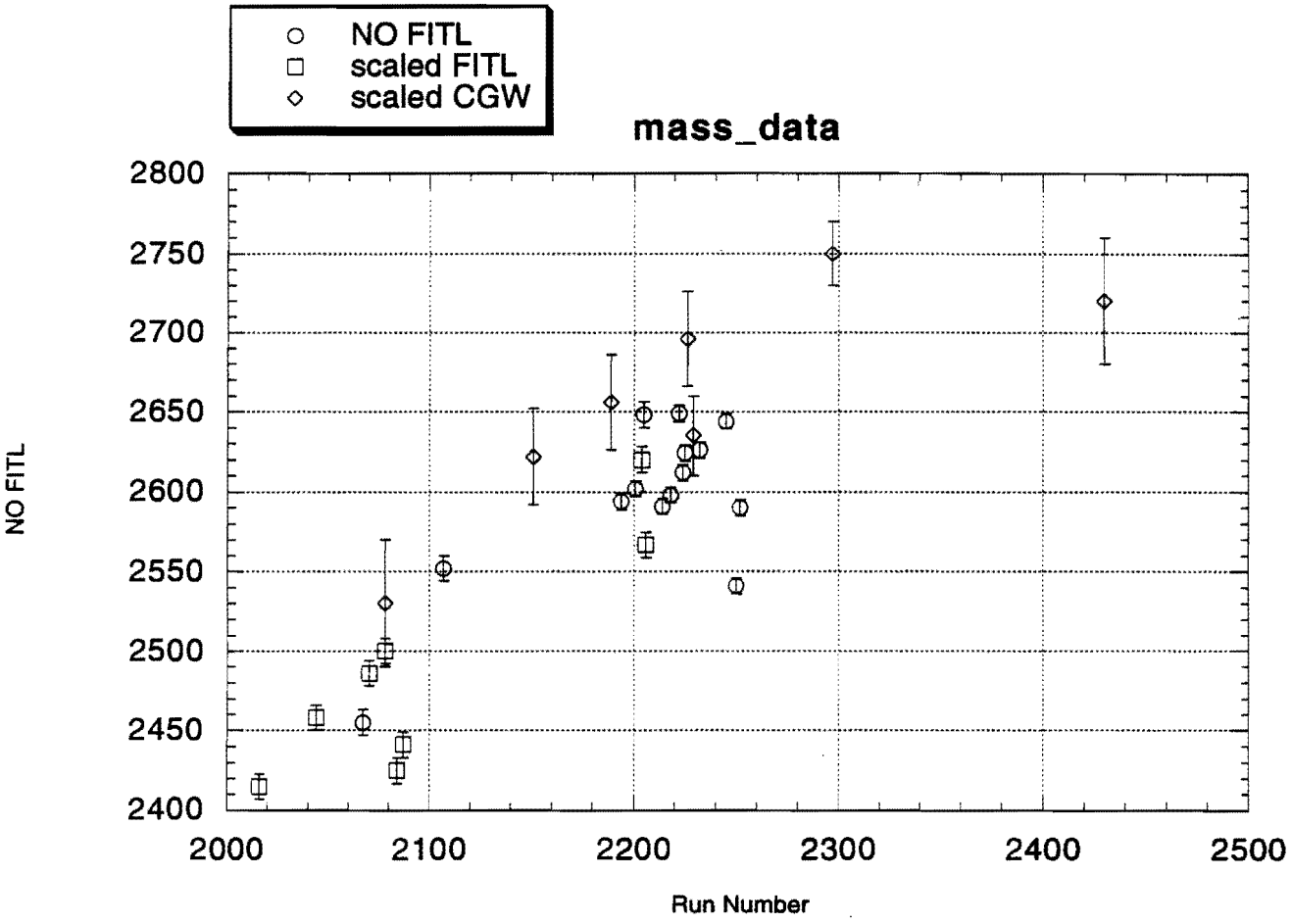
NO FITL
scaled FITL
scaled CGW
mass_data
NO FITL
2800
2750
2700
2650
2600
2550
2500
2450
2400
2000
2100
2200
2300
2400
2500
Run Number

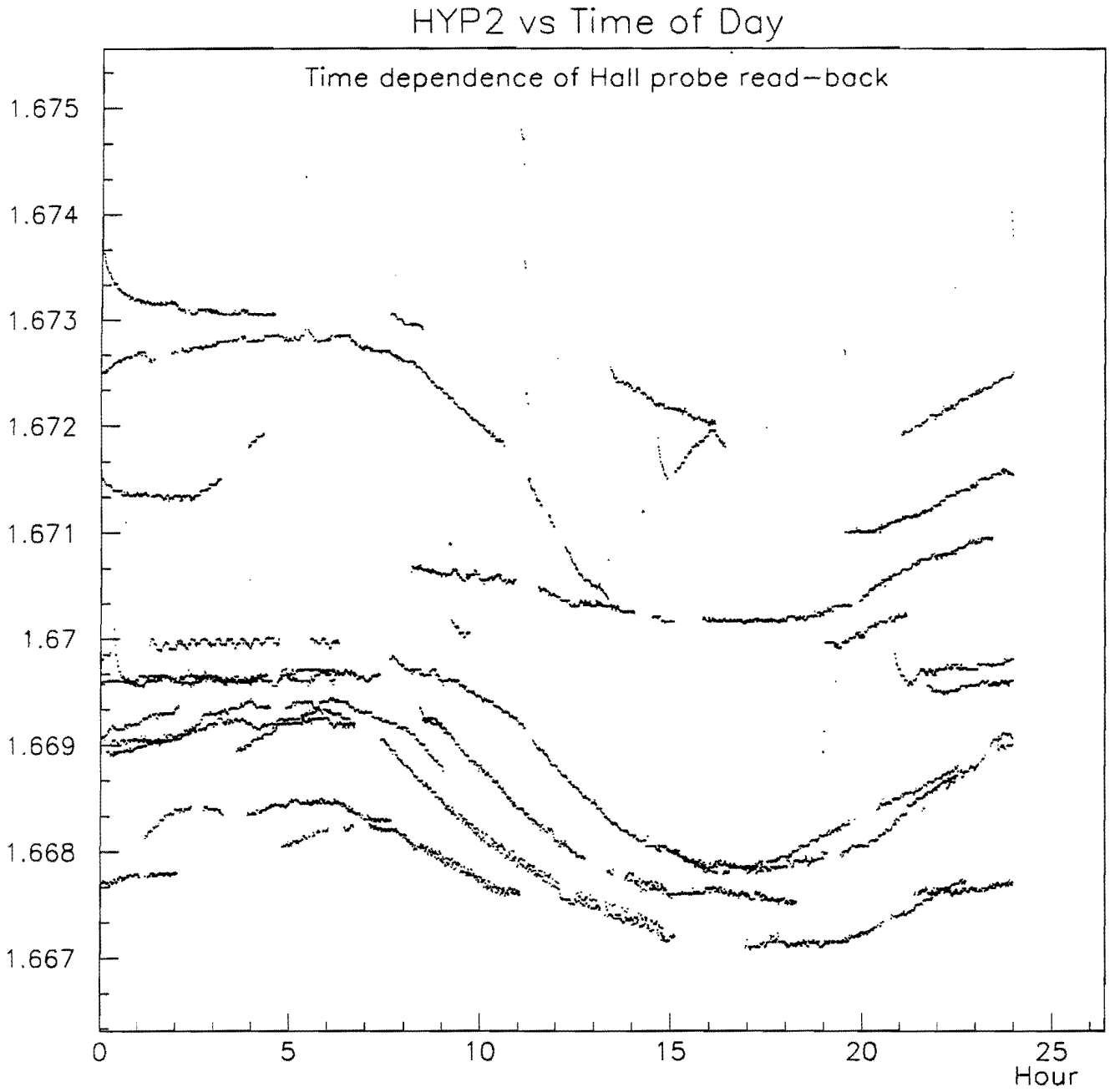
HYP2 vs Time of Day
Time dependence of Hall probe read–back
1.675
1.674
1.673
1.672
1.671
1.67
1.669
1.668
1.667
0
5
10
15
20
25
Hour

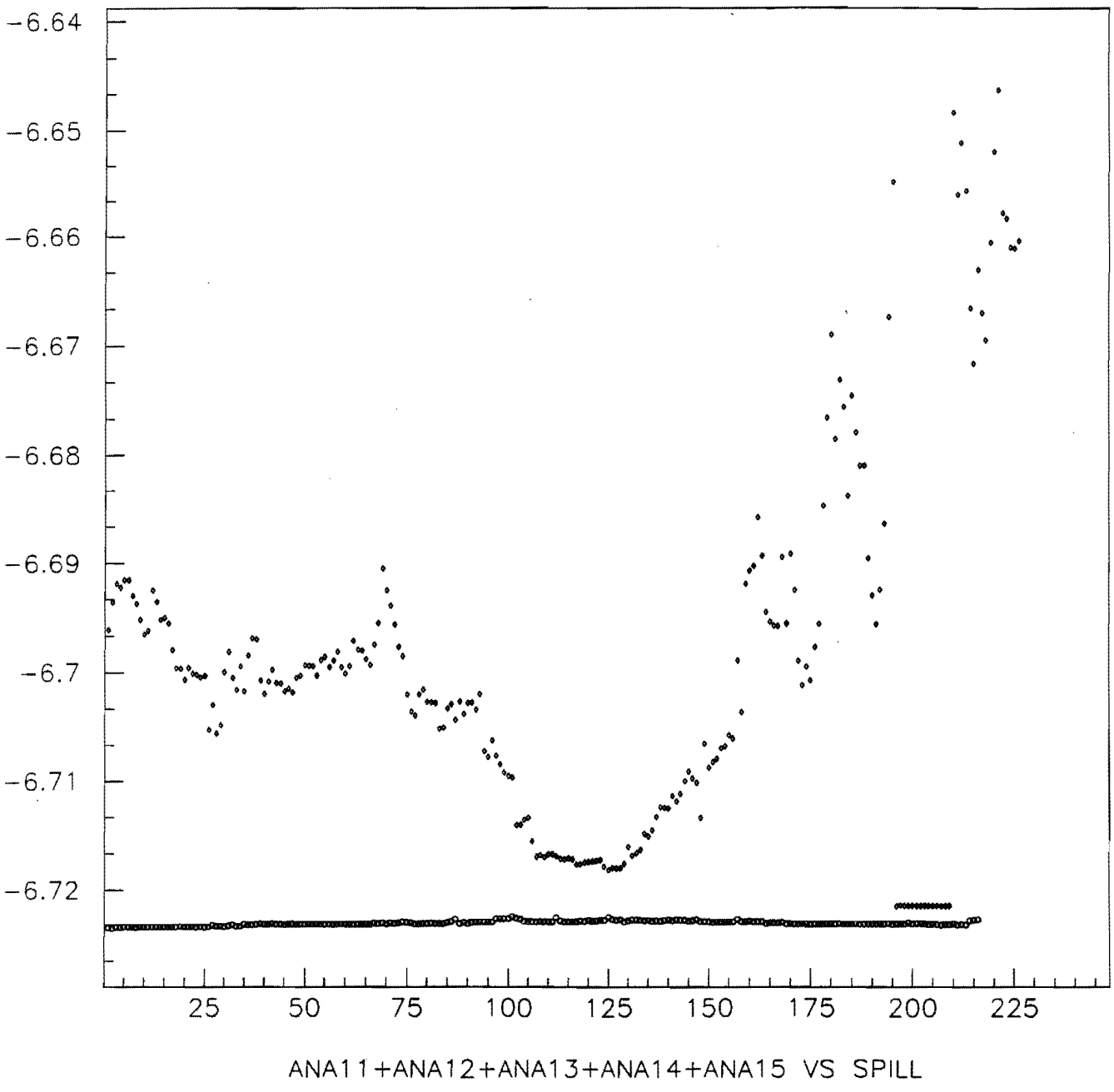
-6.64
-6.65
-6.66
-6.67
-6.68
-6.69
-6.7
-6.71
-6.72
25
50
75
100
125
150
175
200
225
ANA11+ANA12+ANA13+ANA14+ANA15 VS SPILL

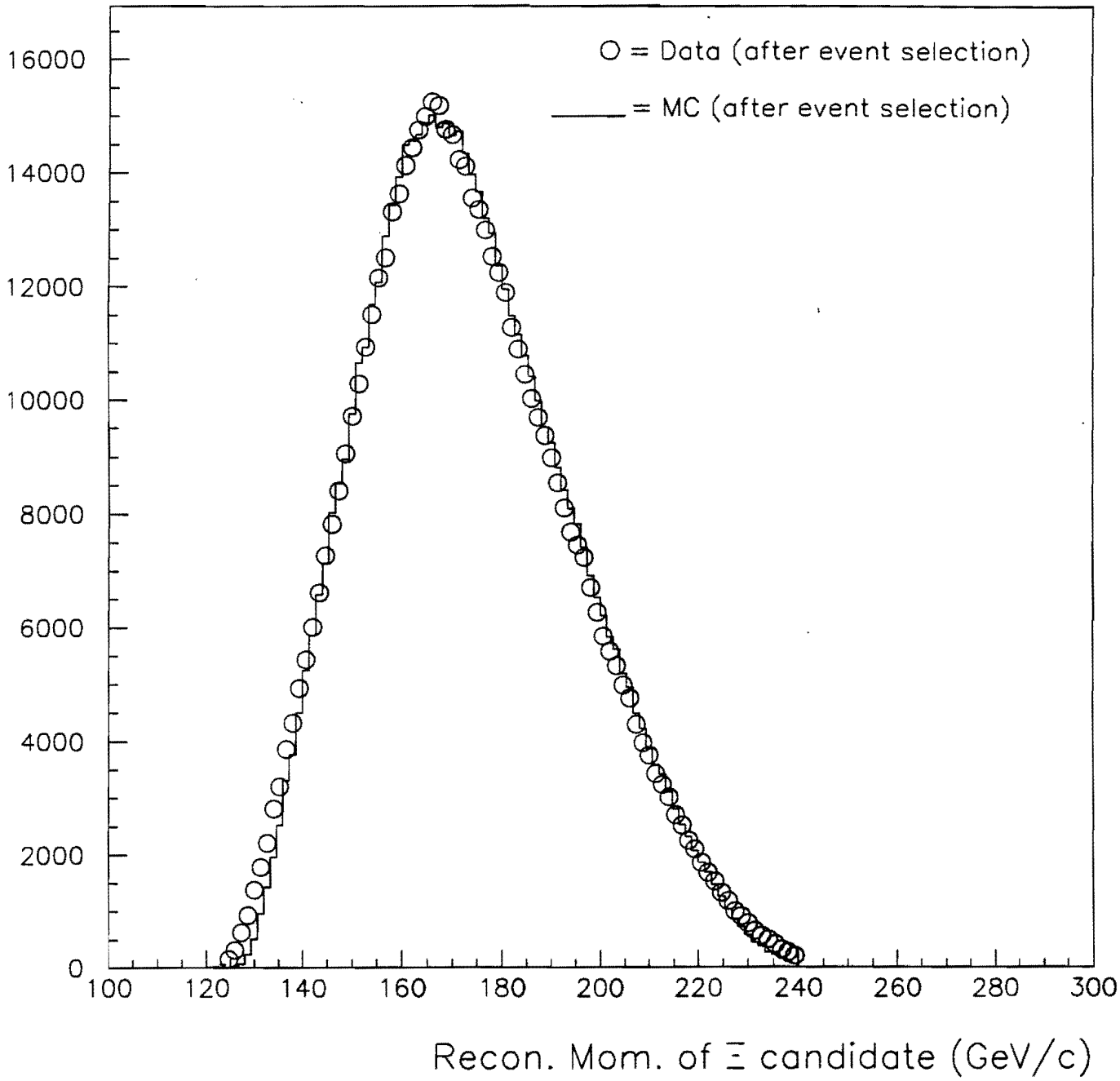
O = Data (after event selection)
_____ = MC (after event selection)
16000
14000
12000
10000
8000
6000
4000
2000
0
100
120
140
160
180
200
220
240
260
280
300
Recon. Mom. of Ξ candidate (GeV/c)

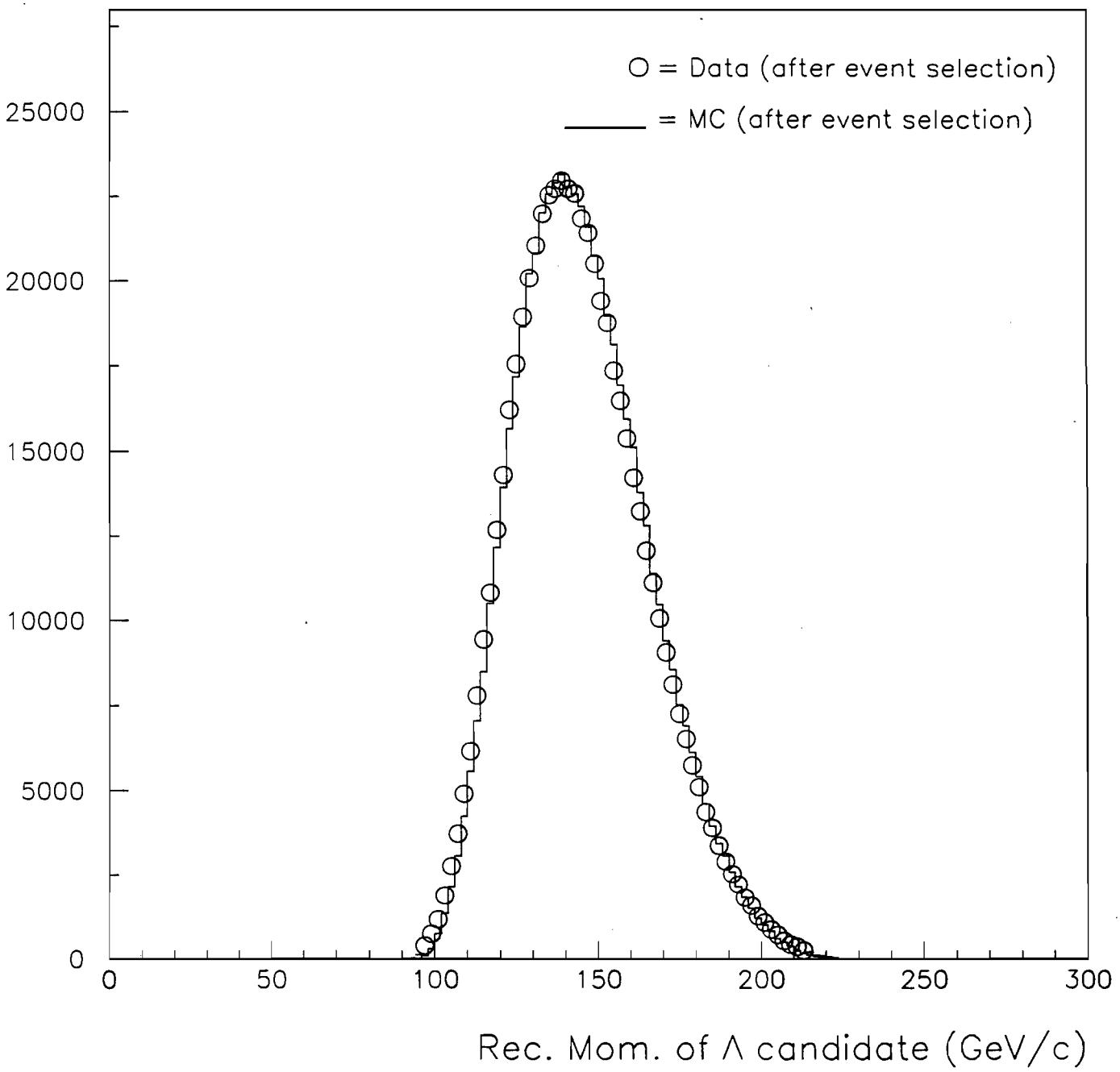
O = Data (after event selection)
= MC (after event selection)
25000
20000
15000
10000
5000
0
0
50
100
150
200
250
300
Rec. Mom. of Λ candidate (GeV/c)

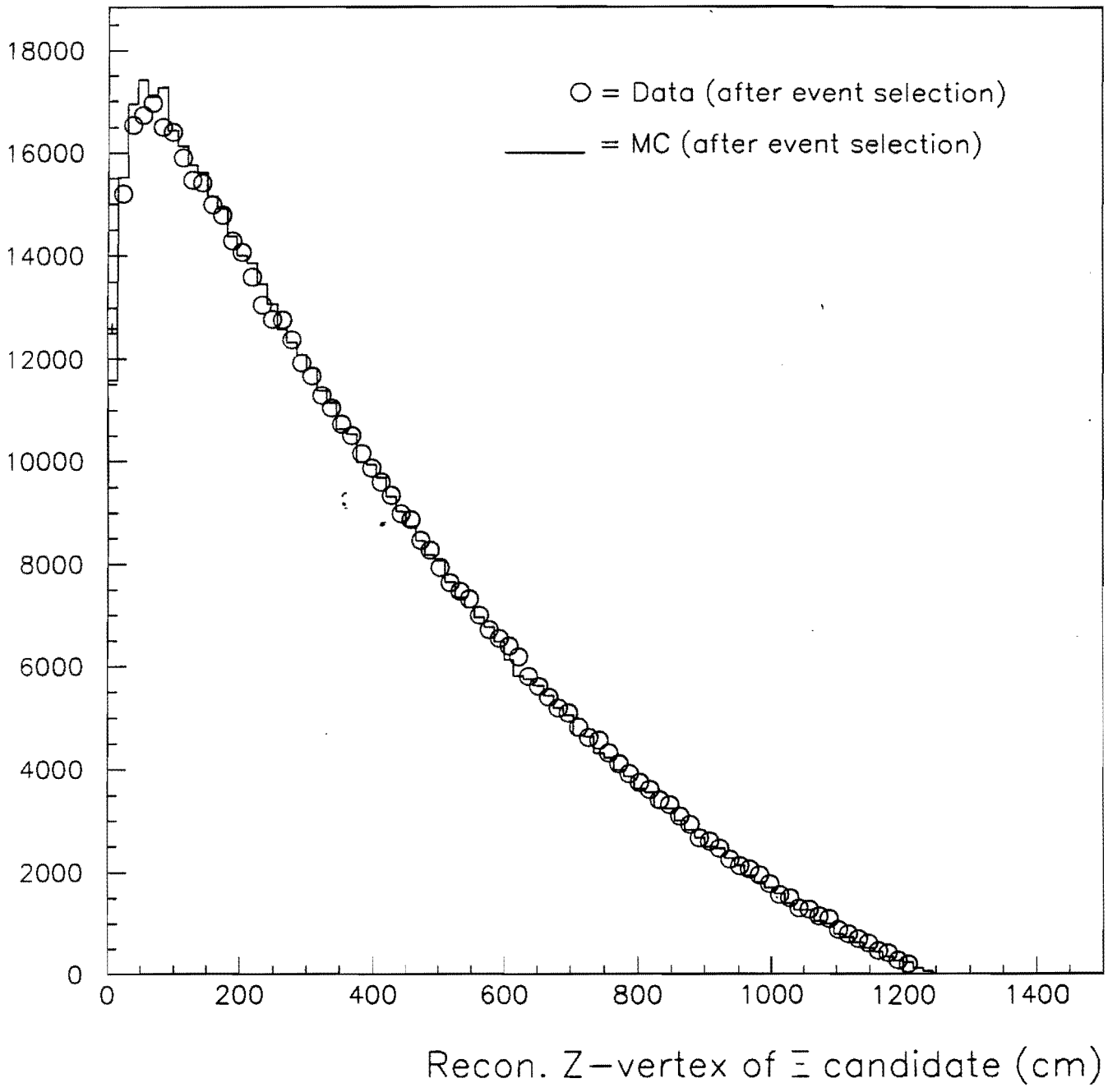
O = Data (after event selection)
= MC (after event selection)
18000
16000
14000
12000
10000
8000
6000
4000
2000
0
0
200
400
600
800
1000
1200
1400
Recon. Z−vertex of Ξ candidate (cm)

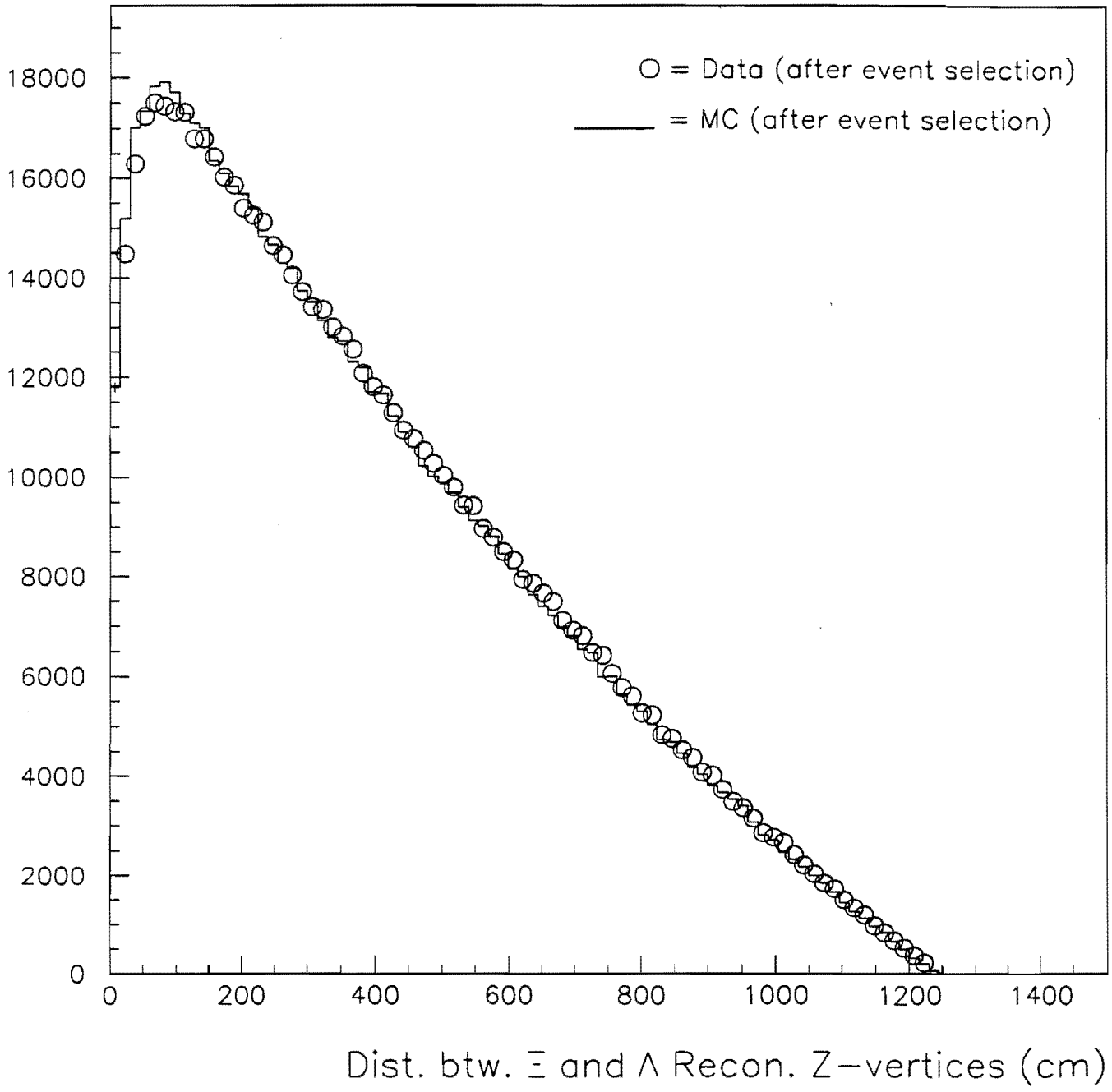
O = Data (after event selection)
= MC (after event selection)
18000
16000
14000
12000
10000
8000
6000
4000
2000
0
0
200
400
600
800
1000
1200
1400
Dist. btw. Ξ and Λ Recon. Z−vertices (cm)

Systematics

Any effect which adds or subtracts events unequally from the Ξ^- and $\overline{\Xi}^+$ proton and antiproton $\cos\theta$ distributions will cause a false asymmetry if not corrected for.

There are three classes of biases.

1. Acceptance differences:
   - Targetting differences.
   - Magnetic field differences.
   - Chamber efficiency differences.
   - Different reconstruction efficiencies due to different interaction cross sections with the material in the spectrometer between the π^- and π^+ and between the p and $\bar{p}$.
2. Different Ξ^- and $\overline{\Xi}^+$ polarization.
   - This means that the Λ is no longer found in a simple helicity state with the polarization magnitude given by α_Ξ, but rather by:

$$\vec{P}_\Lambda = \frac{(\alpha + \vec{P}_\Xi \cdot \hat{p}_\Lambda)\hat{p}_\Lambda + \beta(\vec{P}_\Xi \times \hat{p}_\Lambda) + \gamma(\hat{p}_\Lambda \times (\vec{P}_\Xi \times \hat{p}_\Lambda))}{(1 + \alpha \vec{P}_\Xi \cdot \hat{p}_\Lambda)}$$

   - This results in the Λ and $\overline{\Lambda}$ inhabiting different regions of phase space.
   - Nonzero Ξ polarization can in principal be corrected for.
3. Different backgrounds under the Λ and $\overline{\Lambda}$ and the Ξ^- and $\overline{\Xi}^+$ mass peaks.

Dukes

Our analysis method naturally minimizes potential biases

- The analysis frame axes changes from event to event since we always define the $\hat{z}$ axis to be the direction of the Λ momentum in the Ξ rest frame.

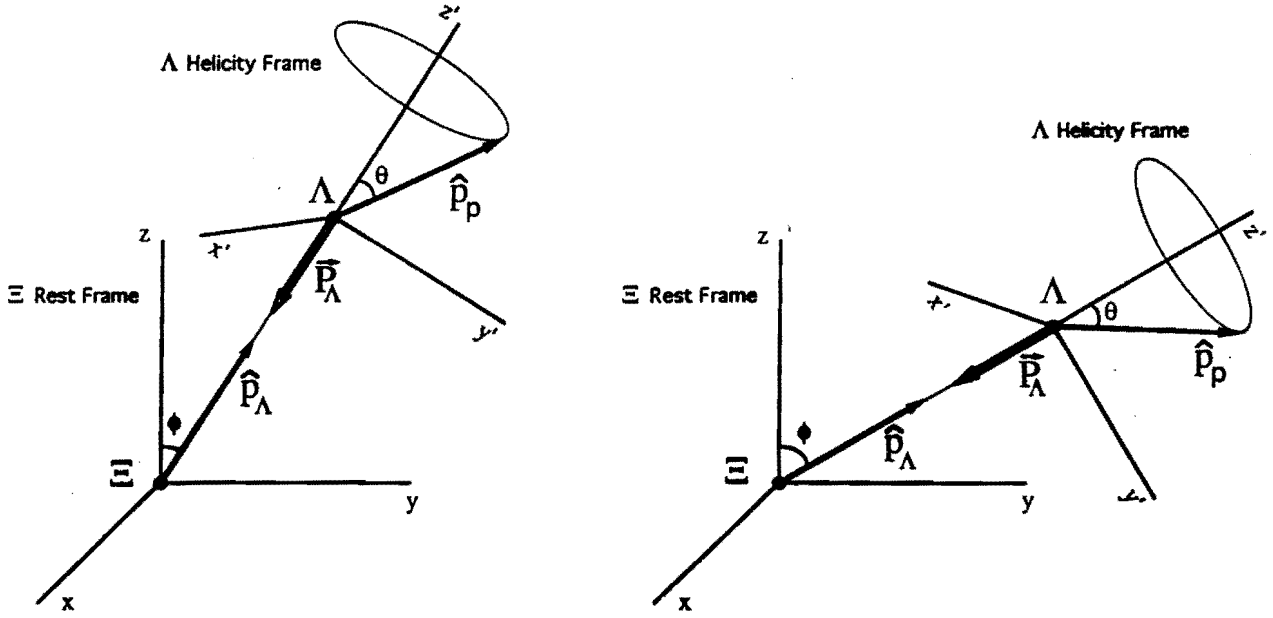

- Acceptance differences localized in a particular part of the apparatus do **not** map into a particular part of the proton (antiproton) $\cos\theta$ distribution.

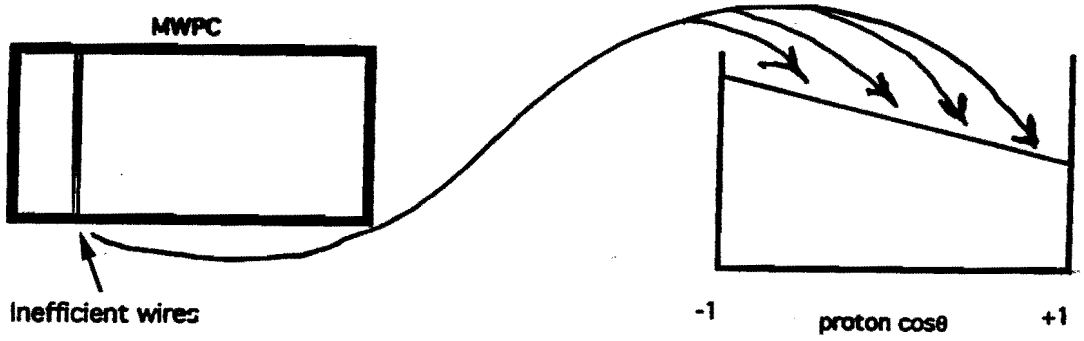

Effect of Ξ Polarization on $A_{\Xi\Lambda}$

- If the Ξ and $\overline{\Xi}$ polarizations are identically zero then the Λ and $\overline{\Lambda}$ are found in pure helicity states with polarizations given by α_Ξ and $\overline{\alpha}_\Xi$.
- Non-zero Ξ and $\overline{\Xi}$ polarizations give polarization components along axes perpendicular to the Λ momentum direction:

$$\vec{P}_d = \frac{(\alpha + \vec{P}_p \cdot \hat{p}_d)\hat{p}_d + \beta(\vec{P}_p \times \hat{p}_d) + \gamma(\hat{p}_d \times (\vec{P}_p \times \hat{p}_d))}{(1 + \alpha \vec{P}_p \cdot \hat{p}_d)}.$$

  where $\vec{P}_d$ is the Λ polarization, $\vec{P}_p$ is the Ξ polarization, and $\hat{p}_d$ is the Λ momentum direction in the Ξ rest frame. The parameters: α, β, and γ are:

$$\begin{aligned} \alpha &= \frac{2\mathrm{Re}(S^*P)}{|S|^2 + |P|^2}, \\ \beta &= \frac{2\mathrm{Im}(S^*P)}{|S|^2 + |P|^2}, \\ \gamma &= \frac{|S|^2 - |P|^2}{|S|^2 + |P|^2}, \end{aligned}$$

- We have generated several hundred million Ξ Monte Carlo events with various polarizations in the horizontal (x) and vertical (y) directions to estimate the bias caused by a non-zero Ξ or $\overline{\Xi}$ polarization.

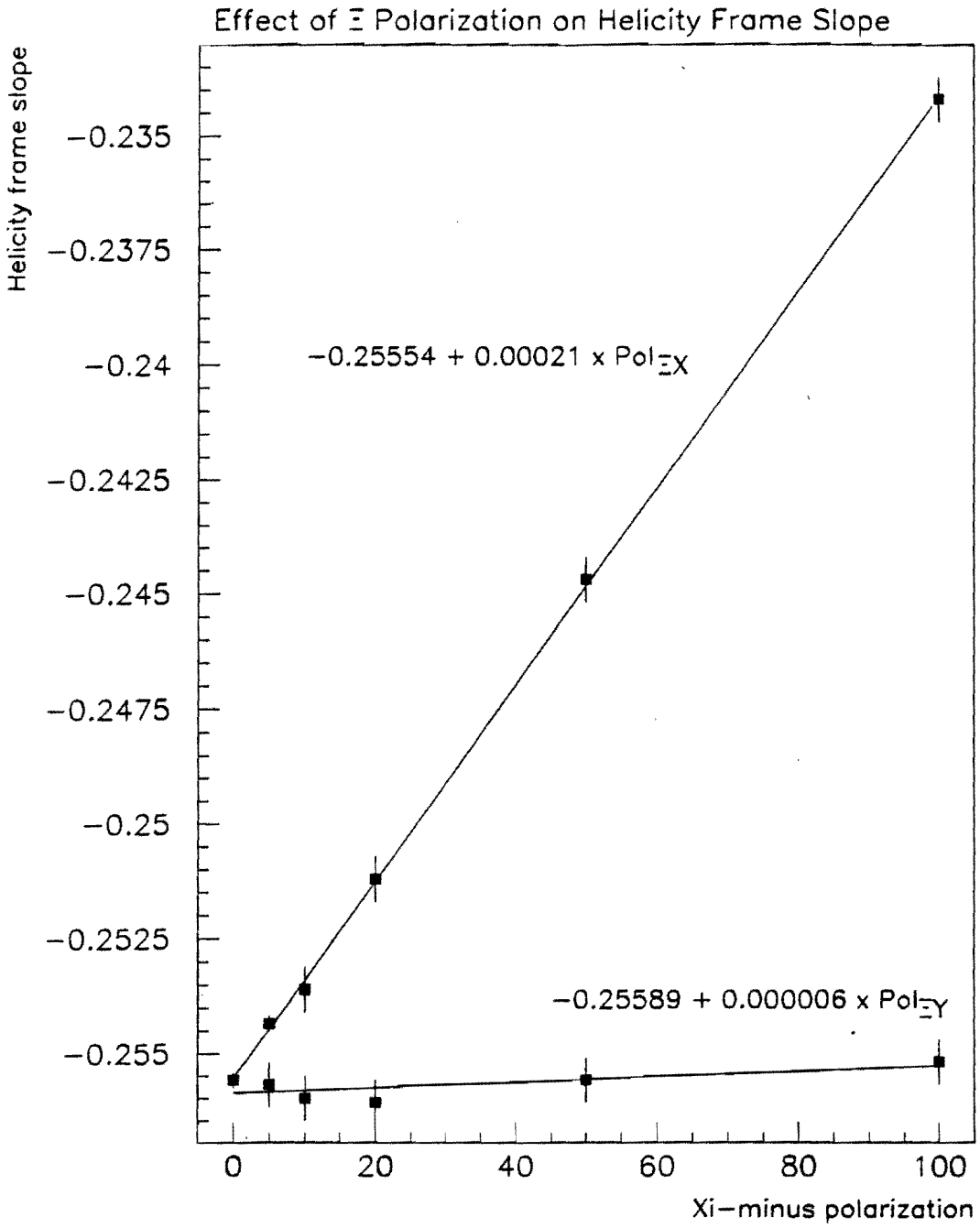
Effect of Ξ Polarization on Helicity Frame Slope
Helicity frame slope
−0.235
−0.2375
−0.24
−0.2425
−0.245
−0.2475
−0.25
−0.2525
−0.255
−0.25554 + 0.00021 x Pol_ΞX
−0.25589 + 0.000006 x Pol_ΞY
0
20
40
60
80
100
Xi−minus polarization

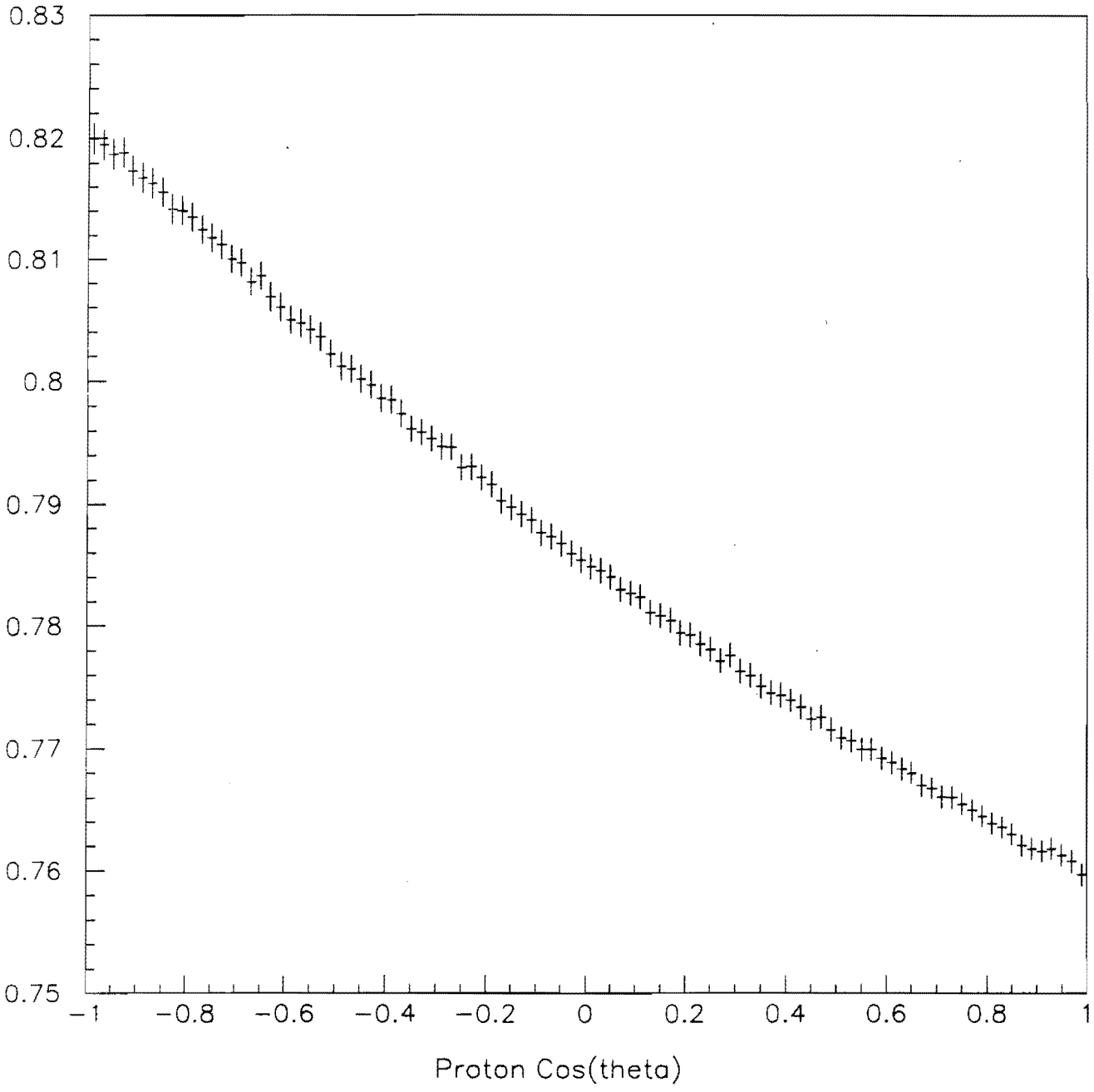
Helicity Frame Acceptance (100 million events)
0.83
0.82
0.81
0.8
0.79
0.78
0.77
0.76
0.75
−1
−0.8
−0.6
−0.4
−0.2
0
0.2
0.4
0.6
0.8
1
Proton Cos(theta)

How Well do we Need to Know the Ξ Polarization?

$$A_{\Xi\Lambda} = \frac{\alpha_\Xi\alpha_\Lambda - \overline{\alpha}_\Xi\overline{\alpha}_\Lambda}{\alpha_\Xi\alpha_\Lambda + \overline{\alpha}_\Xi\overline{\alpha}_\Lambda} = 1.71(\alpha_\Xi\alpha_\Lambda - \overline{\alpha}_\Xi\overline{\alpha}_\Lambda)$$

Call $\alpha_\Xi\alpha_\Lambda = \alpha_\Xi\alpha_\Lambda$ and $\overline{\alpha}_\Xi\overline{\alpha}_\Lambda = \overline{\alpha}_\Xi\overline{\alpha}_\Lambda$. Then

$$A_{\Xi\Lambda} = 1.71(\alpha_\Xi\alpha_\Lambda - \overline{\alpha}_\Xi\overline{\alpha}_\Lambda)$$

If we assume that $\delta(\alpha_\Xi\alpha_\Lambda) = \delta(\overline{\alpha}_\Xi\overline{\alpha}_\Lambda)$,

$$\delta A_{\Xi\Lambda} = 1.71\sqrt{2}\delta(\alpha_\Xi\alpha_\Lambda) = 2.4\delta(\alpha_\Xi\alpha_\Lambda)$$

If we wish the error in $A_{\Xi\Lambda} \leq 1\times10^{-4}$, this implies:

$$\delta(\alpha_\Xi\alpha_\Lambda) \leq 4.1\times10^{-5}$$

Monte Carlo results show that:

$$\begin{aligned}\delta(\alpha_\Xi\alpha_\Lambda) &= 2.1\times10^{-2}\times P_{\Xi x} \\ &= 6.0\times10^{-4}\times P_{\Xi y}\end{aligned}$$

Hence the polarization has to be measured to an accuracy of:

$$\begin{aligned}\delta P_{\Xi x} &\leq 0.2\times10^{-2} \quad \text{(required events : } 3.6\times10^6\text{)} \\ \delta P_{\Xi y} &\leq 6.8\times10^{-2} \quad \text{(required events : } 3.1\times10^3\text{)}\end{aligned}$$

These measurments are easy to make, and are done by looking at the asymmetry in the $\Xi \to \Lambda\pi$ decay distribution, as well as the asymmetry in the daughter $\Lambda \to p\pi$ distribution. This analysis is done along axes parallel to the laboratory axes, and not in the helicity frame.

What Polarization do we Expect?

- At a production angle of 0°, the Ξ and $\overline{\Xi}$ polarization should be zero, if parity is conserved in strong interactions.
- Our production angle, of course, is not exactly zero, so there could be some residual polarization.
- The kinematic behavior of the Ξ and $\overline{\Xi}$ polarizations, at our x_f, is not well known, although all hyperons exhibit similar behavior. Studies of Λ polarization have shown that

$$\mathrm{P} = 0.05 p_T \text{ at } x_f \approx 0.20$$

  Assume the Ξ and $\overline{\Xi}$ polarizations have the same p_T dependence. Since $p_T = 170 \times \theta$, we have $\mathrm{P} = 7.5 \times \theta$, and hence the average production angle, for a bias of less than 1×10^{-4} in $A_{\Xi\Lambda}$ must be less than

$$\begin{aligned} |\theta_x| &\leq 8.0 \times 10^{-3} \text{ rad} \\ |\theta_y| &\leq 0.24 \times 10^{-3} \text{ rad} \end{aligned}$$

- Typical production angles range from

$$\begin{aligned} |\theta_x| &\leq 0.2 \times 10^{-3} \text{ rad} \\ |\theta_y| &\leq 0.1 \times 10^{-3} \text{ rad} \end{aligned}$$

  Mean values are much less!

- **Conclusion:** Expected polarization will be much less than that needed to give a bias of 1×10^{-4}.

Hyperon Polarization Results from the Fermilab Neutral Hyperon Group

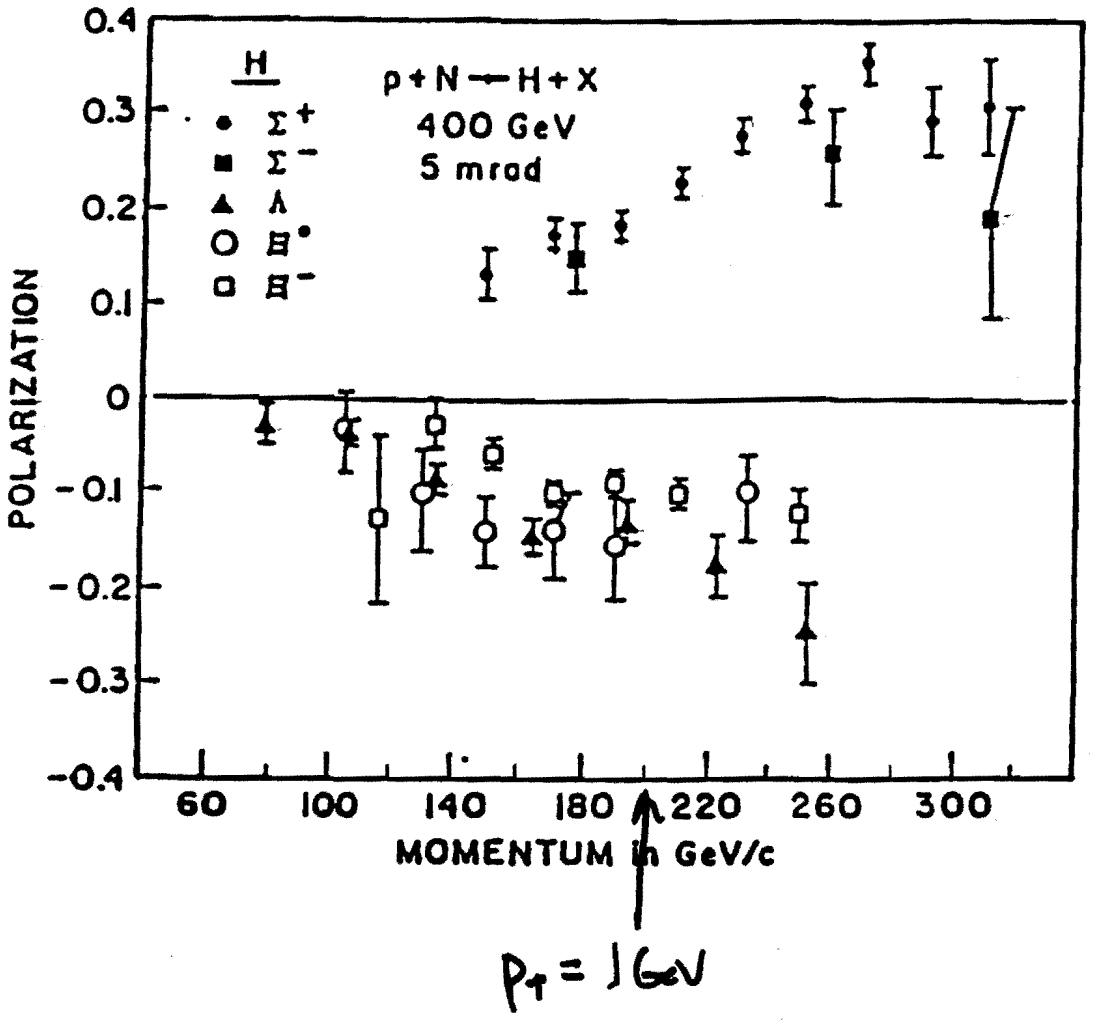

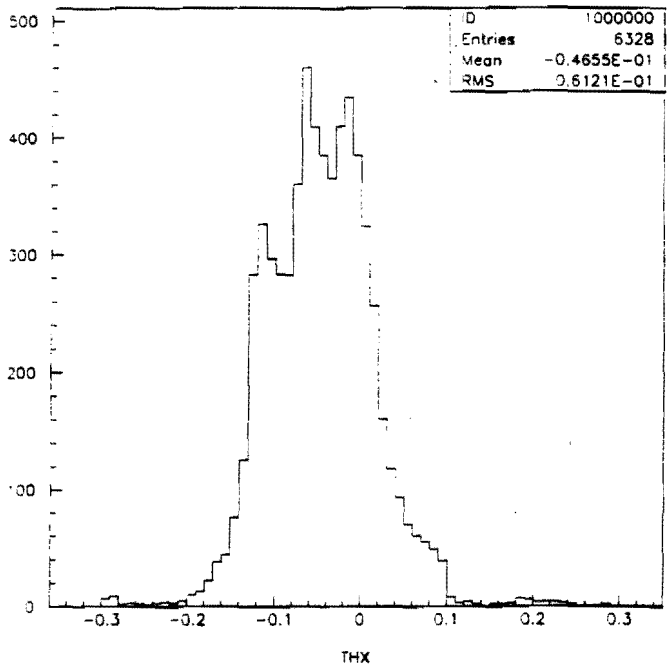
ID 1000000
Entries 6328
Mean -0.4655E-01
RMS 0.6121E-01
500
400
300
200
100
0
-0.3
-0.2
-0.1
0
0.1
0.2
0.3
THX

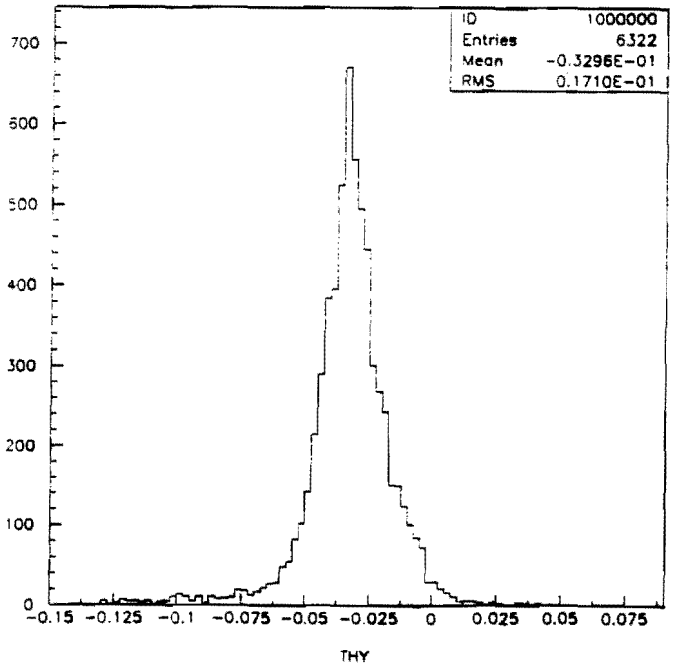
ID 1000000
Entries 6322
Mean -0.3296E-01
RMS 0.1710E-01
700
600
500
400
300
200
100
0
-0.15
-0.125
-0.1
-0.075
-0.05
-0.025
0
0.025
0.05
0.075
THY

Effect of a Momentum Mismatch on $A_{\Xi\Lambda}$

- The slope of the proton $\cos\theta$ distribution is sensitive to the Ξ momentum, so hence the Ξ^- and $\overline{\Xi}^+$ momentum distributions need to be normalized.
- To estimate the effect we have generated 100 million nominal Ξ^- events and 10 million Ξ^- events with a mean momentum boosted by about 1 GeV. The ratio of the two proton $\cos\theta$ distributions is shown below.

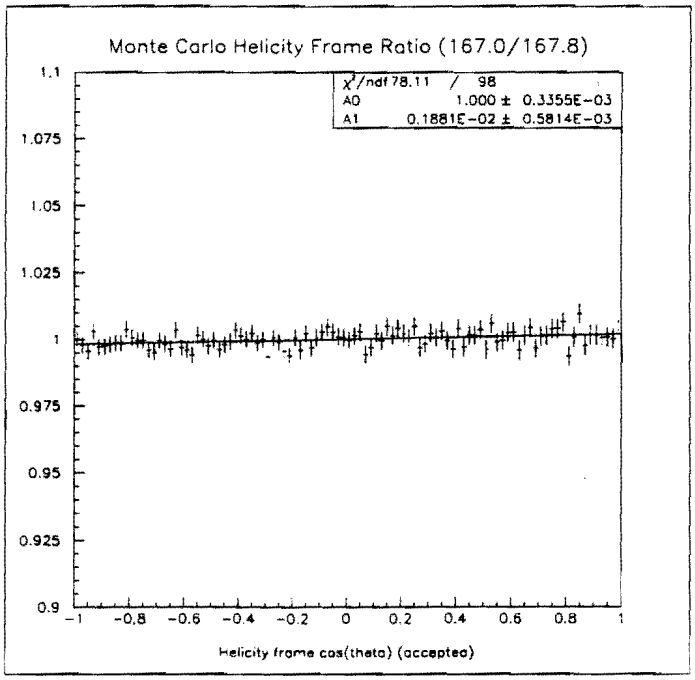

- From the slope in the above plot we deduce that an asymmetry of 1×10^{-4} in $A_{\Xi\Lambda}$ corresponds to a mean momentum difference of 24 MeV.
- Since we can normalize the two momentum distributions to essentially arbitrary accuracy, only a systematic effect such as an error in the magnetic field value (measured to 1×10^{-4}), or the Earth's magnetic field, can produce such an effect.
- These two effects produce a systematic error in the Ξ momentum of about 15 MeV, and hence contribute to $A_{\Xi\Lambda}$ at a level less than 1×10^{-4}.

Dukes

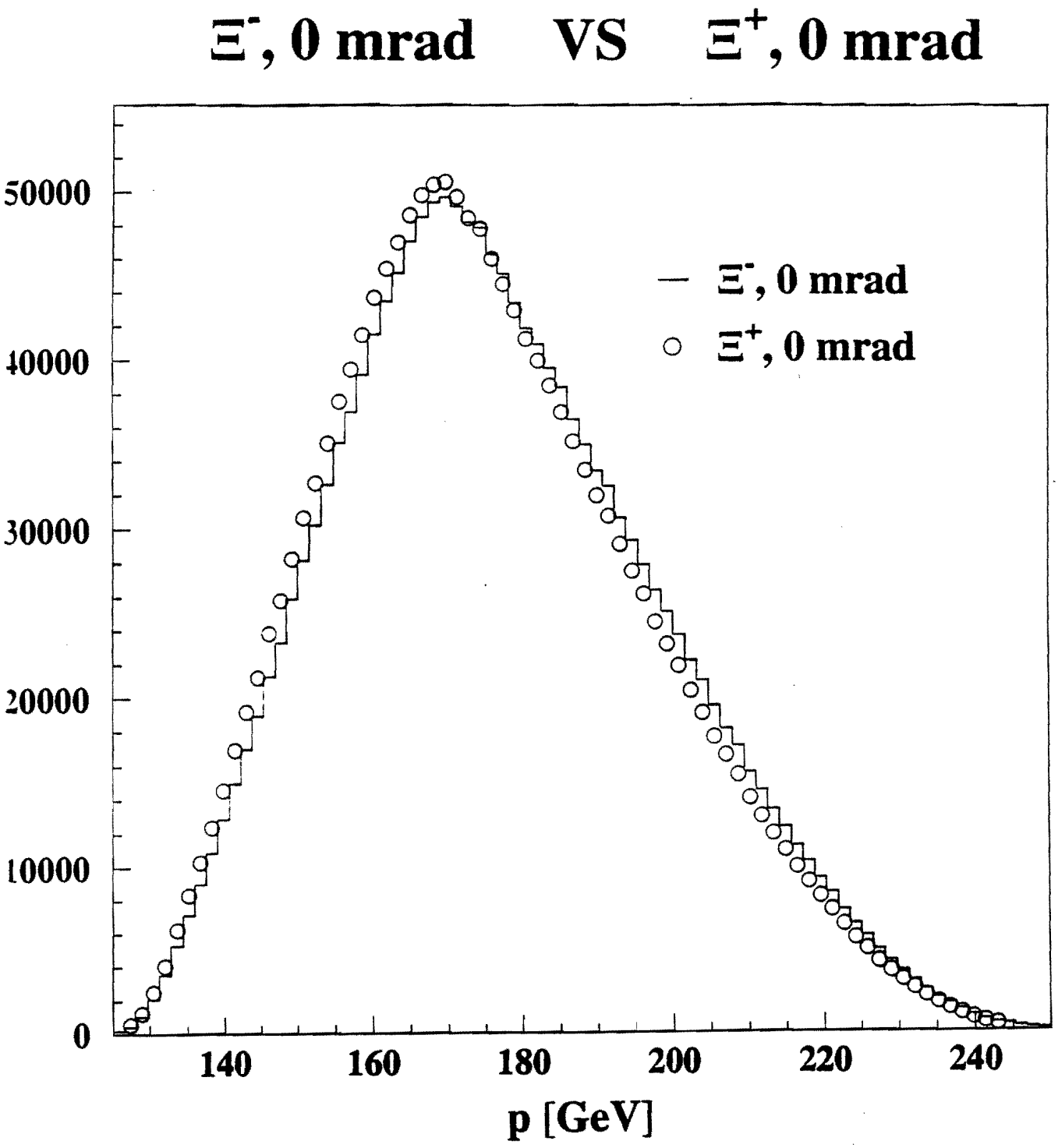
Ξ⁻, 0 mrad VS Ξ⁺, 0 mrad
50000
40000
30000
20000
10000
0
140
160
180
200
220
240
p [GeV]
Ξ⁻, 0 mrad
Ξ⁺, 0 mrad

Effect of the Background on $A_{\Xi\Lambda}$

- The backgrounds under the Ξ^- and $\bar{\Xi}^+$ mass peaks are similar and range from about 5×10^{-3} to 1×10^{-4}, depending on the severity of the cuts.
- By measuring the asymmetry in the Ξ sidebands we can estimate the effect on the proton $\cos\theta$ distribution.

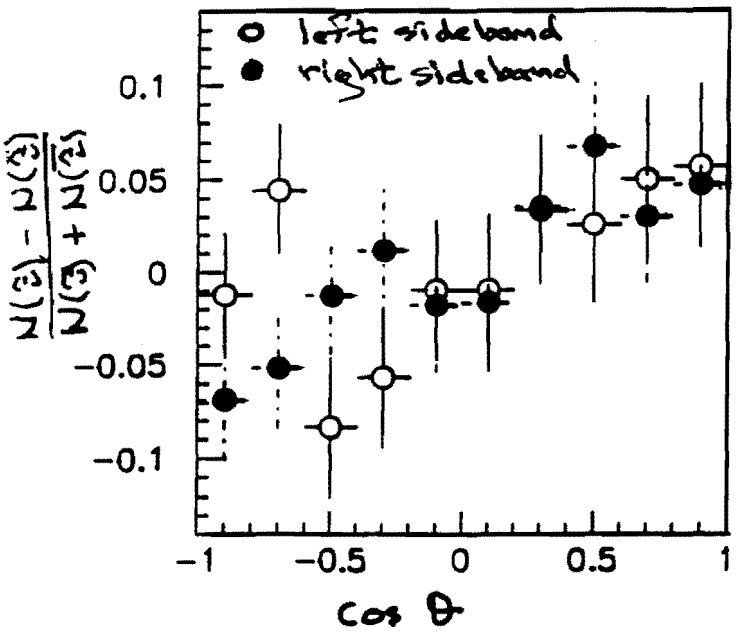

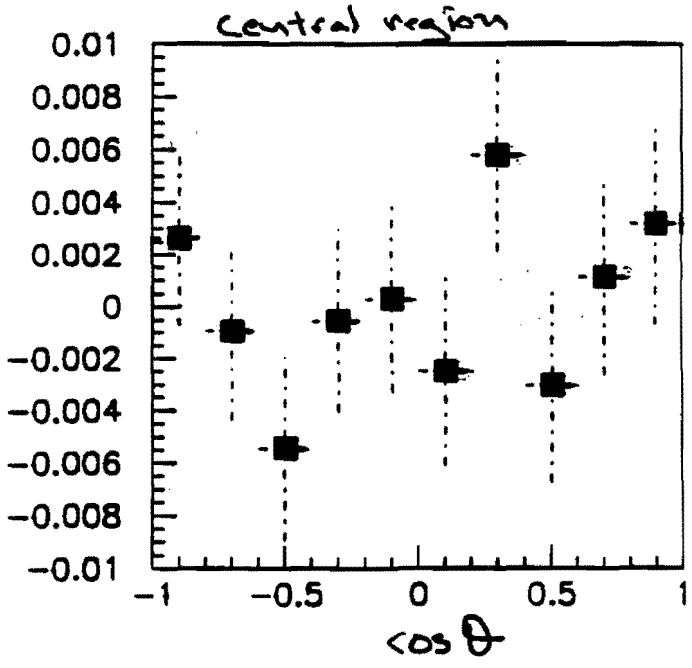

- Our preliminary estimate is a systematic error of $\delta A_{\Xi\Lambda} = 4\times10^{-5}$.
- More work and statistics are needed to firm up this number.

assuming $\frac{S}{B} = \frac{1}{5\times10^{-3}}$

and no attempt to correct for it

Effect of Interactions in the Spectrometer on $A_{\Xi\Lambda}$

- Because the spectrometer represents about 2.3% of an interaction length, both Ξ^- and $\overline{\Xi}^+$ events are lost due to the proton (antiproton) and pions interacting with that material.
- Because the pA and $\overline{p}A$, and the π^-A and π^+A cross sections have a different momentum dependence, the proton and antiproton $\cos\theta$ distributions are affected differently.

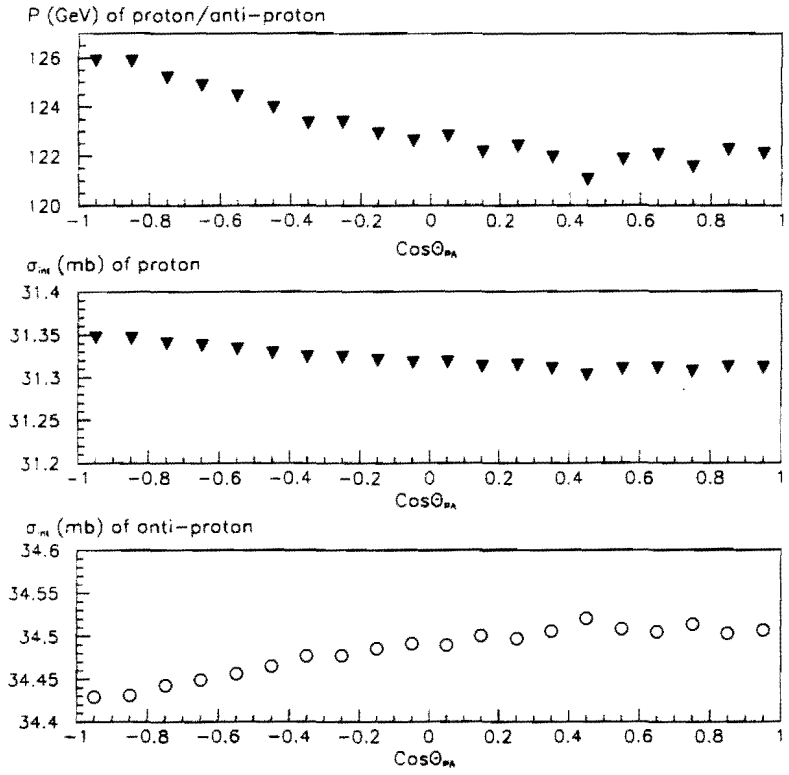

The pions from Ξ decays show similar behavior.

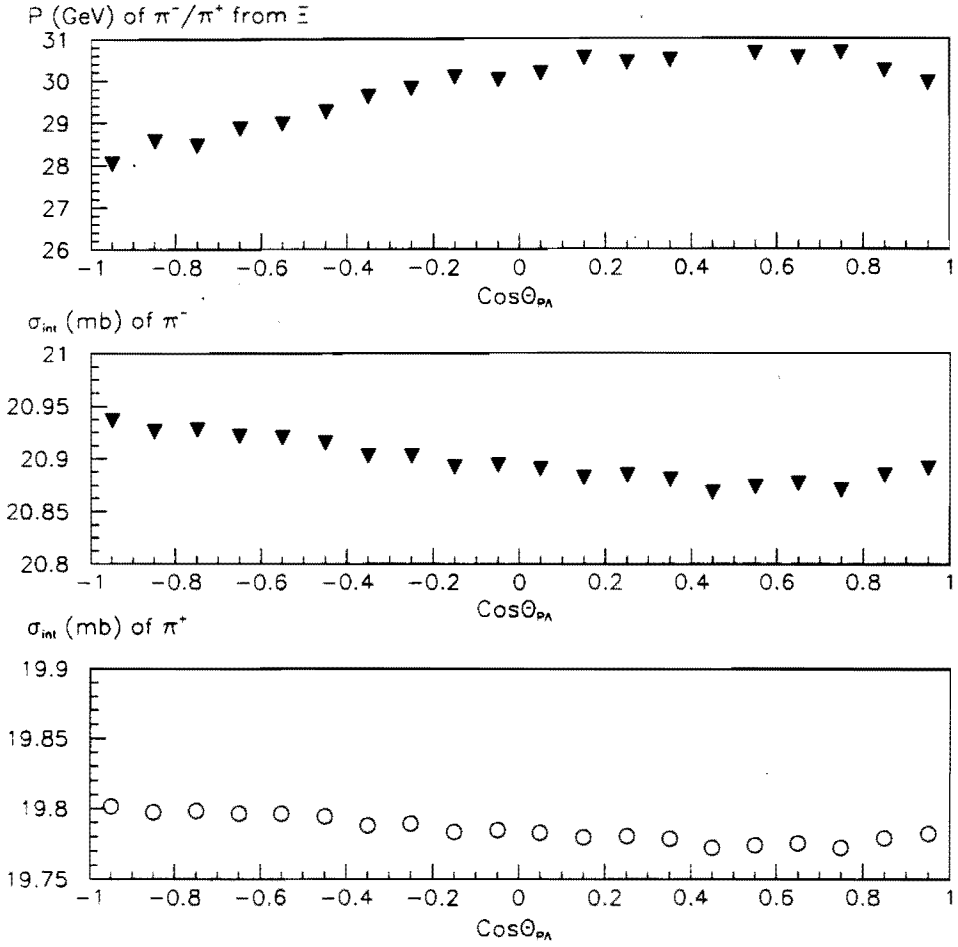

As well as the pions from Λ decays.

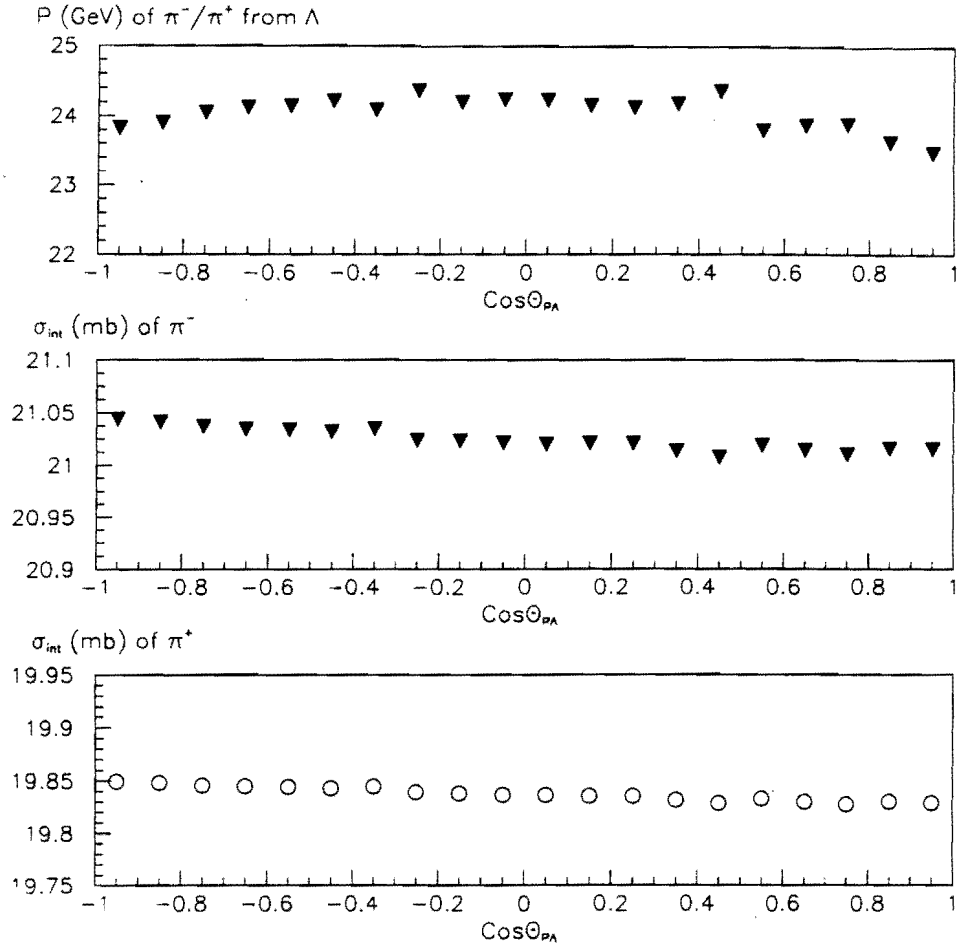

- The proton $\cos\theta$ distribution from Ξ^- decays is hardly affected, but the proton $\cos\theta$ distribution from $\bar{\Xi}^+$ decays does show a systematic effect.

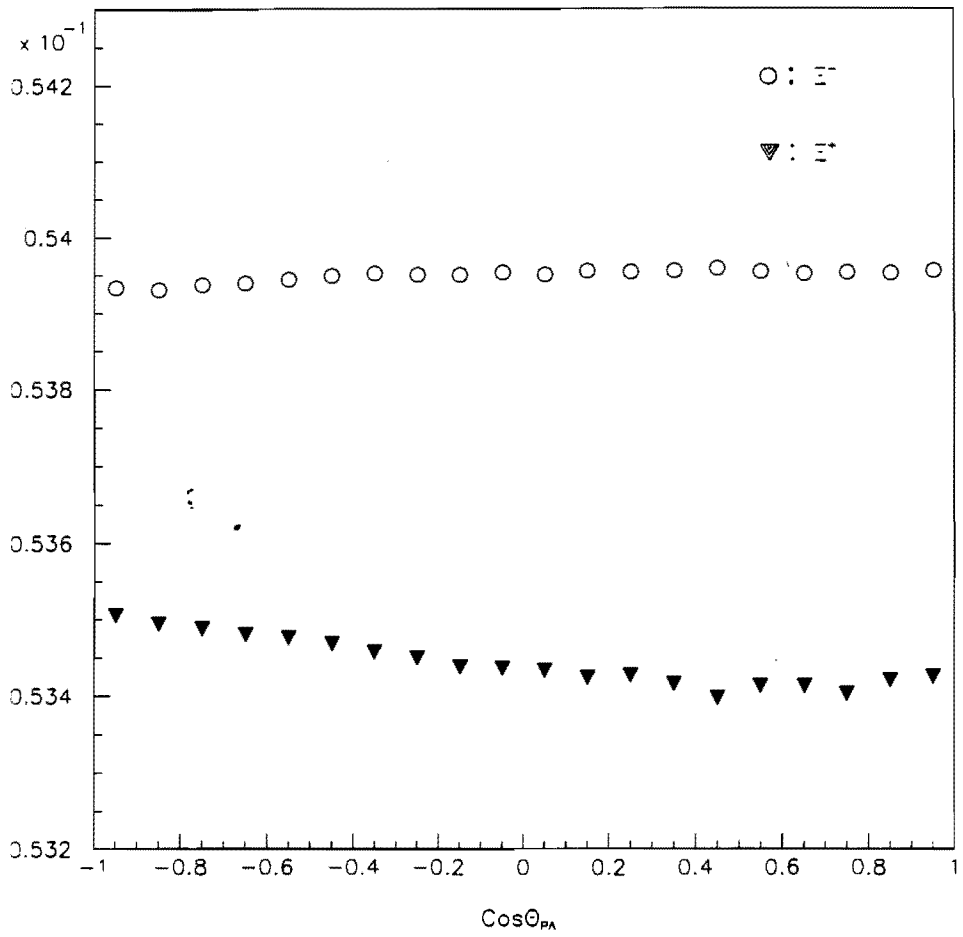

- These plots indicate that, **without correction** this difference in cross sections leads to an error of 1×10^{-4} in $A_{\Xi\Lambda}$.

RAN

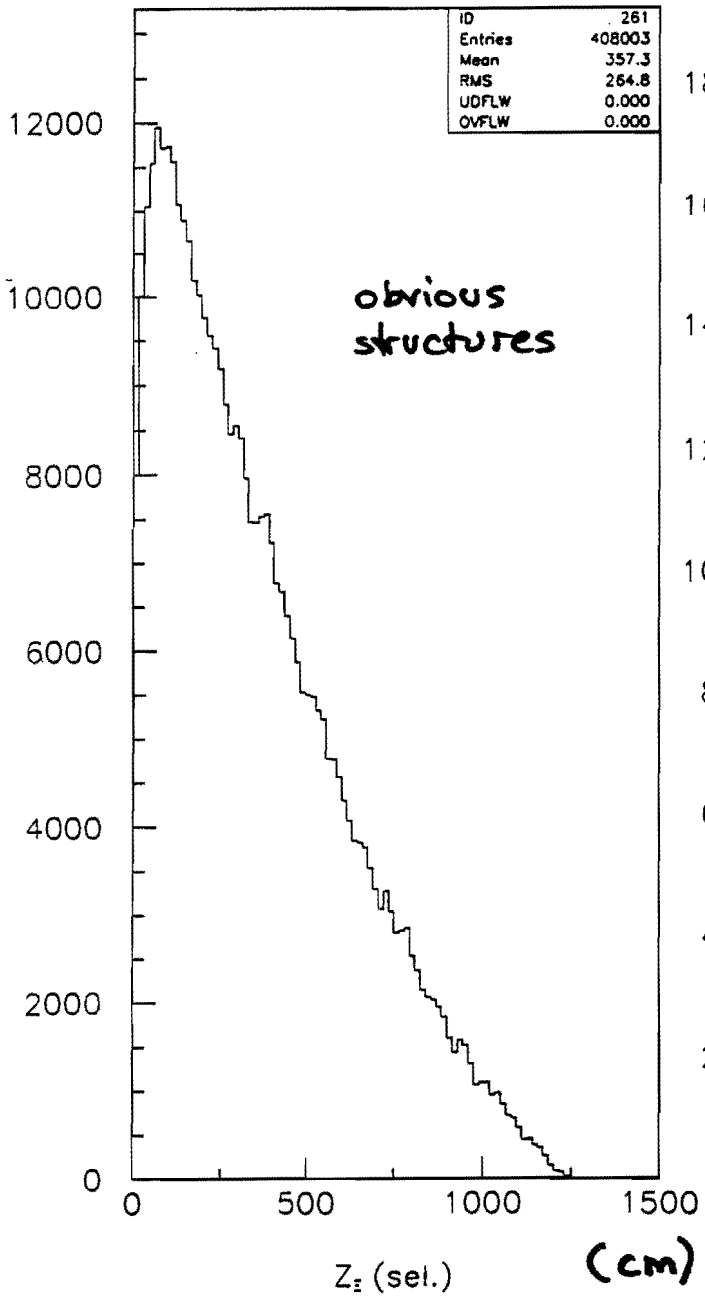

RANLUX

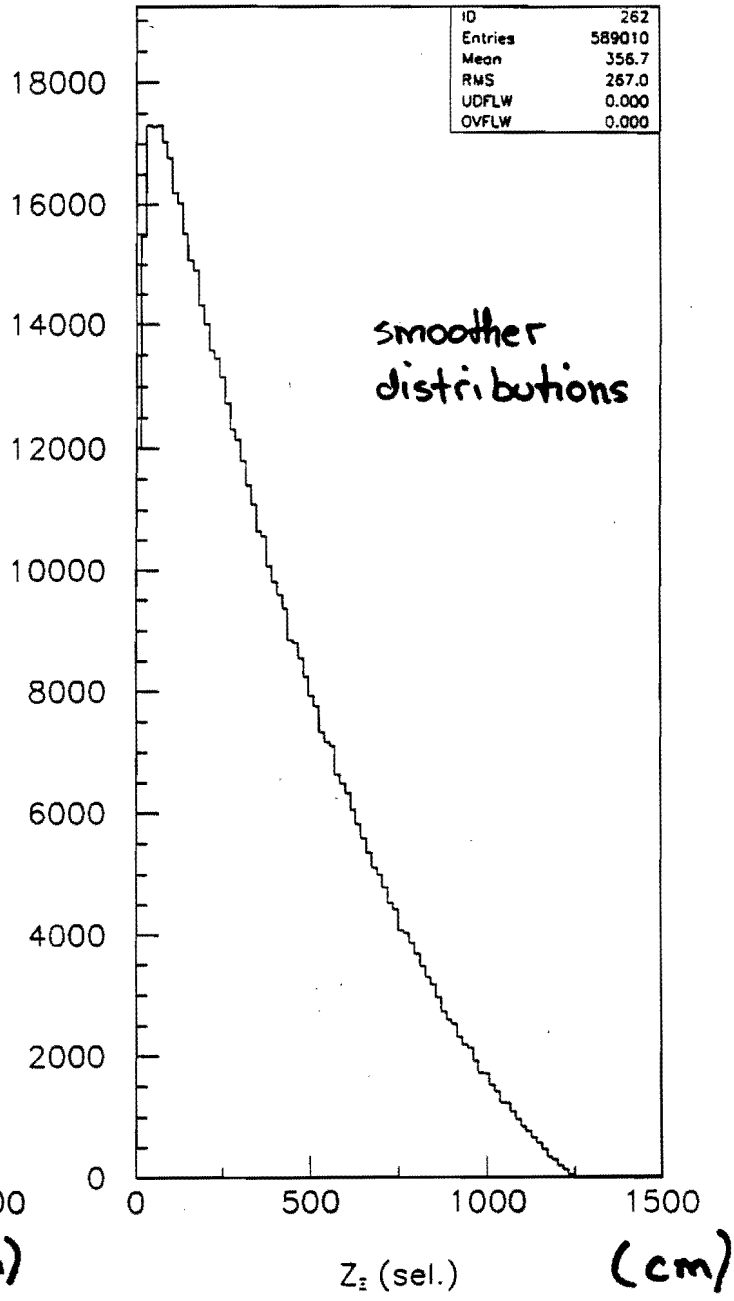

z-decay vertex of Ξ^-

Conclusions

- Systematic studies look good... we've seen nothing that will preclude a successful analysis of the experiment.
- Systematic studies are, of course, still in progress, and will continue until we send off the PRL.
- Farm analysis is going well and at the expected pace.
- We expect to go into high gear with the final version of the track reconstruction code and parameter files by July.
- Work on spectrometer improvements for the 1999 run are underway, but require (modest) funding from the DOE.
- Every month of running in 1999 will increase our data sample by an amount equal to that acquired in the 1997 run.
- The 1999 run provides a unique opportunity for a unique experiment — this physics cannot be done at Main Injector energies.

"In my view, CPV measurements in hyperon decay are at least as important as ϵ'/ϵ. They measure different things not always accessible in the K-decay experiments (even though both are $\Delta s = 1$ effects)."

S. Pakvasa

B. Luk
11/12/93

Fermilab Proposal P-871

Search for CP Violation in the Decays of $\Xi^-/\overline{\Xi}^+$ and $\Lambda^\circ/\overline{\Lambda}^\circ$ Hyperons

J. Antos, Y.C. Chen, C.N. Chiou, C. Ho, A. Sumarokov, and P.K. Teng

Academia Sinica, Nankang, Taipei 11529, Taiwan, Republic of China

G. Abrams, H. Bingham, G. Gidal, P.M. Ho, and K.B. Luk[1]

Lawrence Berkeley Laboratory and the University of California, Berkeley, CA 94720, USA

M. Botlo and E. Wang

Superconducting Super Collider, Dallas, TX 75237, USA

E.C. Dukes[2]

University of Virginia, Charlottesville, VA 22901, USA

T. Alexopoulos, A. Erwin, and M. Thompson

University of Wisconsin, Madison, WI 53706, USA

October 14, 1993

[1]Spokesperson: LUK@CSA.LBL.GOV, (510)486-7054

[2]Spokesperson: DUKES@UVAHEP.PHYS.VIRGINIA.EDU, (804)982-5376

Consider the decay

$$\Lambda \rightarrow p\,\pi^-$$

In the Λ rest frame, the angular distribution of the proton is given by:

$$\frac{dN_p}{d\cos\theta_p} = \frac{1}{2}(1 + \alpha_\Lambda \vec{P}_\Lambda \cdot \hat{p}) = \frac{1}{2}(1 + \alpha_\Lambda P_\Lambda \cos\theta_p)$$

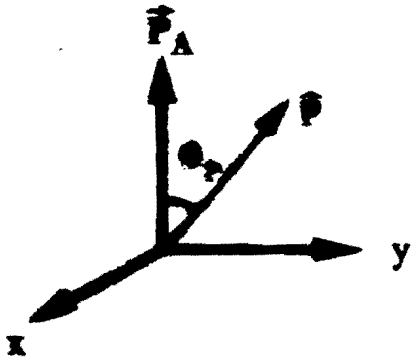

where

$$\alpha_\Lambda = \frac{2Re(S^*P)}{|S|^2 + |P|^2}$$

Under CP transformation,

$$\Lambda \rightarrow p\,\pi^- \quad \rightarrow \quad \bar{\Lambda} \rightarrow \bar{p}\,\pi^+$$
$$\alpha_\Lambda \quad \rightarrow \quad \alpha_{\bar{\Lambda}} = -\alpha_\Lambda$$

CP is violated if

$$\alpha_\Lambda \neq -\alpha_{\bar{\Lambda}}$$

To search for CP violation in the Λ decay, we have to measure the slope of the angular distribution:

$$\text{Slope} = \alpha_\Lambda P_\Lambda$$

However, we need to have know the polarization for both Λ and $\bar{\Lambda}$ in order to determine α_Λ and $\alpha_{\bar{\Lambda}}$.

The best way to guarantee that the Λ and $\bar{\Lambda}$ polarizations are precisely known is to get them from

$$\Xi^- \to \Lambda\pi^- \quad \text{and} \quad \bar{\Xi}^+ \to \bar{\Lambda}\pi^+$$

In this case, the Λ polarization in the Ξ^- rest frame is given by:

$$\vec{P}_\Lambda = \frac{(\alpha_\Xi + \vec{P}_\Xi \cdot \hat{\Lambda})\hat{\Lambda} + \beta_\Xi (\vec{P}_\Xi \times \hat{\Lambda}) + \gamma_\Xi (\hat{\Lambda} \times (\vec{P}_\Xi \times \hat{\Lambda}))}{(1 + \alpha_\Xi \vec{P}_\Xi \cdot \hat{\Lambda})}$$

where

$$\beta = \frac{2\text{Im}(S^* P)}{|S|^2 + |P|^2}$$

$$\gamma = \frac{|S|^2 - |P|^2}{|S|^2 + |P|^2}$$

If $\vec{P}_\Xi = 0$,

$$\vec{P}_\Lambda = \alpha_\Xi \hat{\Lambda}$$

Search For CP Violaton by Carrying out the Λ Helicity Analysis

In the Λ rest frame,

$$\frac{dN_p}{d\cos\theta} = \frac{1}{2}(1 + \alpha_\Lambda \alpha_\Xi \hat{\Lambda}\cdot\hat{p}) = \frac{1}{2}(1 + \alpha_\Lambda \alpha_\Xi \cos\theta)$$

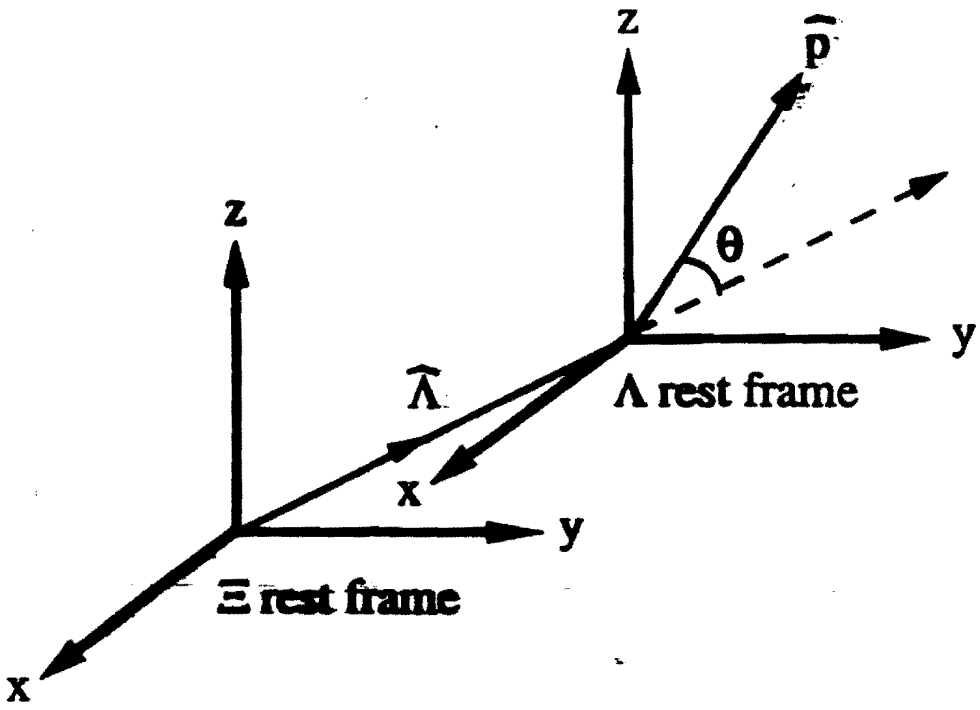

Note:

* The Λ helicity is **NOT fixed** in space, but changes from event to event.
* Many systematics, such as Ξ polarization, are fixed in space, their effects on the Λ helicity measurement is greatly reduced.

If CP is conserved,

$$\alpha_{\Xi}\alpha_{\Lambda} = \alpha_{\bar{\Xi}}\alpha_{\bar{\Lambda}}$$

i.e. the cosθ slopes of the proton and antiproton are identical for the decay sequences:

$$\Xi^- \to \Lambda\,\pi^- \quad (\Lambda \to p\,\pi^-) \qquad \text{and} \qquad \bar{\Xi}^+ \to \bar{\Lambda}\,\pi^+ \quad (\bar{\Lambda} \to \bar{p}\,\pi^+)$$

Define CP asymmetry parameter

$$A = \frac{\alpha_{\Xi}\alpha_{\Lambda} - \alpha_{\bar{\Xi}}\alpha_{\bar{\Lambda}}}{\alpha_{\Xi}\alpha_{\Lambda} + \alpha_{\bar{\Xi}}\alpha_{\bar{\Lambda}}} = A_{\Xi} + A_{\Lambda}$$

where

$$A_{\Xi} = \frac{\alpha_{\Xi} + \alpha_{\bar{\Xi}}}{\alpha_{\Xi} - \alpha_{\bar{\Xi}}}$$

$$A_{\Lambda} = \frac{\alpha_{\Lambda} + \alpha_{\bar{\Lambda}}}{\alpha_{\Lambda} - \alpha_{\bar{\Lambda}}}$$

Theoretical Predictions of CP Asymmetry

* CP violation in Ξ and Λ decays is direct with $\Delta S = 1$

* As in K^0 system the origin is thought to be due to the Penguin diagrams:

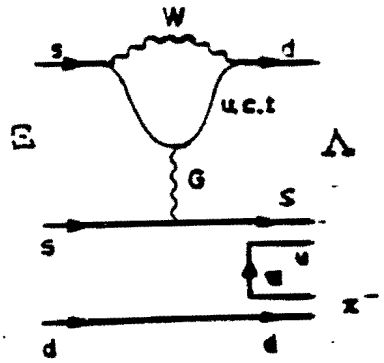

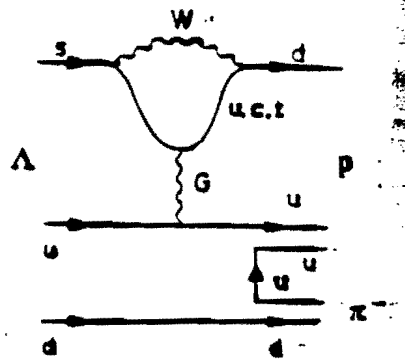

* In terms of the S- and P- wave amplitudes, final-state interaction strong phases δ, and weak CP violation phases ϕ, the partial waves of the hyperon decays are given by:

$$S = \sum_{k=1,3} S_k \, e^{i(\delta_{kS} + \phi_{kS})} \qquad P = \sum_{k=1,3} P_k \, e^{i(\delta_{kP} + \phi_{kP})}$$

and for antihyperon decay amplitudes,

$$\overline{S} = -\sum_{k=1,3} S_k \, e^{i(\delta_{kS} + \phi_{kS})} \qquad \overline{P} = \sum_{k=1,3} P_k \, e^{i(\delta_{kP} + \phi_{kP})}$$

and the CP asymmetry is :

$$A_\Xi \approx -\tan(\delta_{3P} - \delta_{3S}) \sin(\phi_{1P} - \phi_{1S})$$

$$A_\Lambda \approx -\tan(\delta_{1P} - \delta_{1S}) \sin(\phi_{1P} - \phi_{1S})$$

$\delta_{3S} = -18.7°$
$\delta_{3P} = -2.7°$
$\delta_{1S} = 6.0 \pm 1.0°$
$\delta_{1P} = -1.1 \pm 1.0°$

where 1 and 3 refer to the $\Delta I = 1/2$ and $\Delta I = 3/2$ amplitudes.

*

$\Lambda \to p\pi^-$

	$\beta + \bar{\beta}$	$\alpha + \bar{\alpha}$	$\frac{\Gamma - \bar{\Gamma}}{\Gamma + \bar{\Gamma}}$
KM	5×10^{-4}	-0.8×10^{-4}	-5.4×10^{-7}
Higgs	3×10^{-4}	-4×10^{-5}	-7.8×10^{-6}
Left-Right	1×10^{-4}	-1.4×10^{-5}	0

J. F. Donoghue (1986)

$\Xi^- \to \Lambda^0\pi^-$

	$\beta + \bar{\beta}$	$\alpha + \bar{\alpha}$	$\frac{\Gamma - \bar{\Gamma}}{\Gamma + \bar{\Gamma}}$
KM	2×10^{-4}	-0.7×10^{-4}	0
Higgs	1×10^{-3}	-3×10^{-4}	0
Left-Right	$-.6 \times 10^{-4}$	2×10^{-5}	0

Table I. Estimates of CP violating quantities in hyperon decay

*

He, Steger and Valencia (PL B272, 411 (1991))

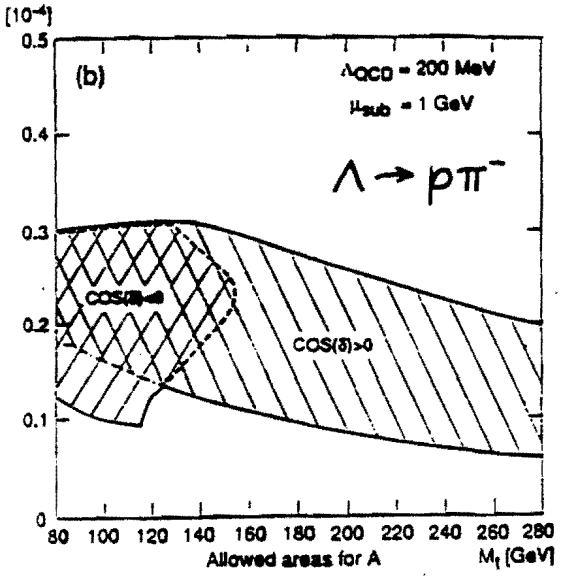

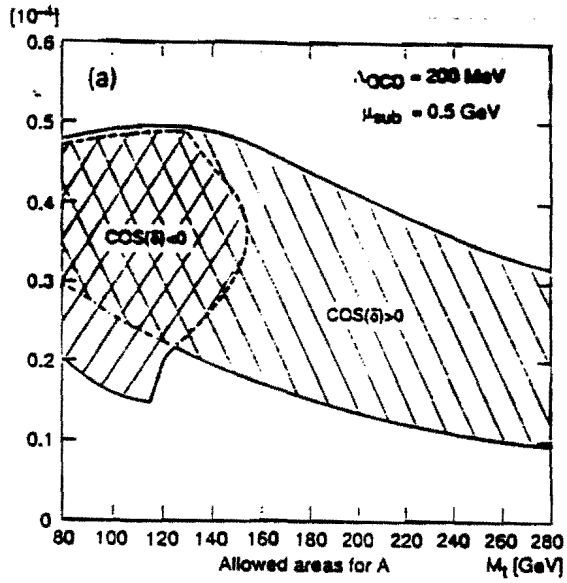

$A_\Xi \approx 2.5 \times 10^{-5}$ to 2.5×10^{-4}

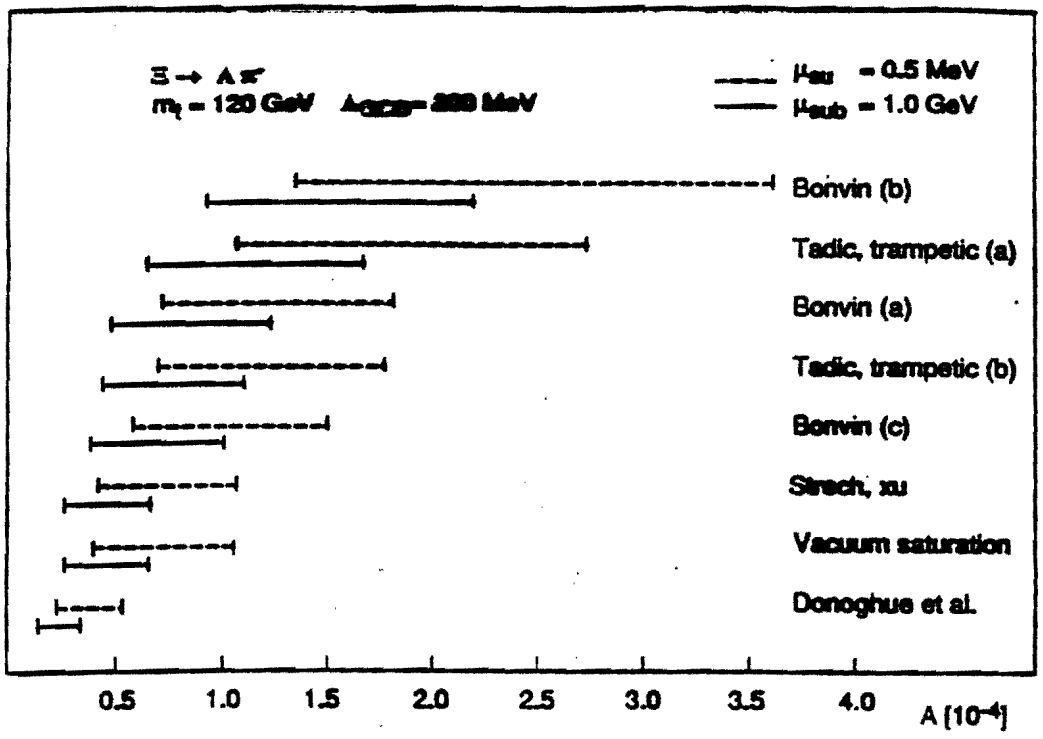

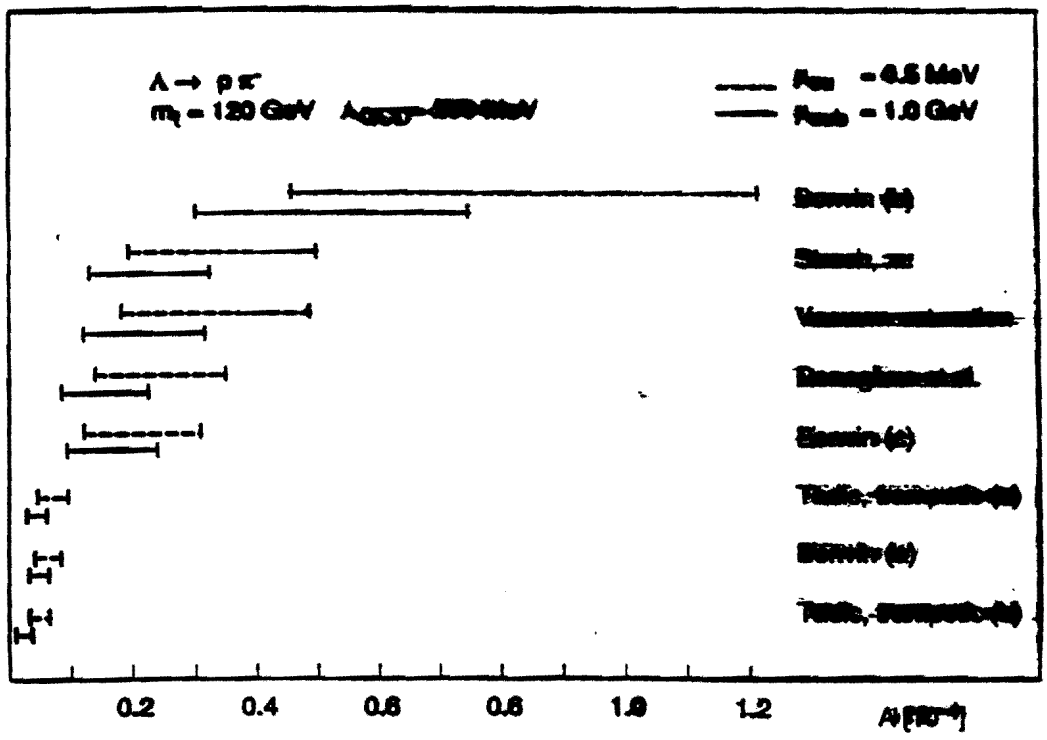

Figure 1: Standard Model predictions for (a) Ξ decay and (b) Λ decay.

The current experimental search for CP violations in hyperon decays:

$$\Lambda \rightarrow p\,\pi^-$$

$\Lambda\bar{\Lambda}$ pairs are produced in exclusive reactions.

$$A_\Lambda = -0.03 \pm 0.06$$

The only search for CP violation in Ξ decay through the sequence:

$$\Xi^- \rightarrow \Lambda\,\pi^- \quad \text{and} \quad \bar{\Xi}^+ \rightarrow \bar{\Lambda}\,\pi^+$$
$$\hookrightarrow p\,\pi^- \qquad\qquad\qquad\qquad \hookrightarrow \bar{p}\,\pi^+$$

comes from a test done in E756.

E756

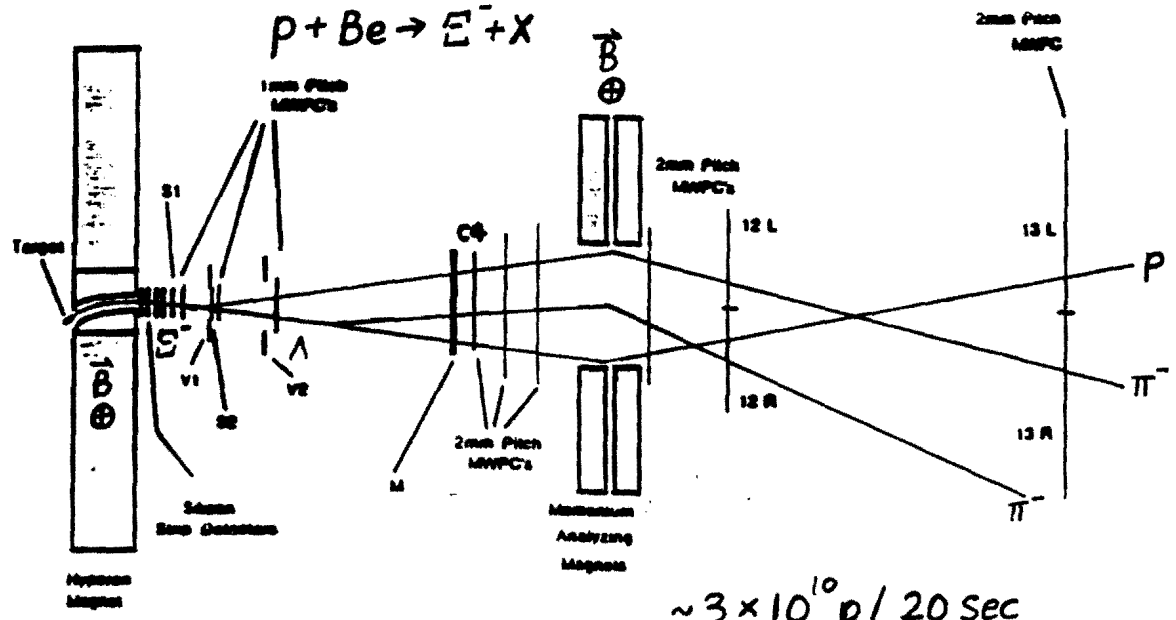

~ 3×10^{10} p / 20 sec

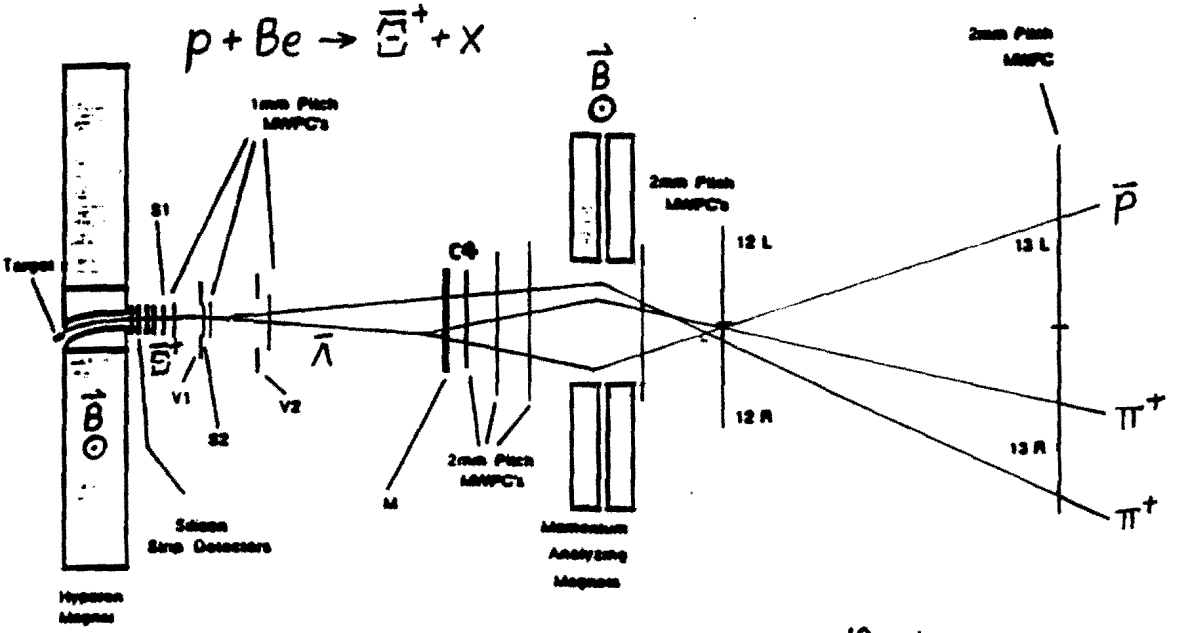

~ 1×10^{10} p / 20 sec

E756 spectrometer can't handle high rate

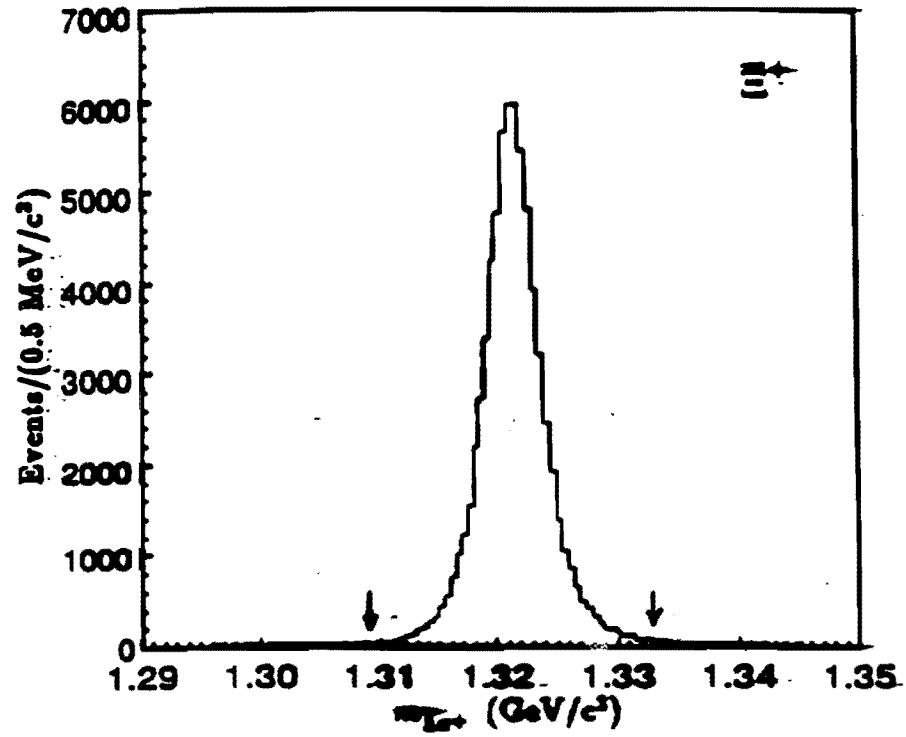
7000
6000
5000
4000
3000
2000
1000
0
Events/(0.5 MeV/c²)
1.29
1.30
1.31
1.32
1.33
1.34
1.35
(GeV/c²)

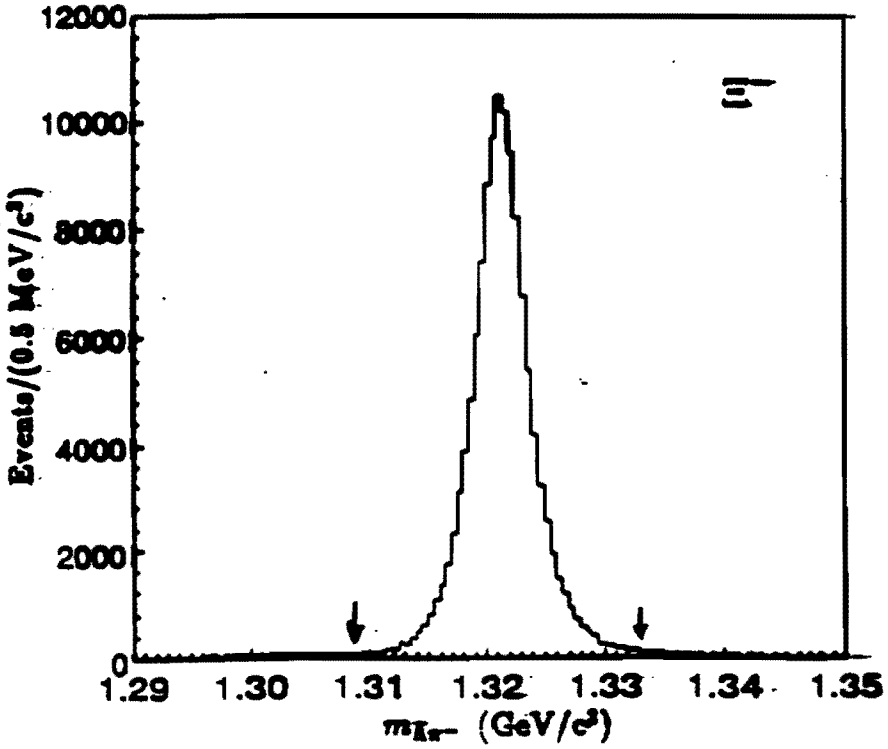
12000
10000
8000
6000
4000
2000
0
Events/(0.5 MeV/c²)
1.29
1.30
1.31
1.32
1.33
1.34
1.35
(GeV/c²)

Without any correction

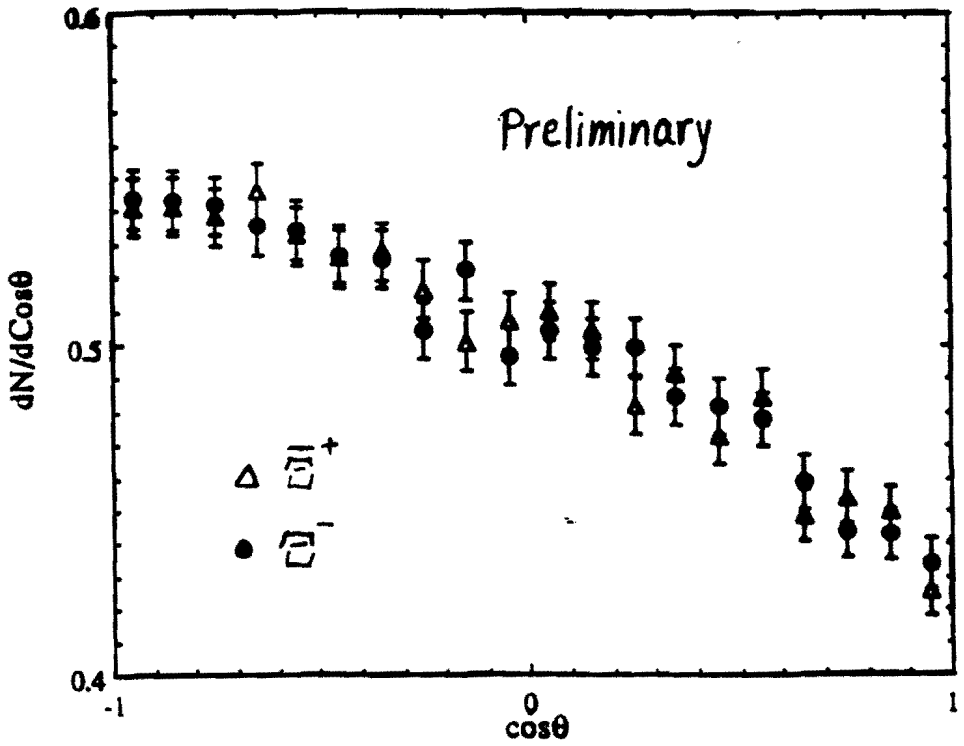

$$A = A_\Lambda + A_\Xi = 0.0017 \pm 0.015$$

P 871

Goal: Search for CP violation in charged Ξ and Λ decays with good sensitivity:

$$\delta(A_\Lambda + A_\Xi) = 10^{-4}$$

Need:

2×10^9 reconstructed $\bar{\Xi}^+ \rightarrow \bar{\Lambda}\, \pi^+$ events

& 2×10^9 reconstructed $\Xi^- \rightarrow \Lambda\, \pi^-$ events

assume 200 days of running with 50% duty factor, we need to get

1,400 $\Xi \rightarrow \Lambda\, \pi$; $\Lambda \rightarrow p\, \pi$ decays per spill-sec

to achieve our goal.

What Is Required?

- High Rate MWPC's
- Good CP Invariant Trigger
- High Rate DAQ
- Modern Offline Capability
- Control of Systematics to a part in 10,000

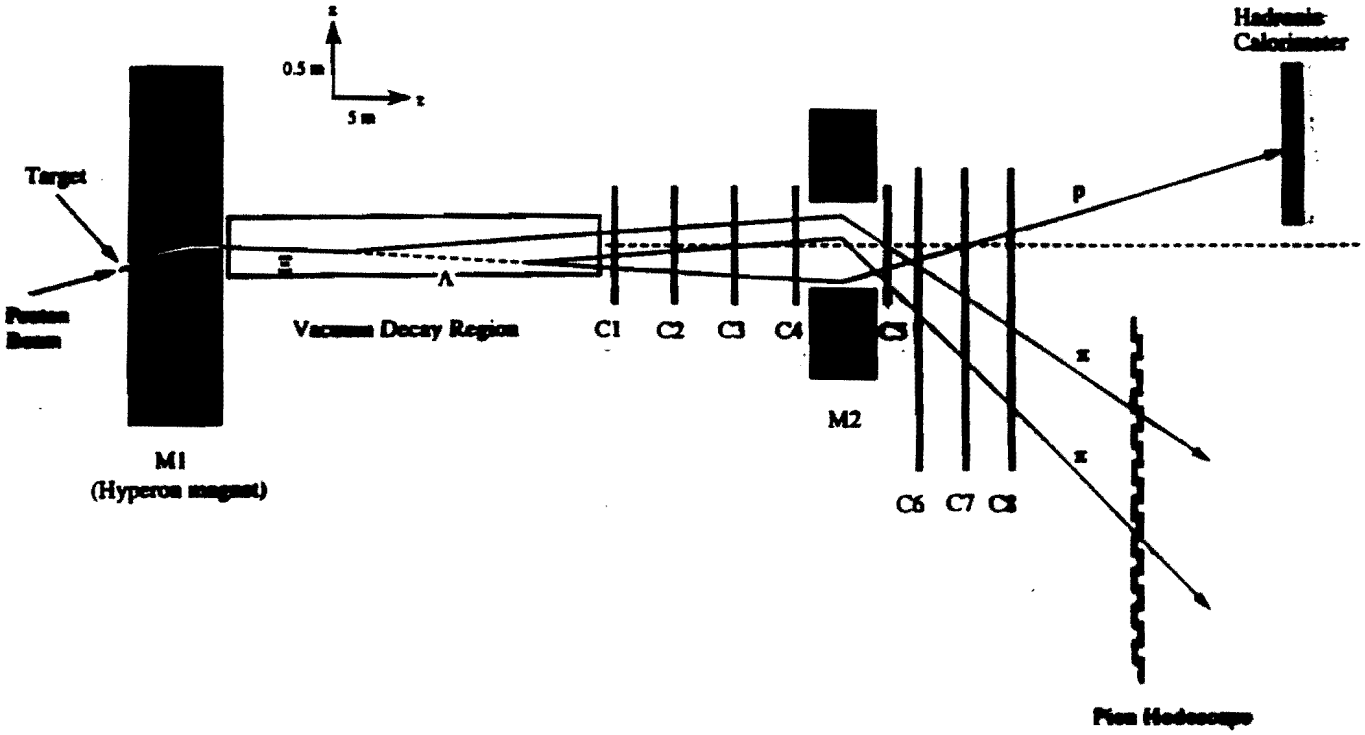
0.5 m
5 m
Target
Proton Beam
M1
(Hyperon magnet)
Vacuum Decay Region
C1
C2
C3
C4
C5
M2
C6
C7
C8
p
π
π
Hadronic Calorimeter
Pion Hodoscope

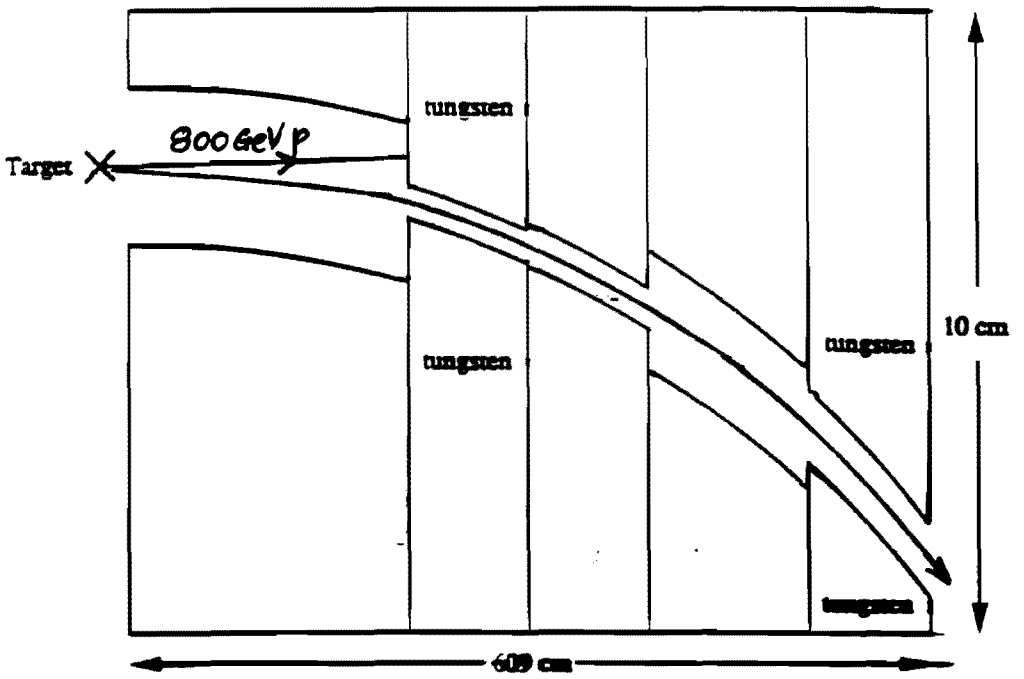

(a) Bend view

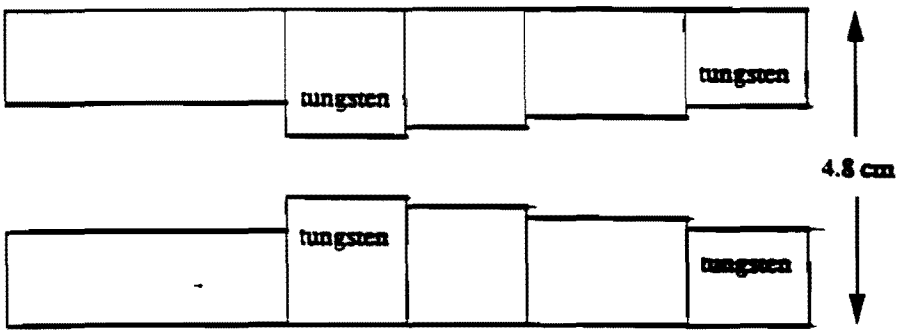

(b) Non-bend view

Solid angle, $\Delta\Omega = 4.88\ \mu$stero.

bend angle, $\theta_{bend} \doteq 22.6$ mrad

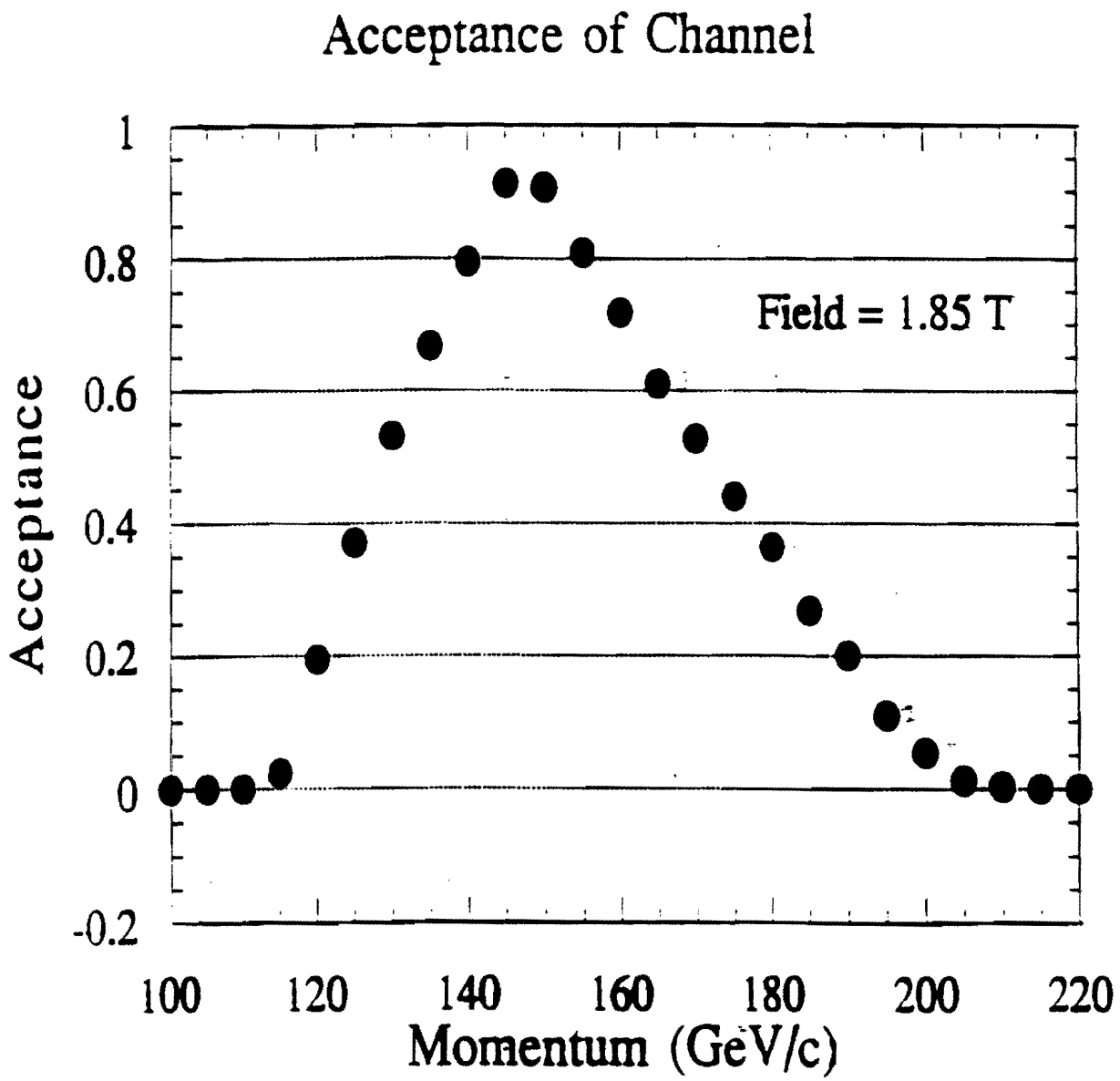

Figure 4: Hyperon channel acceptance.

Wire Chambers

Requirements:

- low mass
- high-rate capability: $4 \times 10^5/cm^2sec$
- redundancy
- modest size: 72×45 cm^2 in front; 200×60 cm^2 in rear.
- fast front end.

These requirements are comparable to those encountered by other experiments.

Solution:

- narrow wire spacing (1mm) MWPC's in front of magnet; 2mm spacing in rear.
- fast gas: 80% CF_4, 20% isobutane.
- anode-cathode gap of 3 mm.
- E771/E789 preamplifier.
- 20,000 total channels.

Front View

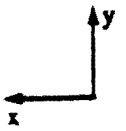

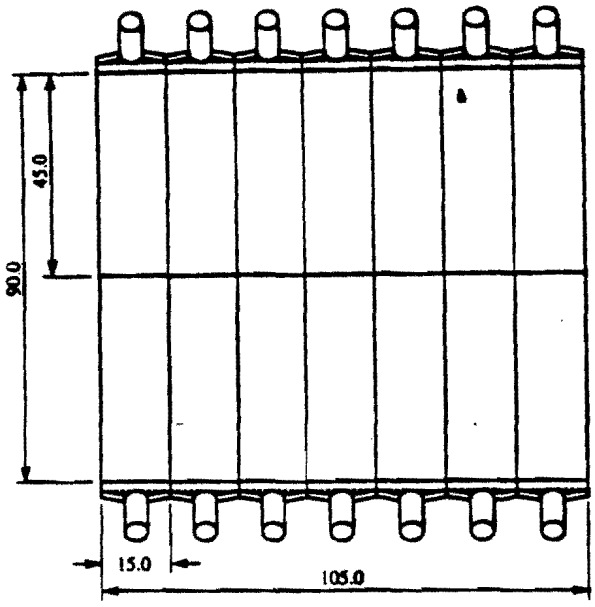

Side View

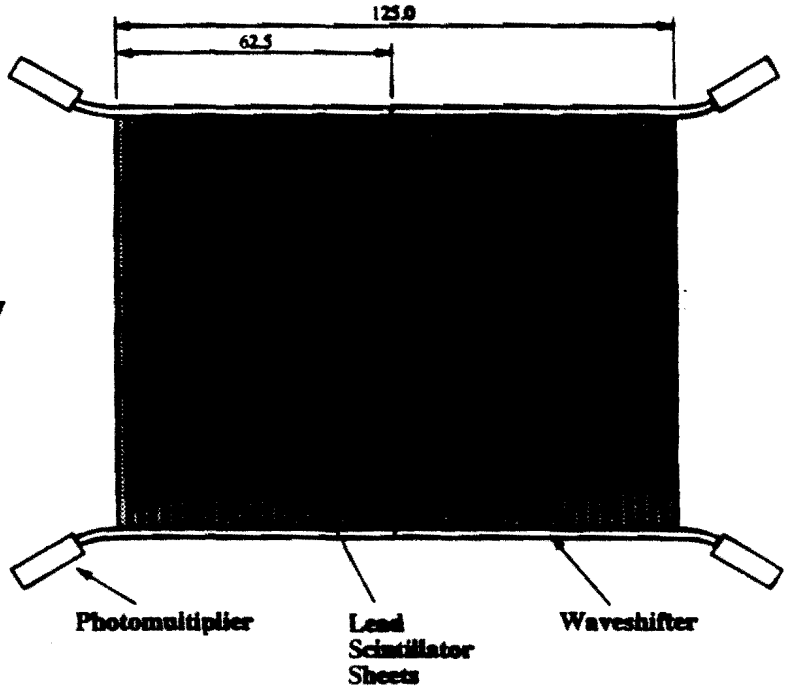

Hadronic Calorimeter

- Requirements: fast, good energy resolution, and uniform efficiency over its entire fiducical area.
- Does not need to be radiation hard or well segmented. Nor is calibration a problem.
- Small: 105 x 90 cm^2, 6 λ_I deep.
- Sampling calorimeter: 50 layers of 0.5 cm scintillator, 2.0 cm Pb (λ_I = 20.3 cm, X_0 = 0.7 cm).
- Segmentation: 7 x 2 x 2 (x,y,z), 28 channels.
- Hadronic energy resolution: $\sigma/E = 60\%/\sqrt{E}$.
- Electromagnetic energy resolution: $\sigma/E = 30\%/\sqrt{E}$.

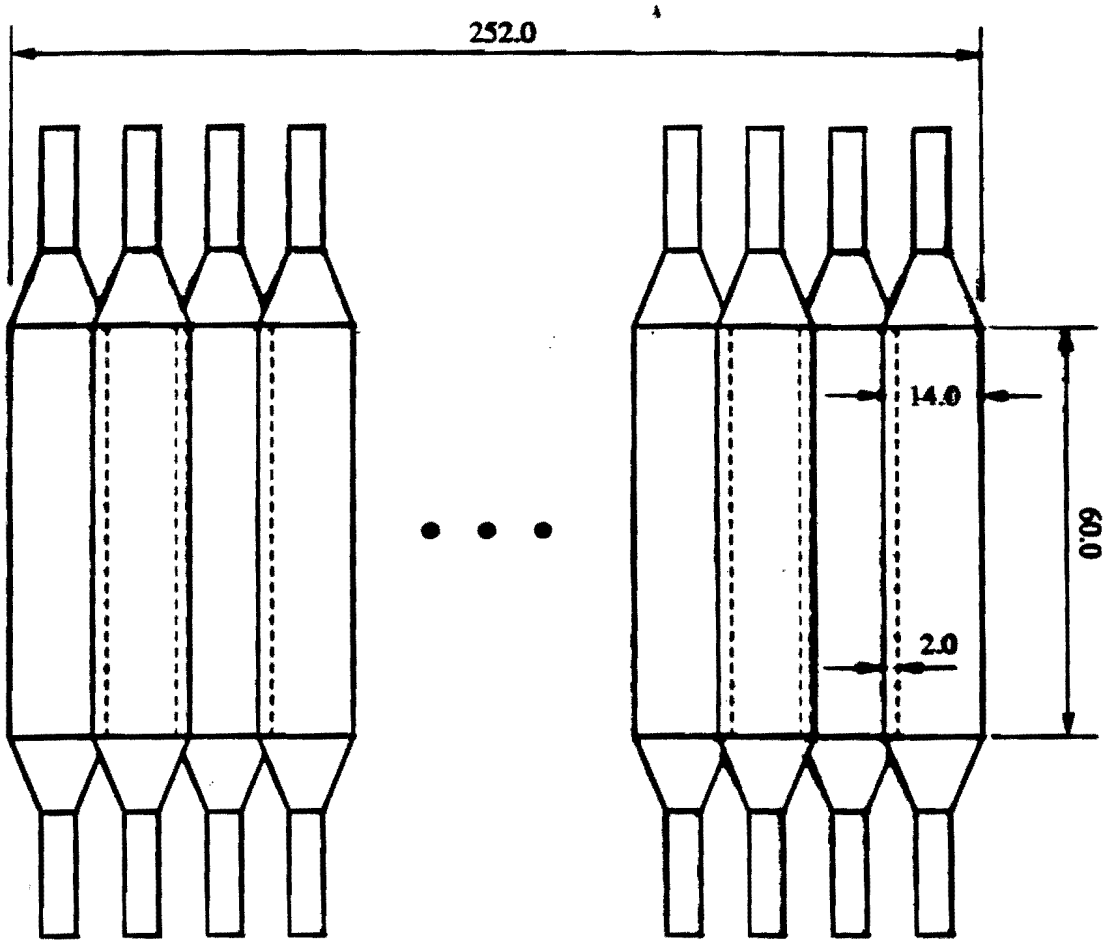
252.0
14.0
60.0
2.0

Yield Calculations

Reaction

$$p + Be \rightarrow Y + x$$

at 800 GeV and 0 mrad.

* Ξ yields are calculated based on Ξ/π ratios measured at CERN and at Fermilab.

* π, K and p yields are calculated with the parametrizations used at Fermilab for designing ν beams.

Ξ, π, K, and p yields per 10^{10} protons.

Particle	At target[1]	At exit of channel[2]
Positive Beam		
Ξ^+	6.5×10^4	8.5×10^3
π^+	6.5×10^7	2.7×10^7
K^+	6.5×10^6	2.7×10^6
p	3.2×10^7	1.3×10^7
Total:	1.0×10^8	4.3×10^7
Negative Beam		
Ξ^-	1.1×10^5	1.5×10^4
π^-	3.6×10^7	1.5×10^7
K^-	2.9×10^6	1.2×10^6
Total:	3.9×10^7	1.6×10^7

Ξ^- and $\bar{\Xi}^+$ acceptance and yields per 10^{10} protons.

	Ξ^-	$\bar{\Xi}^+$
Total entering collimator:	110,000	65,000
Total exiting collimator:	15,000	8,500
BR ($\Xi^- \to \Lambda^\circ\pi^-$)	1.00	1.00
BR ($\Lambda^\circ \to p\pi^-$)	0.641	0.641
Ξ & Λ decaying in vacuum region	0.84	0.84
Geometric acceptance	0.79	0.79
Trigger acceptance	0.88	0.88
Reconstruction efficiency	0.87	0.87
Software event selection cuts	0.88	0.88
Total events passing all cuts:	2,650	1,500

$\epsilon = 0.17$

With 10^{10} protons/s on target,

~1,500 $\bar{\Xi}^+ \to \bar{\Lambda}\,\pi^+$ events/s

~2,650 $\Xi^- \to \Lambda\,\pi^-$ events/s

Comparison of P871 and E756 $\bar{\Xi}^+$ Yields.

	E756	P871	Gain
Run time	8 days	100 days	12.5
Channel solid angle	2.36 μsr	4.88 μsr	2
$< x_F >$	0.4	0.2	7
$< p_T >$	0.75 GeV/c	0.0 GeV/c	7
Proton intensity	1×10^{10}	2×10^{11}	20
Lifetime	0.5	0.6	1.2
Total:			29,400

μ fluence determined in E756

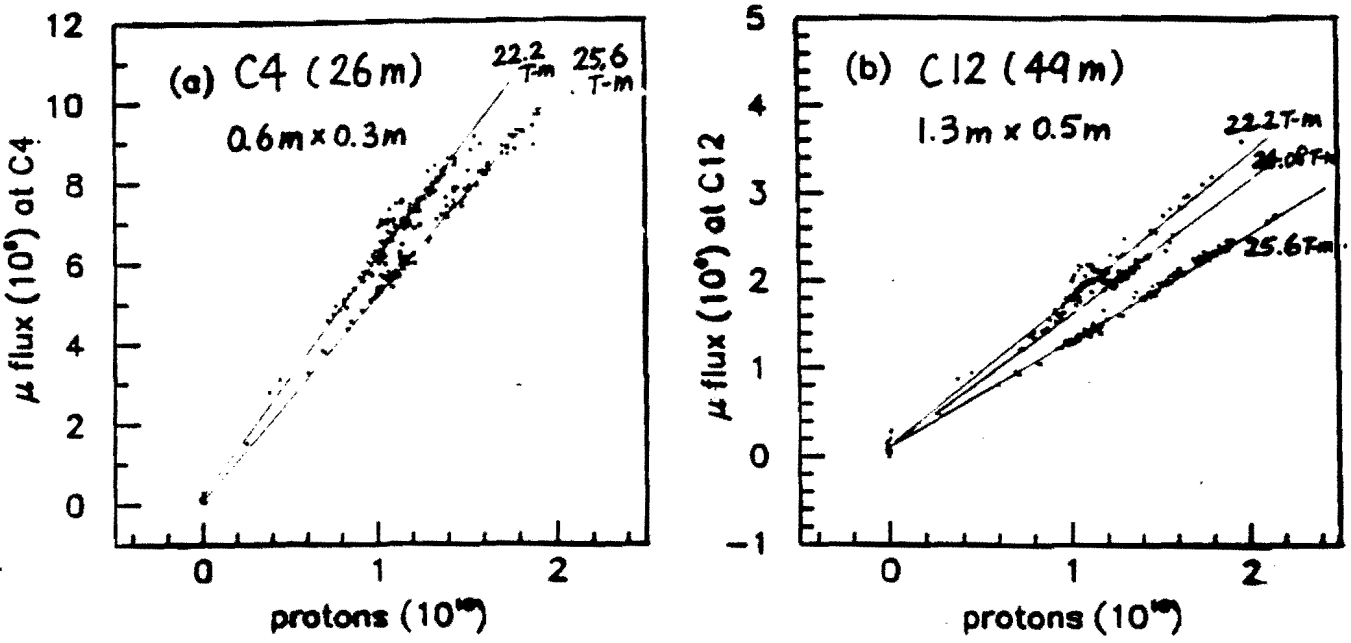

p + Be @ 0 mrad

* agree with measurements done with a scintillator telescope in E756 by E761 colleagues
* extrapolated μ fluence expected in P871

$\sim 7 \times 10^6 \mu / 10^{10}$ protons @ 26m

$\sim 2 \times 10^6 \mu / 10^{10}$ protons @ 50m

can be reduced by more shielding

Trigger Rate:

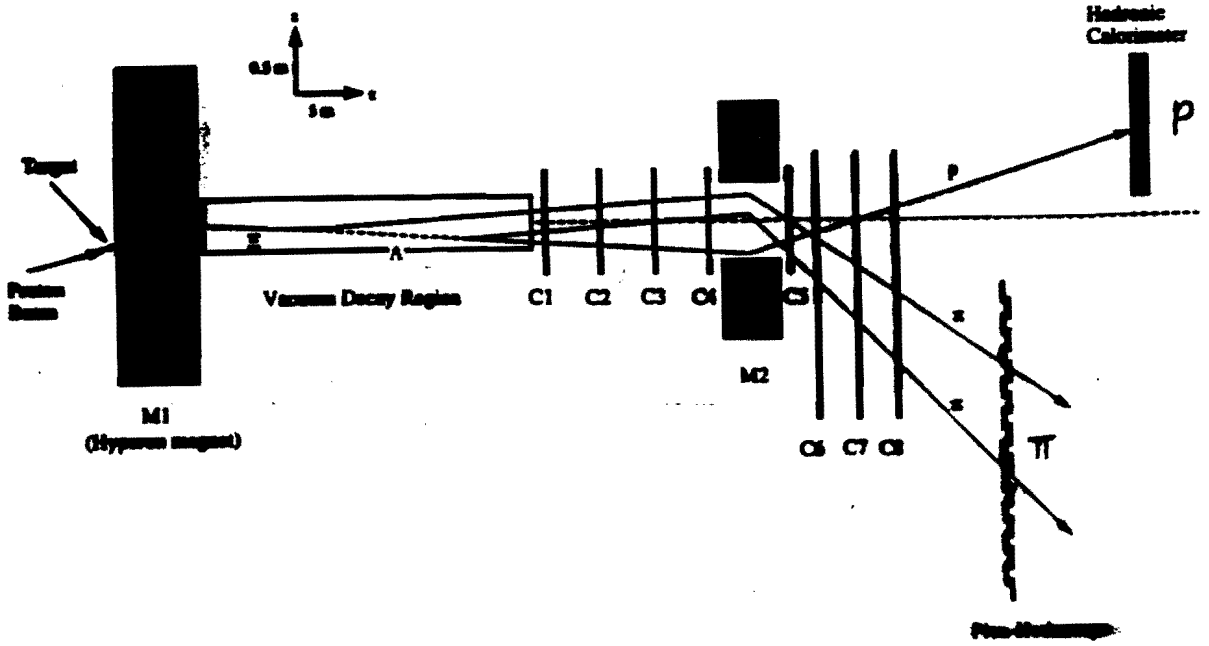

	Beam Particle	Ξ^+
@ exit	4.3 MHz	8.5 kHz
1% interact	430 kHz	
p·π trigger	< 30 kHz	2.2 kHz

Total trigger rate < 35 kHz, including triggers due to μ satisfying the calorimeter energy requirement along with accidentals.

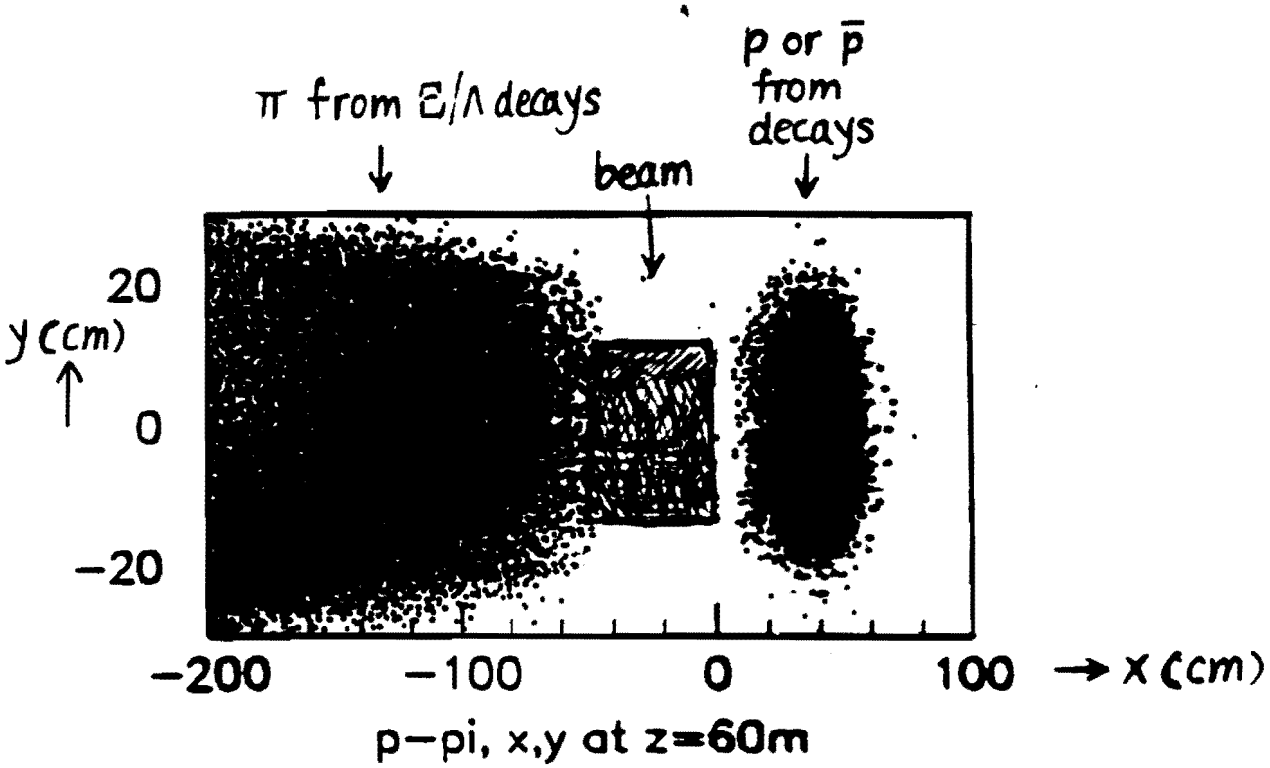
π from Ξ/Λ decays
p or p̄ from decays
beam
20
y (cm)
0
−20
−200
−100
0
100
x (cm)
p−pi, x,y at z=60m

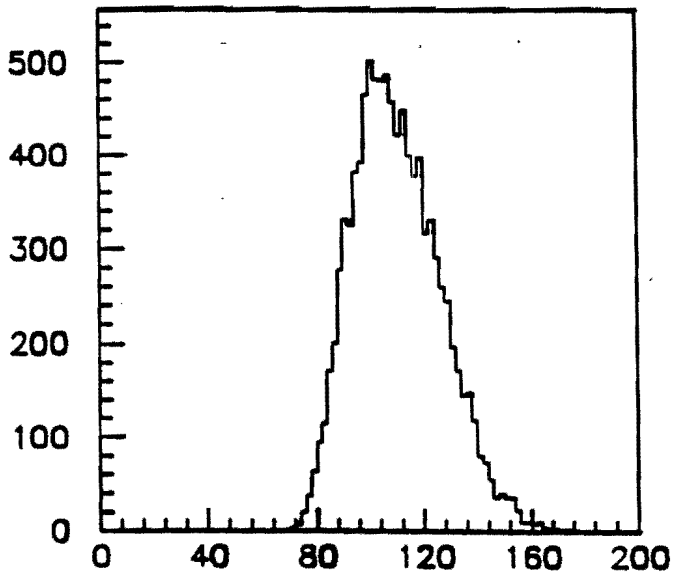

The proton momentum from Λ decays. The momentum is in GeV/c.

[redacted] DATE 15/10/93 [redacted]

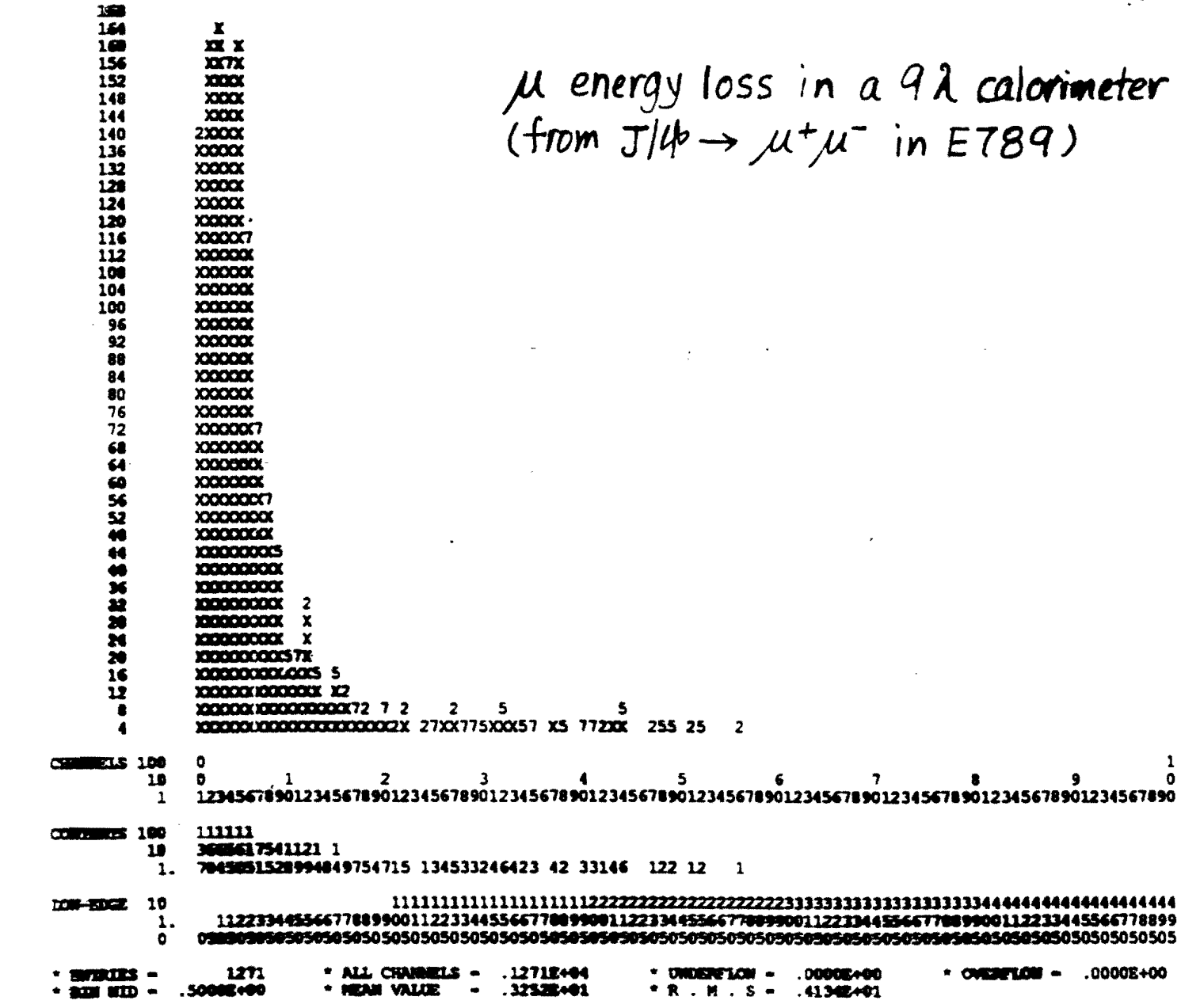

CHANNELS 100 0 1
10 0 1 2 3 4 5 6 7 8 9 0
1 1234567890123456789012345678901234567890123456789012345678901234567890123456789012345678901234567890

CONTENTS 100 111111
10 [redacted]
1. [redacted]

DON-EDGE 10 1111111111111111111122222222222222222222233333333333333333334444444444444444444
1. 1122334455667788990011223344556677889900112233445566778899001122334455667788990011223344556677889900
0 [redacted]

* ENTRIES = 1271 * ALL CHANNELS = .1271E+04 * UNDERFLOW = .0000E+00 * OVERFLOW = .0000E+00
* SUM MID = .5000E+00 * MEAN VALUE = .3252E+01 * R . M . S = .4134E+01

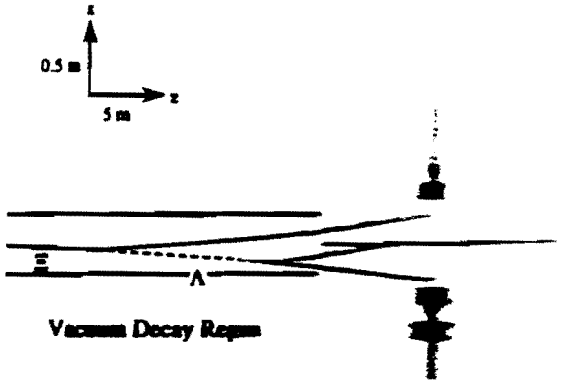

a)

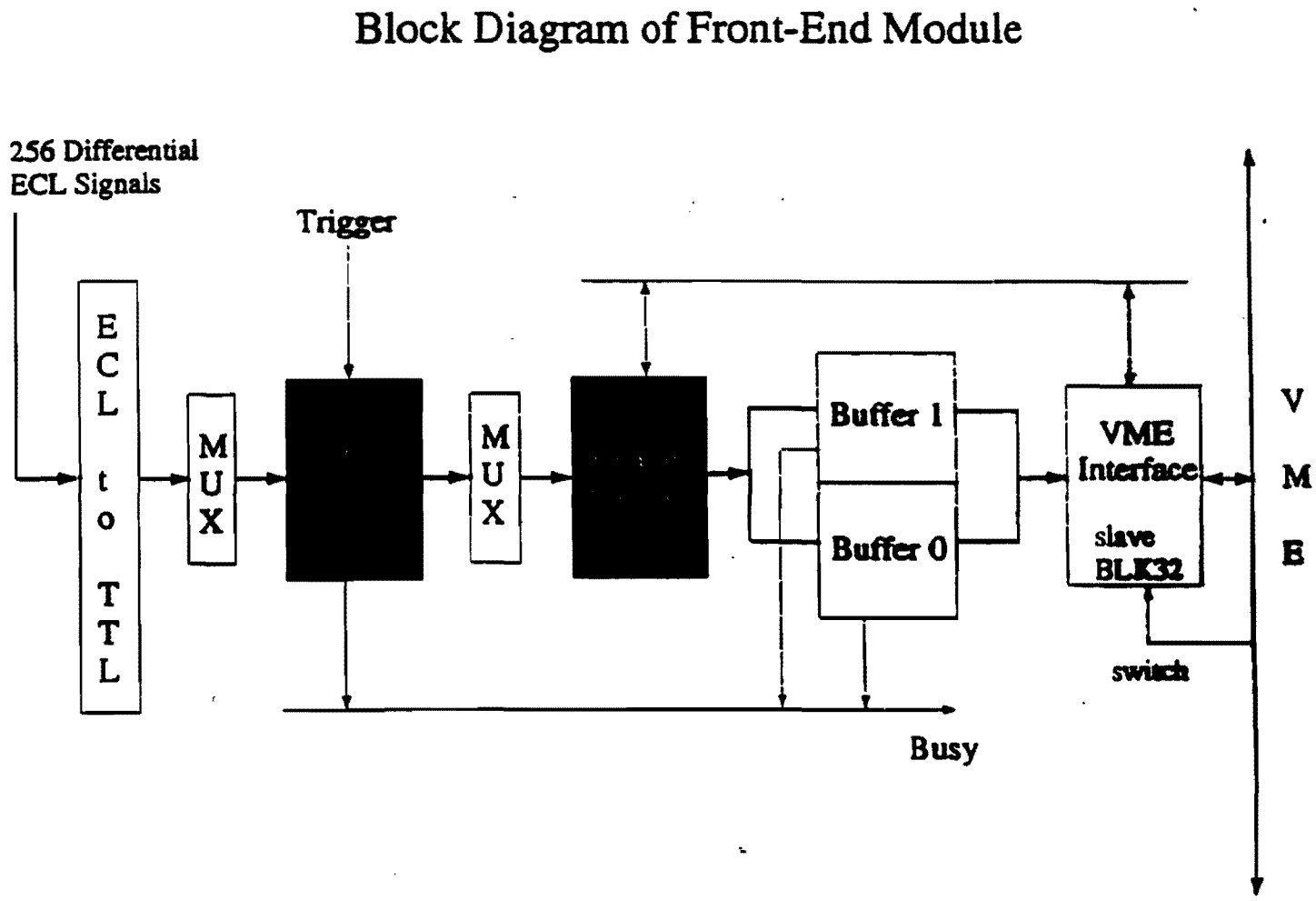

Figure 12: Block diagram of a front-end module.

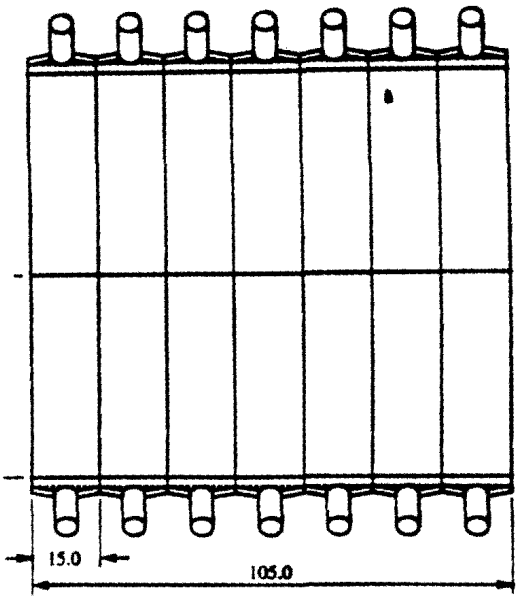
15.0
105.0

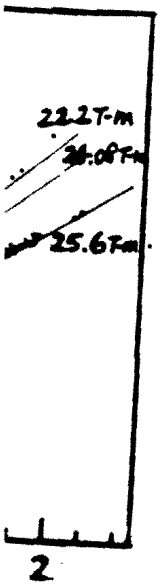
22.2T-m
25.6T-m
2

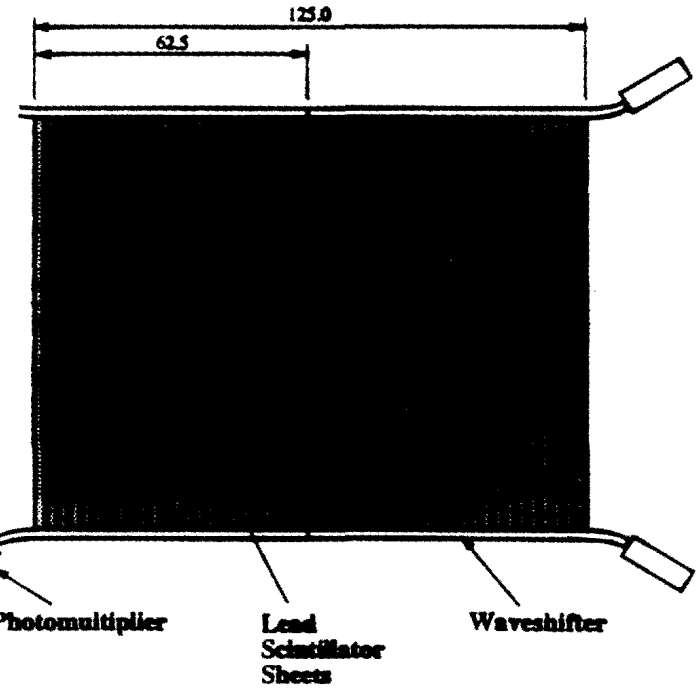
125.0
62.5
Photomultiplier
Lead
Scintillator
Sheets
Waveshifter

lator

Estimated Costs.

	New Equipment	Available Equipment and Labour
Beam line equipment and setup costs	—	[illegible]
Hyperon magnet	—	[illegible]
Hyperon channel	$ 50K	—
Evacuated decay pipe	—	$ 10K
Installation of analysis magnet	—	$ 10K
Portacamp facility	—	$ 50K
Mechanical and electrical support	—	$ 50K
Electronics from PREP	—	$200K
Terminals and network hookups	—	$ 20K
DAQ system	$200K	—
Wire chamber fabrication and testing	$200K	—
Cables for chamber readout	$100K	—
Chamber readout electronics	$800K	—
Scintillators and associated electronics	$ 30K	—
8mm tapes	$ 50K	—
Offline computers and peripherals	$100K	—
Hadronic calorimeter	$100K	—
Total cost:	$1,630K	$640K

[redacted] ID= [redacted] DATE 15/10/93 .NO= 11


```
      168
      164          X
      160         XX X
      156         XX7X
      152         XXXX
      148         XXXX
      144         XXXX
      140        2XXXX
      136        XXXXX
      132        XXXXX
      128        XXXXX
      124        XXXXX
      120        XXXXX
      116        XXXXX7
      112        XXXXXX
      108        XXXXXX
      104        XXXXXX
      100        XXXXXX
       96        XXXXXX
       92        XXXXXX
       88        XXXXXX
       84        XXXXXX
       80        XXXXXX
       76        XXXXXX
       72        XXXXXX7
       68        XXXXXXX
       64        XXXXXXX
       60        XXXXXXX
       56        XXXXXXX7
       52        XXXXXXXX
       48        XXXXXXXX
       44        XXXXXXXX5
       40        XXXXXXXXX
       36        XXXXXXXXX
       32        XXXXXXXXX  2
       28        XXXXXXXXX  X
       24        XXXXXXXXX  X
       20        XXXXXXXXX57X
       16        XXXXXXXXXXXX5 5
       12        XXXXXXXXXXXXX X2
        8        XXXXXXXXXXXXXXXX72 7 2    2    5          5
        4        XXXXXXXXXXXXXXXXXXXXX2X 27XX775XXX57 X5 77ZXX  255 25   2

CHANNELS 100    0                                                                                                   1
         10     0        1         2         3         4         5         6         7         8         9          0
          1     12345678901234567890123456789012345678901234567890123456789012345678901234567890123456789012345678901234567890

CHANNELS 100    111111
         10     3685617541121 1
          1.    7045851528994849754715 134533246423 42 33146  122 12   1

DON-EDGE  10                          1111111111111111111112222222222222222222223333333333333333333344444444444444444444
          1.     11223344556677889900112233445566778899001122334455667788990011223344556677889900112233445566778899
          0     0202020505050505050505050505050505050505050505050505050505050505050505050505050505050505050505050505
```

* ENTRIES = 1271 * ALL CHANNELS = .1271E+04 * UNDERFLOW = .0000E+00 * OVERFLOW = .0000E+00
* BIN MID = .5000E+00 * MEAN VALUE = .3253E+01 * R . M . S = .4134E+01

How can we address the differences in polarization and acceptance?

Consider two samples of $\bar{\Xi}^{+}$'s prepared under different conditions,

Sample 1:

$$n_1 = \frac{dN_1}{d\cos\theta} = \frac{A_1}{2}(1+\alpha_\Lambda \alpha_{\bar{\Xi}} \cos\theta)$$

Sample 2:

$$n_2 = \frac{dN_2}{d\cos\theta} = \frac{A_2}{2}(1+\alpha_\Lambda \alpha_{\bar{\Xi}} \cos\theta)$$

Take the ratio,

$$R = \frac{n_1}{n_2} = \frac{A_1}{A_2}$$

Express $R = a + b\cos\theta$

if $A_1 = A_2$, $b = 0$., and $a = 1$.

Offline Computing Needs:

Total number of triggers = 1.3×10^{11}

Total number of 20 Gb 8 mm tapes = 2,700

CPU time/event on a HP-735 = 3 ms

Total CPU time = 700 SpecInt92-year

With a cluster of 20 HP-735 workstations (76 SpecInt92 each) can process the entire data set in one calendar year.

CPU time/Monte Carlo event = 10 ms

Monte Carlo studies will require comparable amounts of computing power.

Based on 1.4 x 10^7 $\Xi^- \to \Lambda \pi^-$ decays from E756,

$< p_{+\theta} >^1$	$< p_{-\theta} >^2$	Δp (GeV/c) ^{3}	ΔP_Ξ ^{4}	b	χ^2/DOF
317.665	319.066	-1.40	0.23	-0.0017 ± 0.0027	1.02
318.739	319.342	-0.60	0.25	$+0.0023 \pm 0.0029$	0.90
385.484	383.453	2.03	0.26	-0.0016 ± 0.0017	1.20
427.339	425.845	1.49	0.28	-0.0030 ± 0.0024	0.74
458.834	454.323	4.51	0.29	-0.0063 ± 0.0047	0.93
478.983	478.419	0.56	0.25	-0.0125 ± 0.0044	1.03

Combined $b = 0.00025 \pm 0.00104$

The cosθ acceptance of proton w.r.t. $\hat{\Lambda}$ is insensitive to polarization difference and acceptance difference in the lab.

What are the potential systematic problems ?

1. Difference in Polarization

2. Difference in Spectrometer acceptance (beam, target, magnets)

3. Difference in interaction cross sections between particles and antiparticles

4. Difference in reconstruction of hyperons and antihyperons

5. Difference in backgrounds under the Λ-π invariant mass peak

.

.

Problem of Secondary Interactions in the Spectrometer

p and $\bar{p}$, as well as π^- and π^+, interact differently in matter. This may cause a difference in the cosθ dependence of the reconstruction efficiency.

Detailed simulation of the effects of secondary interactions is in progress:

$$\Xi^- \rightarrow \Lambda\, \pi^- \quad \hookrightarrow p\, \pi^- \qquad \text{and} \qquad \bar{\Xi}^+ \rightarrow \bar{\Lambda}\, \pi^+ \quad \hookrightarrow \bar{p}\, \pi^+$$

events are generated with the P871 Monte Carlo. Secondary interactions of the p and $\bar{p}$ with material in the spectrometer are simulated using PYTHIA.

* Events are reconstructed using the E756 tracking program.

* With 5×10^6 generated events, each having a secondary interaction (equivalent to 5×10^8 events with 1% interaction probability), no statistically significant difference between the p and $\bar{p}$ cosθ distributions has been observed.

* Further studies are in progress.

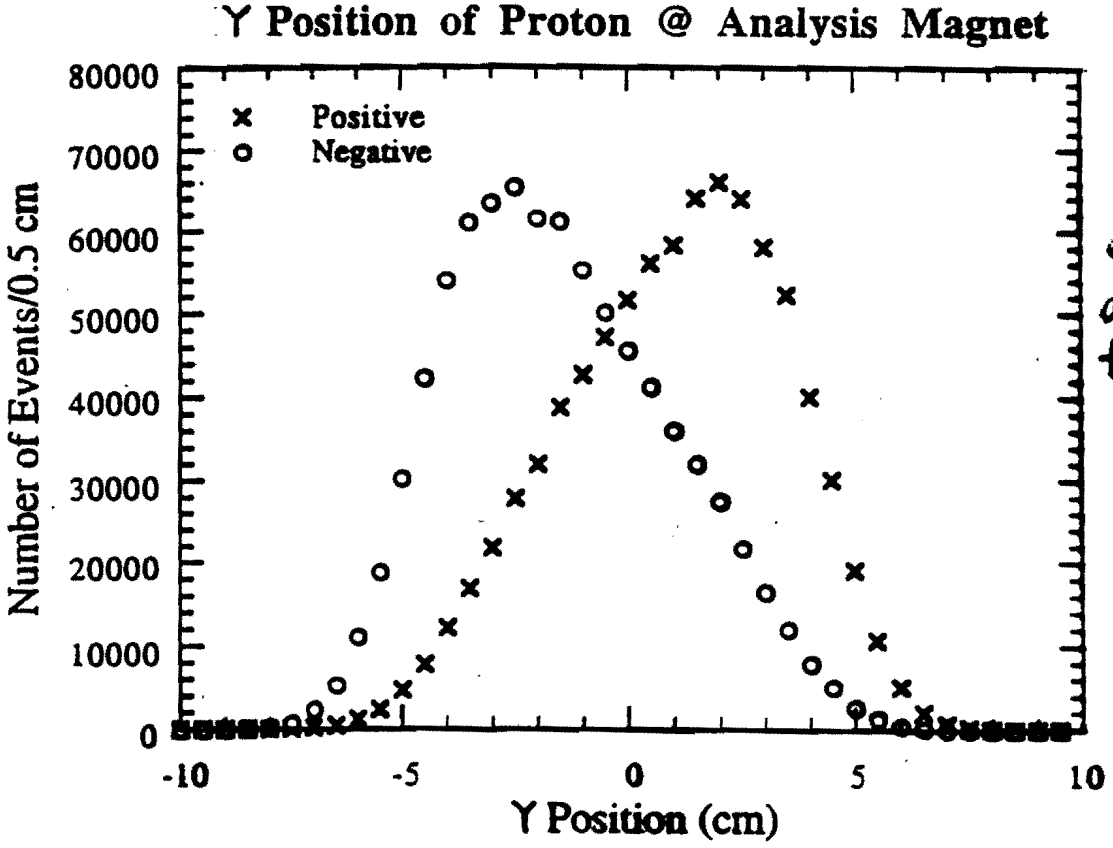

due to difference in targeting angle

$p + Be \rightarrow \Xi^- + X$

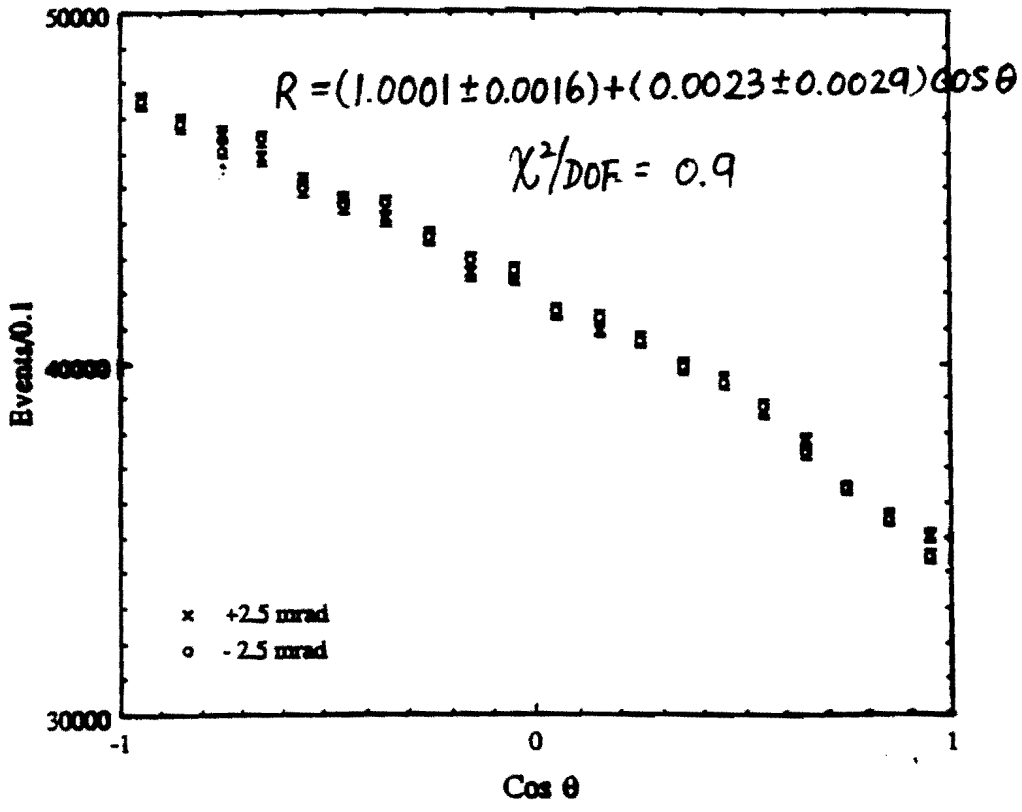

E756 data

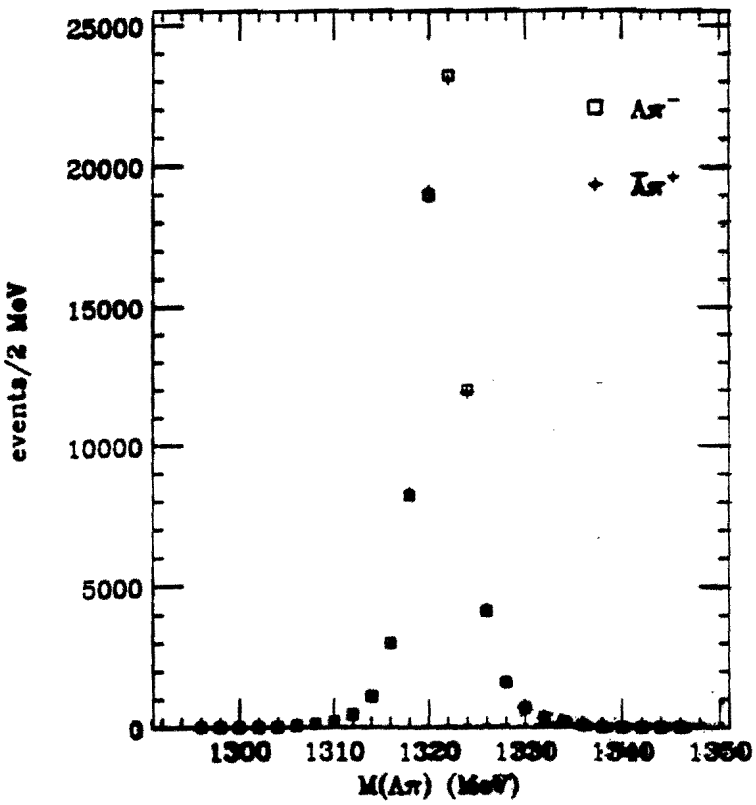

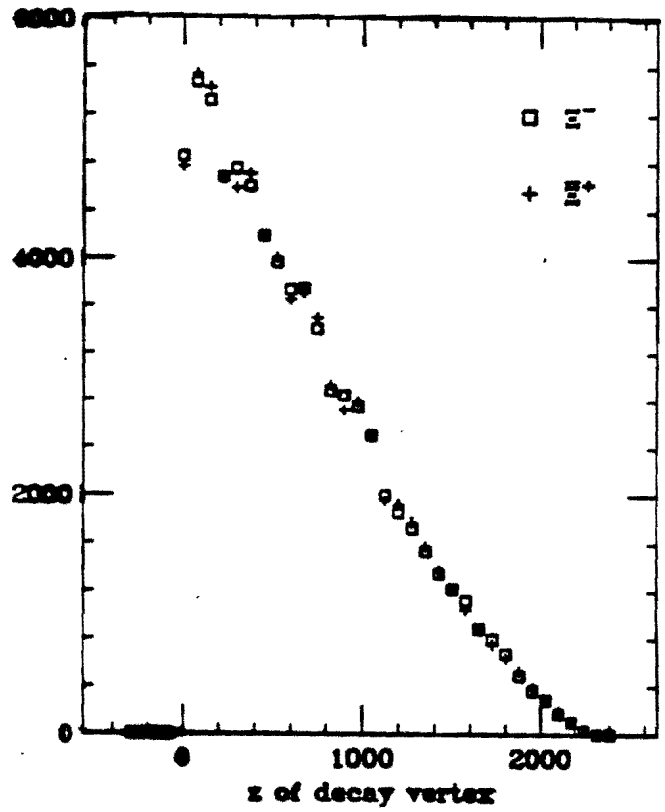

Reconstruction program does not bias Ξ^- or $\bar{\Xi}^+$ decays

Reconstructed $\bar{\Xi}$ events with interactions

$\bar{\Xi}^+$

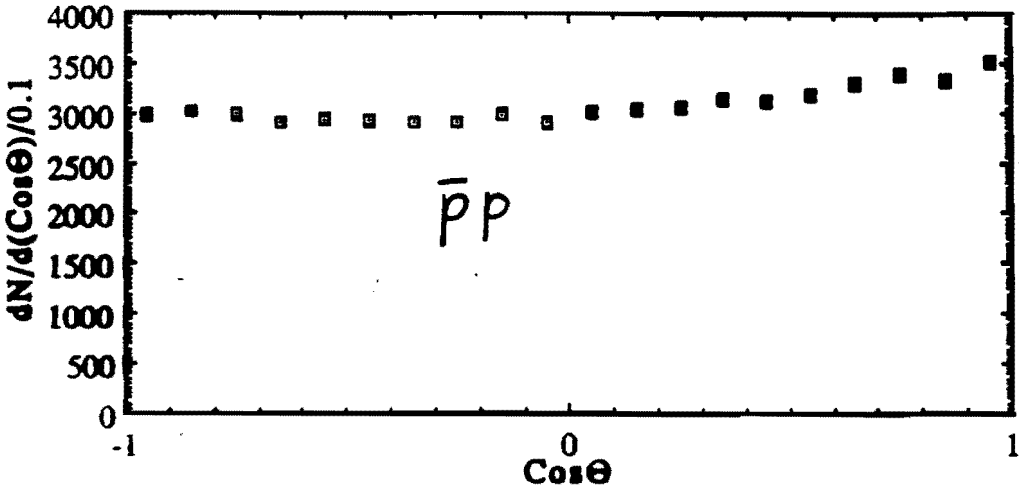

Ξ^-

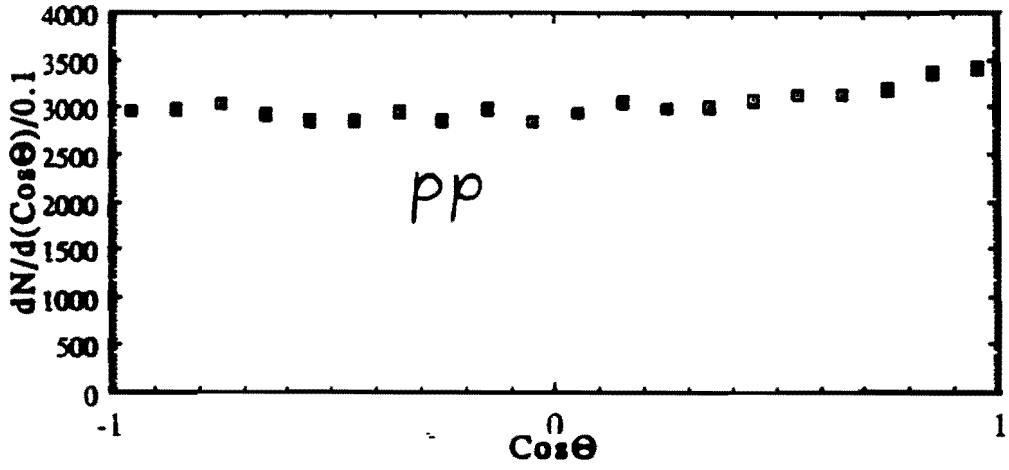

This implies a sensitivity of

$(2.9 \pm 1.7) \times 10^{-4}$

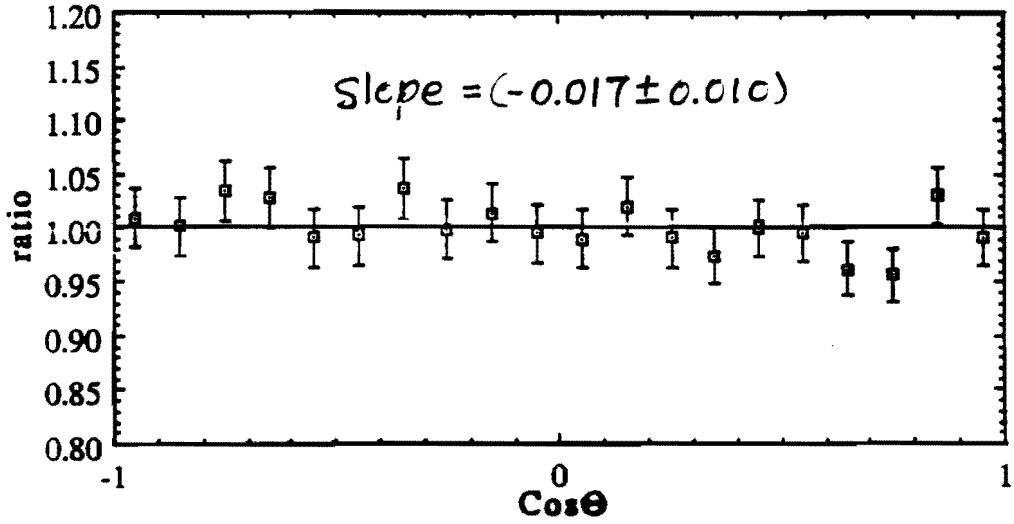

*** COMPARAISON 1 *** XISQR: 80.15 NDF: 19 XISQR/NDF: 4.218

COEF: .1140E+01

PLOT 173 EVTS (X): 835082 PLOT 176 EVTS (0): 732397.0

NORMALIZATION: 835084

BIN	BIN VALUE	XISQR	X	O	* COS(PROTON,PAKET) IN PAS DE 551
1	-1.00	1.585	35886	35442	.
2	-.900	14.019	39859	38872	.
3	-.800	1.134	41304	40980	.
4	-.700	.369	42567	42364	.
5	-.600	1.213	43148	42814	.
6	-.500	1.387	43618	43259	.
7	-.400	1.829	43790	43377	.
8	-.300	.118	43855	43750	.
9	-.200	.140	43428	43314	.
10	-.100E+00	10.695	43694	42700	.
11	.000E+00	2.214	43164	42713	.
12	.100	.604	43649	43312	.
13	.200	.203	43825	43687	.
14	.300	3.040	43542	44076	.
15	.400	.347	43804	43664	.
16	.500	1.606	42472	42855	.
17	.600	4.941	41717	42304	.
18	.700	17.406	40088	41320	.
19	.800	1.031	38754	39047	.
20	.900	16.265	34048	35166	.

$$\cos\theta_x = (\hat{x} \times \hat{\Lambda}) \cdot \hat{f}$$

*** COMPARAISON 2 *** XISQR: 224.55 NDF: 19 XISQR/NDF: 11.819

COEF: .1140E+01

PLOT 173 EVTS (X): 835081 PLOT 176 EVTS (0): 732397.0

NORMALIZATION: 835078

BIN	BIN VALUE	XISQR	X	O	* COS(PROTON,PAKET) IN PAS DE 549
1	-1.00	29.855	35396	36917	.
2	-.900	37.595	38736	40523	.
3	-.800	12.533	40855	41909	.
4	-.700	17.509	41563	42821	.
5	-.600	9.234	42338	43258	.
6	-.500	.217	42694	42835	.
7	-.400	10.895	42611	43614	.
8	-.300	1.171	42999	43328	.
9	-.200	.843	43302	43023	.
10	-.100E+00	.017	43121	43081	.
11	.000E+00	.133	43099	43210	.
12	.100	1.452	43313	42947	.
13	.200	.016	43052	43014	.
14	.300	5.329	43334	42634	.
15	.400	10.868	43873	42869	.
16	.500	2.003	43155	42726	.
17	.600	20.507	42992	41630	.
18	.700	11.978	42096	41064	.
19	.800	20.796	39971	38649	.
20	.900	31.601	36581	35026	.

$$\cos\theta_y = (\hat{y} \times \hat{\Lambda}) \cdot \hat{f}$$

*** COMPARAISON 3 *** XISQR: 14.04 NDF: 19 XISQR/NDF: .739

COEF: .1140E+01

PLOT 173 EVTS (X): 835082 PLOT 176 EVTS (0): 732397.0

NORMALIZATION: 835084

BIN	BIN VALUE	XISQR	X	O	* COS(PROTON,PAKET) IN PAS DE 623
1	-1.00	.108	49472	49579	.
2	-.900	1.549	48868	48868	.
3	-.800	.033	46659	46716	.
4	-.700	.009	44479	44458	.
5	-.600	.041	42623	42562	.
6	-.500	.458	40868	40269	.
7	-.400	.002	38809	38877	.
8	-.300	.213	36977	37107	.
9	-.200	.003	35669	35684	.
10	-.100E+00	.322	34346	34500	.
11	.000E+00	.207	34015	34691	.
12	.100	2.508	35676	36115	.
13	.200	.901	36806	37113	.
14	.300	.361	38219	38391	.
15	.400	.459	40167	40366	.
16	.500	1.730	42783	42386	.
17	.600	.944	44366	44666	.
18	.700	.514	46584	46358	.
19	.800	3.325	48410	47825	.
20	.900	.358	49566	49761	.

$$\cos\theta_z = (\hat{z} \times \hat{\Lambda}) \cdot \hat{f}$$

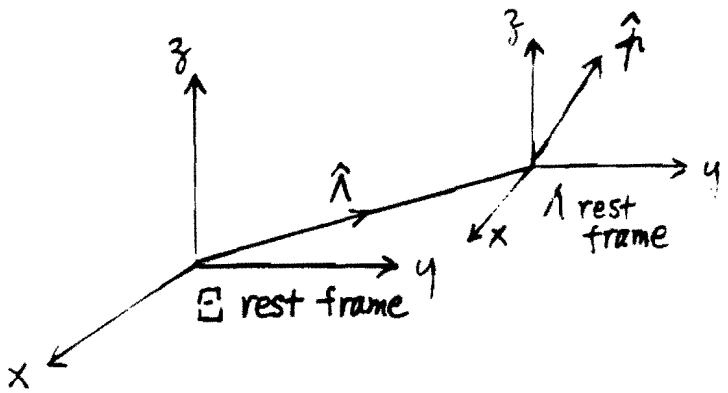

Conclusions

- After 30 years of experimental effort, the origin of CP violation remains unknown.
- In particular, despite an impressive amount of experimental effort, 1) no experiment has seen CP violation outside of the neutral kaon system, and 2) there is no compelling evidence for direct CP violation.
- P871 addresses both of these important experimental questions in a very cost effective manner.

"We must continue to seek the origin of the CP symmetry violation by all means at our disposal. We know that improvements in detector technology and quality of accelerators will permit even more sensitive experiments in the coming decades. We are hopeful, then, that at some epoch, perhaps distant, this cryptic message from nature will be deciphered."

J. Cronin, 1981

Fermilab Proposal P-871
Revised Version

Search for CP Violation in the Decays of $\Xi^-/\overline{\Xi}^+$ and $\Lambda/\overline{\Lambda}$ Hyperons

J. Antos, Y.C. Chen, C.N. Chiou, C. Ho, A. Sumarokov, and P.K. Teng
Academia Sinica, Nankang, Taipei 11529, Taiwan, Republic of China

M. Botlo
Brookhaven National Laboratory, Upton, NY 11973, USA

G. Abrams, C. Ballagh, H. Bingham, D. Chapman, G. Gidal, P.M. Ho, K.B. Luk[1], and J. Lys
Lawrence Berkeley Laboratory and University of California, Berkeley, CA 94720, USA

L. Pinsky
University of Houston, Houston, TX 77204, USA

L. Lederman
Illinois Institute of Technology, Chicago, IL 60616, USA

M. Jenkins and K. Clark
University of South Alabama, Mobile, AL 36688, USA

E.C. Dukes[2], K. Nelson, D. Pocanic
University of Virginia, Charlottesville, VA 22901, USA

T. Alexopoulos, A. Erwin, and M. Thompson
University of Wisconsin, Madison, WI 53706, USA

March 26, 1994

[1]Spokesperson: LUK@CSA.LBL.GOV, (510)486-7054
[2]Spokesperson: DUKES@UVAHEP.PHYS.VIRGINIA.EDU, (804)982-5376

We pray for the second coming of CP *violation ...*

A. Pais

Abstract

We propose to perform a sensitive search for *CP* violation in Ξ^- ($\overline{\Xi}^+$) and Λ ($\overline{\Lambda}$) decays. Unpolarized Ξ^- ($\overline{\Xi}^+$) hyperons are produced by protons and momentum selected with a magnetic channel. The decay sequences $\Xi^- \to \Lambda\pi^-$ ($\overline{\Xi}^+ \to \overline{\Lambda}\pi^+$) and $\Lambda \to p\pi^-$ ($\overline{\Lambda} \to \bar{p}\pi^+$) are detected with a simple wire chamber spectrometer with high-rate capability. By studying the angular distribution of the proton (antiproton) with respect to the helicity axis in the Λ ($\overline{\Lambda}$) rest frame, the product of the decay parameters $\alpha_\Lambda\alpha_\Xi$ ($\alpha_{\overline{\Lambda}}\alpha_{\overline{\Xi}}$) can be extracted. Any difference between $\alpha_\Lambda\alpha_\Xi$ and $\alpha_{\overline{\Lambda}}\alpha_{\overline{\Xi}}$ is evidence that *CP* symmetry is violated. In a typical Fermilab fixed target run, 4×10^9 Ξ^- and $\overline{\Xi}^+$ decays can be collected, enabling a measurement of the relevant asymmetry to 10^{-4} sensitivity, comparable to the level of standard model predictions for the asymmetry and well over two orders of magnitude better than the present limit. A non-zero asymmetry would be the first evidence of *CP* violation outside of the neutral kaon system and would be unambiguous evidence of direct *CP* violation.

Contents

List of Tables

[1] Assuming a 21% λ_I Be target.

1 Introduction

In the 30 years since the discovery of *CP* violation [1], our understanding of the phenomenon has improved little despite a long series of beautiful experiments. It still remains a small peculiarity unique to the neutral kaon system. Although *CP* violation can be accommodated nicely within the framework of the standard model, its origin and magnitude remain a profound mystery and many questions need to be answered before we can claim to have an understanding of it. Perhaps foremost among these is whether *CP* violation is a phenomenon unique to the neutral kaon system or a property shared by other particles. The standard model tells us that it should be evident elsewhere — in the decays of hyperons and neutral B mesons for example — but no experiment has been able to achieve the necessary sensitivity to see *CP* violation outside of the neutral kaon system. Another outstanding question is whether *CP* violation occurs only in $|\Delta S| = 2$ weak transitions — as is predicted by the superweak model of Wolfenstein [2] — or is also evident in direct $|\Delta S| = 1$ decays, as is predicted by the standard model. Despite an impressive experimental effort, both at Fermilab [3] and CERN [4], the question remains open.

For some time it has been known that *CP* violation should manifest itself in the decays of hyperons: in differences in the angular distribution of the daughter baryons between particle and antiparticle [5]. The asymmetries are expected to be small and were presumed to be difficult if not impossible to measure experimentally. In the past decade, however, considerable advances have been made in the development and operation of very high-rate spectrometers. It is no longer inconceivable for an experiment to acquire in a year's time the order of a billion events needed to measure such asymmetries. Recently E756 at Fermilab — an experiment measuring both the $\overline{\Xi}^+$ magnetic moment and polarization [6] — has shown that copious numbers of $\overline{\Xi}^+$ hyperons can be acquired with a simple trigger and with very little background. Analysis of the difference between the daughter decay distributions in the Ξ^- and the $\overline{\Xi}^+$ samples — the signature for *CP* asymmetry — shows no evidence of false asymmetries. This is extremely encouraging considering the fact that the experiment was by no means optimized to measure small asymmetries between Ξ^- and $\overline{\Xi}^+$ decays. The E756 collaboration expects to report a result with a sensitivity of about 10^{-2} which is better than any previous measurement.

In light of these facts, we have examined the possibility of measuring *CP* violation in a dedicated experiment analyzing the non-leptonic decays of charged Ξ and Λ hyperons. We find that in a standard Fermilab fixed target run a sensitivity of 10^{-4} can be achieved in the comparison of the α decay parameters of the Ξ^- ($\overline{\Xi}^+$) and Λ ($\overline{\Lambda}$). This is a

sensitivity on the order of the theoretical predictions of the standard model (as well as other models of *CP* violation), and over two orders of magnitude better than the world average experimental limit of -0.03 ± 0.06 [7] in $\Lambda(\overline{\Lambda})$ decays. Observation of an asymmetry would provide the first evidence of *CP* violation outside of the neutral kaon system as well as evidence of direct *CP* violation. Because of the importance of *CP* violation to our understanding of the standard model we feel that this experiment should be pursued vigorously at Fermilab. We emphasize that the experiment can be done with relatively modest effort and expenditure.

2 Physics of CP Violation in Hyperon Decays

2.1 Signatures for CP Violation in Hyperon Decays

The phenomenology of *CP* violation in hyperon decays has been discussed in several excellent references (see Ref. [9] for example). We briefly review it here. Because the nonleptonic weak decays of spin 1/2 hyperons violate parity they can decay into admixtures of both *S*- and *P*-wave final states:

$$\begin{aligned} S &= +S_1 e^{i(\delta_1^S+\phi_1^S)} + S_3 e^{i(\delta_3^S+\phi_3^S)}, \\ \overline{S} &= -S_1 e^{i(\delta_1^S-\phi_1^S)} - S_3 e^{i(\delta_3^S-\phi_3^S)}, \\ P &= +P_1 e^{i(\delta_1^P+\phi_1^P)} + P_3 e^{i(\delta_3^P+\phi_3^P)}, \\ \overline{P} &= +P_1 e^{i(\delta_1^P-\phi_1^P)} + P_3 e^{i(\delta_3^P-\phi_3^P)}. \end{aligned}$$

Here δ and ϕ are the strong and weak phases, and the subscripts 1 and 3 refer to the $\Delta I = 1/2$ and $\Delta I = 3/2$ isospin transitions. Note that under the combined operation of *CP* the *S*-wave amplitudes and the weak phases change sign.

In terms of the *S*- and *P*-wave amplitudes, the hyperon non–leptonic decays are conventionally described by the Lee–Yang variables: α, β, and γ [8]:

$$\begin{aligned} \alpha &= \frac{2\mathrm{Re}(S^*P)}{|S|^2+|P|^2}, \\ \beta &= \frac{2\mathrm{Im}(S^*P)}{|S|^2+|P|^2}, \\ \gamma &= \frac{|S|^2-|P|^2}{|S|^2+|P|^2}, \end{aligned}$$

where $\alpha^2+\beta^2+\gamma^2 = 1$. Often one sees (in the Particle Data Booklet, for example) the parameterization given in terms of α and ϕ where:

$$\begin{aligned} \beta &= \sqrt{1-\alpha^2}\sin\phi, \\ \gamma &= \sqrt{1-\alpha^2}\cos\phi. \end{aligned}$$

Note that ϕ given above is not the same as the weak phase defined previously. Measured values of α, β, γ, and ϕ are given in the Table 1 for the Ξ^- and Λ hyperons.

The decay distribution of the daughter spin 1/2 baryon in the rest frame of the parent hyperon (the Λ in the decay $\Xi^- \to \Lambda\pi^-$, for example) is given by:

$$\frac{dP}{d\Omega} = \frac{1}{4\pi}(1+\alpha\vec{P}_p\cdot\hat{p}_d), \tag{1}$$

where $\vec{P}_p$ is the parent hyperon polarization and $\hat{p}_d$ is the daughter baryon momentum direction in the rest frame of the parent. The daughter itself is polarized with a

Table 1: Ξ^- and Λ hyperon decay parameters [7].

Mode	α	β	γ	ϕ
$\Xi^- \to \Lambda\pi^-$	-0.456 ± 0.014	0.062 ± 0.062	0.888 ± 0.008	$(4 \pm 4)^\circ$
$\Lambda \to p\pi^-$	0.642 ± 0.013	-0.087 ± 0.047	0.762 ± 0.012	$(-6.5 \pm 3.5)^\circ$

polarization given by:

$$\vec{P}_d = \frac{(\alpha + \vec{P}_p \cdot \hat{p}_d)\hat{p}_d + \beta(\vec{P}_p \times \hat{p}_d) + \gamma(\hat{p}_d \times (\vec{P}_p \times \hat{p}_d))}{(1 + \alpha \vec{P}_p \cdot \hat{p}_d)}. \tag{2}$$

Note that in the case of an unpolarized parent the daughter is in a helicity state with a polarization given by the parent α.

Under the operation of CP both α and β reverse sign whereas γ is unchanged. If CP is conserved, the magnitudes of α and β remain the same under the transformation. Hence to search for CP violation in hyperon decays one looks for a difference in either the α or β parameters, or in the partial decay rate ($\Gamma \propto |S|^2 + |P|^2$) between the particle and antiparticle. Observables that are sensitive to CP asymmetries include:

$$\Delta = \frac{\Gamma - \overline{\Gamma}}{\Gamma + \overline{\Gamma}}, \tag{3}$$

$$A = \frac{\alpha + \overline{\alpha}}{\alpha - \overline{\alpha}}, \tag{4}$$

$$B = \frac{\beta + \overline{\beta}}{\beta - \overline{\beta}}, \tag{5}$$

$$B' = \frac{\beta + \overline{\beta}}{\alpha - \overline{\alpha}}, \tag{6}$$

where overlined quantities refer to the antihyperon.

2.2 Experimental Strategy

The four observables for hyperon decays that are sensitive to CP asymmetries are given in Eqs. (3)–(6). The small theoretical predictions for Δ (see the next section) and the difficulty in measuring small differences in rates makes the possibility of finding CP violation through Δ very unlikely. To search for CP violations through measurements of either B or B' requires hyperons and antihyperons with identical or precisely determined polarizations because the β decay parameter can only be determined by measuring the daughter polarization from a polarized parent. Both Ξ^- and $\overline{\Xi}^+$ hyperons have been shown to be polarized when produced with finite transverse momentum by protons in

inclusive production [6]. However, the magnitude of the polarizations is only 10% at a p_t of about 1 GeV/c and an x_F of 0.4, requiring a prohibitive number of Ξ^- and $\overline{\Xi}^+$ hyperons to measure the *CP* asymmetry in β. Furthermore, the polarizations of the Ξ^- and $\overline{\Xi}^+$ are almost certainly different at the required sensitivity level, making measurements of the differences in β extremely difficult. Hence we propose to search for *CP*-odd asymmetries in the parameter A of Eq. (4).

Determining A requires measuring the α parameters of the hyperon and antihyperon. The α parameter is determined by either: 1) measuring the decay asymmetry of a hyperon of known polarization, or 2) measuring the daughter polarization from either a polarized or unpolarized hyperon. Measurement of the α parameter is much easier with unpolarized hyperons if the daughter decay analyzes its own polarization. The Ξ^- and $\overline{\Xi}^+$ hyperons are ideal candidates because they decay with large branching ratios (100%) into Λ and $\overline{\Lambda}$ whose polarizations can be measured through their parity violating weak decay. Unpolarized Ξ^- and $\overline{\Xi}^+$ hyperons are produced by targeting at 0° incident angle.

The daughter Λ polarization from an unpolarized Ξ decay is simply:

$$\vec{P}_\Lambda = \alpha_\Xi \hat{p}_\Lambda, \tag{7}$$

where $\hat{p}_\Lambda$ is the direction of the Λ momentum in the rest frame of the Ξ^-. The Λ is found in a helicity state with polarization given by the Ξ^- alpha parameter: $|\vec{P}_\Lambda| = 0.456$. A difference between the Λ and $\overline{\Lambda}$ polarizations is direct evidence of *CP* violation.

The Λ ($\overline{\Lambda}$) polarization is measured through the decay asymmetry given by:

$$\frac{dP}{d\Omega} = \frac{1}{4\pi}(1 + \alpha_\Lambda \vec{P}_\Lambda \cdot \hat{p}_p), \tag{8}$$

where $\hat{p}_p$ is the direction of the proton (antiproton) momentum in the Λ ($\overline{\Lambda}$) rest frame. Since $\vec{P}_\Lambda = \alpha_\Xi \hat{p}_\Lambda$, the asymmetry in the decay proton (antiproton) direction in the Λ ($\overline{\Lambda}$) rest frame is given by the product of the Λ ($\overline{\Lambda}$) and Ξ^- ($\overline{\Xi}^+$) alpha parameters:

$$\frac{dP}{d\cos\theta} = \frac{1}{2}(1 + \alpha_\Lambda \alpha_\Xi \cos\theta), \tag{9}$$

where θ is the polar angle the proton (antiproton) makes with respect to the Λ ($\overline{\Lambda}$) polarization direction. It should be emphasized that ***in the absence of CP violation the proton and antiproton distributions should be identical***, as should be every other kinematic variable from the Ξ^- and $\overline{\Xi}^+$ decays.

Because we measure the product of the Λ and Ξ alpha parameters, the *CP* asymmetry extracted is the sum of the Λ and Ξ asymmetries given in Eq. (4) (see Appendix 1):

$$\mathcal{A} = \frac{\alpha_\Lambda \alpha_\Xi - \alpha_{\overline{\Lambda}} \alpha_{\overline{\Xi}}}{\alpha_\Lambda \alpha_\Xi + \alpha_{\overline{\Lambda}} \alpha_{\overline{\Xi}}} = A_\Lambda + A_\Xi, \tag{10}$$

where A_Λ and A_Ξ are defined by:

$$A_\Lambda = \frac{\alpha_\Lambda + \alpha_{\overline{\Lambda}}}{\alpha_\Lambda - \alpha_{\overline{\Lambda}}}, \tag{11}$$

$$A_\Xi = \frac{\alpha_\Xi + \alpha_{\overline{\Xi}}}{\alpha_\Xi - \alpha_{\overline{\Xi}}}. \tag{12}$$

Hence the measured asymmetry is sensitive to *CP* violation in both Λ and Ξ^- alpha parameters. Theoretical predictions indicate that any cancellation is highly unlikely.

2.3 Theoretical Predictions

Model independent expressions for the observables given in Eqs. (3)-(6) have been explicitly calculated [9]. To leading order they are, for $\Lambda \to p\pi^-$ decay:

$$\Delta \cong \sqrt{2}\frac{S_3}{S_1}\sin(\delta_3^S - \delta_1^S)\sin(\phi_3^S - \phi_1^S) \tag{13}$$

$$A \cong -\tan(\delta_1^P - \delta_1^S)\sin(\phi_1^P - \phi_1^S), \tag{14}$$

$$B \cong \cot(\delta_1^P - \delta_1^S)\sin(\phi_1^P - \phi_1^S), \tag{15}$$

$$B' \cong -\sin(\phi_1^P - \phi_1^S), \tag{16}$$

and for $\Xi^- \to \Lambda\pi^-$ decay:

$$\Delta = 0, \tag{17}$$

$$A \cong -\tan(\delta_3^P - \delta_3^S)\sin(\phi_1^P - \phi_1^S), \tag{18}$$

$$B \cong \cot(\delta_3^P - \delta_3^S)\sin(\phi_1^P - \phi_1^S). \tag{19}$$

The *CP* asymmetry Δ results from the interference between the $|\Delta I| = 1/2$ and $|\Delta I| = 3/2$ amplitudes whereas the other asymmetries are due to the interference of *S*- and *P*-waves. Δ vanishes in Ξ decays because there is only one isospin channel. Note that *CPT* invariance only guarantees the total decay width or lifetime be the same for the particle and the anti-particle.

Calculations of *CP* asymmetries in hyperon decays are difficult and the predicted asymmetries vary (see Ref. [9,10,11,12,13,14,15,16,17]). For example, predictions of the asymmetry *A* given by Eq. (4) range from 10^{-3} to 10^{-5}. To calculate the magnitude of the asymmetries requires the values of ϵ, ϵ', the top quark mass and the hadronic matrix elements. Results are not reliable to better than an order of magnitude [16].

The hierarchy of the observables given above can be reliably estimated. Because the $|\Delta I| = 1/2$ amplitudes are about 20 times larger than the $|\Delta I| = 3/2$ amplitudes and because $\sin(\delta_i) \approx 1/10$, Donoghue *et al.* find that $\Delta \approx A/10 \approx B'/100$ [9]. In only B' do the strong interaction final state phases cancel out, and the predicted magnitude is the largest of all the asymmetries. *A* is suppressed by the small value of the final state

phase shifts whereas Δ is further suppressed by the $|\Delta I| = 1/2$ rule. Unfortunately, as mentioned in the previous section, measuring B or B' is prohibitively difficult because a hyperon parent with precisely known polarization is needed.

The magnitudes of the predicted CP asymmetries are model dependent. Theories with no $|\Delta S| = 1$ CP-odd effects, such as the superweak model and models with a very heavy neutral Higgs, predict no CP asymmetries [9]. Models in which $|\Delta S| = 1$ CP nonconservation is dominant, such as the Weinberg model [18], predict asymmetries which are on the order of those calculated in the standard model.

In the standard model CP violation effects are due solely to the complex phase in the Cabbibo–Kobayashi–Maskawa matrix [19] and hence CP asymmetries can only arise from matrix elements which involve transitions to the third quark generation. These are thought to be dominated by the gluon penguin diagram [20] shown in Fig. 1 for both kaon and hyperon decays. The standard model predictions vary quite a bit. For example, Donoghue [14] predicts asymmetries in A which range from $-(0.3 \rightarrow 4.0)\times 10^{-4}$ for Λ ($\overline{\Lambda}$) hyperons and $-(0.4 \rightarrow 4.8)\times 10^{-4}$ for Ξ^- ($\overline{\Xi}^+$) hyperons, where much of the uncertainty is due to the incomplete knowledge of the hadronic matrix elements. To illustrate the range of expected values in the standard model, Valencia [21] has compiled predictions based on the method of Xe, Steger, and Valencia [16] with the matrix elements calculated using several different models. These are shown in Fig. 2. Non standard models further widen the range.

2.3.1 Differences Between Direct CP Violation in Kaons and Hyperons

Although there is a close relationship between direct CP violation in kaon and hyperon decays, the differences are important. The most promising method of looking for direct CP violation in neutral kaons is by measuring ϵ'/ϵ where:

$$1 - 6Re(\frac{\epsilon'}{\epsilon}) \approx \left| \frac{\frac{A(K_l \rightarrow \pi^0\pi^0)}{A(K_s \rightarrow \pi^0\pi^0)}}{\frac{A(K_l \rightarrow \pi^+\pi^-)}{A(K_s \rightarrow \pi^+\pi^-)}} \right| . \tag{20}$$

The ratio ϵ'/ϵ can be written in the form [23]:

$$\frac{\epsilon'}{\epsilon} = -\frac{1}{\sqrt{2}|\epsilon|}\frac{1}{ReA_0}\frac{ReA_2}{ReA_0}\left[ImA_0 - \frac{ReA_0}{ReA_2}ImA_2\right], \tag{21}$$

where A_0 and A_2 are the amplitudes leading to isospin-zero and isospin-two final states. Direct CP violation in kaon decays arises from the interference of isospin $I = 0$ and $I = 2$ final states whereas the direct CP violation which is responsible for the difference in alpha parameters between hyperon and antihyperon is due to the interference between S-wave and P-wave final states.

Another difference between the two different examples of direct CP violation is that in standard model calculations the value of ϵ'/ϵ is very sensitive to the top quark mass

whereas $A = (\alpha + \overline{\alpha})/(\alpha - \overline{\alpha})$ is not. The reason for this sensitivity in kaon decays is that the two terms in Eq. 21 with opposite sign have been shown to have the same phase [22] and hence tend to cancel. The amplitude A_0 is due to the *QCD* penguin diagram whereas amplitude A_2 is due to the electroweak penguin diagram, which involves exchanges of Z° and γ. Although the latter amplitude is expected to be much smaller than the former, its importance in Eq. 21 is amplified by the fact that the factor ReA_0/ReA_2 is quite large due to the small size of ReA_2 relative to ReA_0. The electroweak penguin also has a contribution that increases as m_t^2. Hence ϵ'/ϵ diminishes with increasing top mass, vanishing at a top quark mass of about 220 GeV/c^2 and becoming negative thereafter [23]. The dependence on the top quark mass is shown in Fig. 3 for both ϵ'/ϵ and $A_\Lambda = (\alpha_\Lambda + \alpha_{\overline{\Lambda}})/(\alpha_\Lambda - \alpha_{\overline{\Lambda}})$. Should the top quark mass be very heavy — and the CDF and D0 limits are getting ever higher — then we have the unfortunate situation where, even if the standard model explanation of direct *CP* violation is correct, the theory mimics the superweak theory for ϵ'/ϵ.

3 Comparison with Other Past and Proposed Hyperon CP Violation Experiments

The only data on *CP* violation in hyperon decays comes from the comparison of the alpha parameters in Λ and $\overline{\Lambda}$ decays. The experimental limits are weak: the world average compiled by the Particle Data Group is $A = (\alpha_\Lambda + \alpha_{\overline{\Lambda}})/(\alpha_\Lambda - \alpha_{\overline{\Lambda}}) = -0.03 \pm 0.06$ [7]. The three published results are given in Table 2 below. Each of the three experiments used a different technique — and none used the technique we propose here. Their bounds are all limited by statistical, not systematic errors. The first result in Table 2 is from an ISR experiment (R608) which produced Λ and $\overline{\Lambda}$ in $pp \rightarrow \Lambda X$ and $p\overline{p} \rightarrow \overline{\Lambda} X$ reactions. They quote $\alpha P(\overline{\Lambda})/\alpha P(\Lambda) = -1.04 \pm 0.29$. We have converted their result to a limit on A assuming the polarization is the same for Λ and $\overline{\Lambda}$. The data sample consisted of 10,000 $\overline{\Lambda}$'s and 17,000 Λ's. The large error is due to the small polarization of the Λ and $\overline{\Lambda}$.

The second result is from the DM2 detector in the Orsay e^+e^- colliding ring DCI. They ran on the J/ψ resonance and used the decays $J/\psi \rightarrow \Lambda\overline{\Lambda}$. The branching ratio is small — 1.4×10^{-3} [7] — which is why with a total of 8.6×10^6 J/ψ decays only 770 events were used in the analysis. Nevertheless, because of the large Λ polarization, their sensitivity is comparable to the R608 measurement. The third result is from a LEAR experiment (PS185) producing Λ hyperons in the threshold reaction $p\overline{p} \rightarrow \Lambda\overline{\Lambda}$. The polarization of the two Λ's is assumed to be equal by C-parity conservation in strong interactions. A total of 4,063 $\Lambda\overline{\Lambda}$ pairs was used in the analysis.

Table 2: Experimental limits on $A = (\alpha_\Lambda + \alpha_{\overline{\Lambda}})/(\alpha_\Lambda - \alpha_{\overline{\Lambda}})$.

Mode	Limit	Experiment
$p\overline{p} \rightarrow \Lambda X$, $p\overline{p} \rightarrow \overline{\Lambda} X$	0.02 ± 0.14	R608 [24]
$e^+e^- \rightarrow J/\psi \rightarrow \Lambda\overline{\Lambda}$	0.01 ± 0.10	DM2 [25]
$p\overline{p} \rightarrow \Lambda\overline{\Lambda}$	-0.07 ± 0.09	PS185 [26]

There has been considerable interest at CERN in pursuing these measurements to better precision with an improved higher luminosity LEAR (SuperLEAR) [27]. CERN has decided not to pursue this, largely due to budget constraints, and it appears that the LEAR program will end in 1995. A proposal has also been submitted to Fermilab to construct a similar facility dedicated to searching for *CP* violation in Λ ($\overline{\Lambda}$) decays [28]. This experiment requires the main ring injector upgrade to produce the necessary amount of antiprotons as well as the construction of a dedicated storage ring. Hence it entails a large financial commitment on the part of the lab. Both the LEAR and Fermilab storage ring proposals claim a sensitivity on the order of this proposal.

There has also been interest in pursuing hyperon *CP* violation at a tau-charm factory through the decay process $J/\psi \to \Lambda\overline{\Lambda}$. Even with optimistic assumptions on the luminosity and monochromaticity, the expected asymmetry reach is only 5×10^{-4} [29] and hence is not competitive with this proposal.

Only in fixed target experiments at either Fermilab or CERN can sufficient statistics be collected to provide a sensitivity at the 1×10^{-4} level.

4 Yields

4.1 Required Yields

The goal of this experiment is to search for direct *CP* violation in Λ and Ξ^- decays by determining the observable $\mathcal{A} = (\alpha_\Lambda \alpha_\Xi - \alpha_{\overline{\Lambda}} \alpha_{\overline{\Xi}})/(\alpha_\Lambda \alpha_\Xi + \alpha_{\overline{\Lambda}} \alpha_{\overline{\Xi}})$ with a sensitivity at the 10^{-4} level. The number of events needed to measure the asymmetry to this precision is 2×10^9 each for Ξ^- and $\overline{\Xi}^+$ (see Appendix 2). For a nominal Fermilab fixed target run of 200 days; 2×10^7 events per day, 14,000 events per spill, or 700 events per spill second are required. Assuming a 50% duty factor 1,400 *reconstructed* Ξ events per spill second are needed.

4.2 Ξ^- and $\overline{\Xi}^+$ Yields

A magnetic channel with a solid angle of 4.88 μsr selects Ξ^- and $\overline{\Xi}^+$ hyperons with small x_F and a mean p_t of 0 GeV/c, ensuring that the average production polarization is very small if not zero. The $\overline{\Xi}^+$ to π^+ ratio has been measured in p + Cu collisions at 400 GeV [30]. The ratio is about 1×10^{-3} at an x_F of 0.27 and a p_t between 0.0 GeV/c and 0.8 GeV/c which is approximately the kinematic acceptance of the magnetic channel. The π, K, and p yields can be estimated fairly reliably using the parameterization of Malensek [31] which has been used extensively at Fermilab in the design of beam lines. They have been cross-checked with a Pythia simulation which agrees to about 20%. Table 3 is a summary of the yields entering and exiting the magnetic channel for a production angle of 0 mrad and for 1×10^{10} 800 GeV protons incident on a 8.84 cm long (0.21 λ_I) Be target. The acceptance of the magnetic channel is shown in Fig. 8. The estimated number of $\overline{\Xi}^+$'s, with momentum between 110 GeV and 215 GeV, entering the collimator is 65,000 per 1×10^{10} protons. This yields 8,500 $\overline{\Xi}^+$'s at the exit of the collimator where the loss due to decay in the channel has been taken into account.

We have cross-checked the $\overline{\Xi}^+$ yield in several different ways, all of which agree to within a factor of two. The most straightforward estimate is based on E756 measurements. In four full days of running E756 collected 8×10^4 $\overline{\Xi}^+$'s. An increase in yield of about 25,000 over E756 is needed. How that increase is attained is given in Table 4. Note that only a factor of 20 increase in proton intensity is needed. Much of the increase in yield comes from running the experiment for 100 full days rather than 4. Decreasing both the p_T (necessary to produce unpolarized Ξ's) and x_F also provides substantial increases in the yield.

The Ξ^- cross section at low x_F and small transverse momentum has not been measured at high energies. However, the invariant cross section of Ξ^- hyperons produced by 800 GeV protons on Be at 2.5 mrad has been measured by E756. The result is similar to the E495 measurement of the Ξ° cross section at 5 mrad with 400 GeV protons [32]. (In the CERN hyperon experiment the Ξ^- and Ξ° production cross sections were found

Table 3: Ξ, π, K, and p yields per 10^{10} protons[a].

Particle	Yields at Collimator Entrance[b]	Exit[c]
Negative Beam		
Ξ^-	1.1×10^5	1.5×10^4
π^-	3.6×10^7	1.5×10^7
K^-	2.9×10^6	1.2×10^6
Total:	3.9×10^7	1.6×10^7
Positive Beam		
$\overline{\Xi}^+$	6.5×10^4	8.5×10^3
π^+	6.5×10^7	2.7×10^7
K^+	6.5×10^6	2.7×10^6
p	3.2×10^7	1.3×10^7
Total:	1.0×10^8	4.3×10^7

[a]Assuming a 21% λ_I Be target.
[b]Inside a cone with a solid angle of 4.88 μsr centered along the incident beam direction.
[c]Decay loss and channel acceptance have been taken into account.

to be identical [33].) Hence we use the parameterization given by E495 for Ξ° production to estimate the Ξ^- yield at 0 mrad. The number of Ξ^-'s at the collimator exit is approximately 15,000.

After correcting for the probability that the Ξ^- ($\overline{\Xi}^+$) and Λ ($\overline{\Lambda}$) decay in the vacuum region, the spectrometer acceptance, and the branching fraction of $\Lambda \to p\pi^-$ (64%), approximately 4,100 (2,300) events remain. Taking the trigger efficiency, reconstruction efficiency and event selection cuts into account, the final number of Ξ^- ($\overline{\Xi}^+$) is about 2,500 (1,400) per 1×10^{10} protons (see Table 5). The thoroughly tested E756 Monte Carlo and reconstruction programs have been used to estimate the efficiencies.

4.3 Muon Background

Muon background has not been a serious problem for any of the hyperon experiments done at Fermilab the past 15 years. For example, E555 [34], E756, and E800 have all run at much higher target interaction rates than contemplated in P871 with no untoward effects. Nevertheless, we have taken care in the design of the P871 spectrometer to minimize effects due to muon halo.

To estimate the actual muon flux we again rely on data from E756. In that experi-

Table 4: Comparison of P871 and E756 $\bar{\Xi}^+$ yields.

	E756	P871	Gain
Run time	4 days	50 days	12.5
Channel solid angle	2.36 μsr	4.88 μsr	2
$< x_F >$	0.4	0.2	7
$< p_T >$	0.75 GeV/c	0.0 GeV/c	7
Proton intensity (s^{-1})	5×10^8	1×10^{10}	20
Lifetime	0.5	0.6	1.2
Total:			29,400

ment ungated scalers recorded: 1) the singles rate in an upstream wire chamber (a 2 mm pitch MWPC (*C4*) with an active area of 10"×20" and located at 26 m from the exit of the hyperon magnet), 2) the singles rate in a downstream wire chamber (a 2 mm pitch MWPC (*C12*) with an active area of 15"×47" and positioned behind the analysis magnet at 49 m from the exit of the hyperon magnet), and 3) a single track trigger ("*pion*") defined by a small aperture scintillator telescope. Approximately 90% of the "*pion*" triggers were fully reconstructed in the offline analysis and were successfully traced back to the target. In Fig. 4 is shown the muon fluence in the upstream and downstream wire chambers as a function of number of protons for three different hyperon magnetic field settings. The targeting angle in all cases was 0 degrees. The muon fluence is defined as the difference between the singles rate of the MWPC and the "*pion*" trigger rate. The muon fluence has little dependence on the hyperon magnetic field integral: it increases slightly as the hyperon magnet field integral decreases. An independent measurement of the muon fluence using a lead-scintillator telescope agrees with these results [35]. We also cross-checked the rates with those measured by E800 in similar conditions [36] and find comparable rates.

From these measurements we estimate a muon rate in P871 of approximately 7×10^6 Hz in the upstream chambers and 2×10^6 Hz in the downstream chambers. The reduction in rate in the downstream chambers is due to the shielding and sweeping of the analysis magnet since the solid angles subtended by the upstream and downstream chambers are approximately the same. This rate will not be a problem for the wire chambers. Nor is it a problem for the trigger elements: the pion hodoscope is subdivided such that the muon rate in any individual counter is small, and the calorimeter used for the proton (antiproton) trigger is essentially muon blind.

Table 5: Ξ^- and $\overline{\Xi}^+$/ acceptance and yields per 10^{10} protons.

	Ξ^-	$\overline{\Xi}^+$
Total entering collimator:	110,000	65,000
Total exiting collimator:	15,000	8,500
Spectrometer Acceptance		
BR ($\Xi^- \to \Lambda\pi^-$)	1.00	
BR ($\Lambda \to p\pi^-$)	0.641	
Ξ^- & Λ decay in vacuum region	0.50	
Geometric acceptance	0.87	
Trigger acceptance	0.99	
Reconstruction efficiency	0.73	
Software selection cuts	0.84	
Overall acceptance (and BR):	0.17	
Total events passing all cuts:	2,540	1,440

5 Experimental Design

The design of the apparatus is based on 15 years of experience in doing hyperon physics at Fermilab, and in particular, the experience gathered in E756 [6]. The spectrometer is relatively simple. The emphasis is on good acceptance, high efficiency, and high-rate capability. The Ξ^- and $\overline{\Xi}^+$ events will be produced, trigger selected and analyzed under almost identical conditions.

Although the spectrometer described in this section is similar to E756, it is vastly superior in rate capability. The wire chambers and readout used in E756 were built 20 years ago and are not suitable for high-rate experiments. The maximum trigger rate in E756 was about 500 Hz. We intend to increase this rate by over two orders of magnitude.

Figures 5 and 6 show the plan and elevation views of the apparatus. The spectrometer, approximately 60 m long and 2 m wide, consists of a hyperon magnet (M1), 8 wire chamber stations (C1–C8), a pair of momentum analyzing magnets (M2), a hodoscope for triggering on the pions from Ξ and Λ decay, and a small hadronic calorimeter for triggering on the proton (antiproton) from Λ ($\overline{\Lambda}$) decay. To change from Ξ^- to $\overline{\Xi}^+$ running will require that the polarity of all the magnets be changed and that the target be changed.

5.1 Beam

The hyperons will be produced by an 800 or 900 GeV primary proton beam with an intensity of 2×10^{11} per 20 second spill. The beam should have a Gaussian profile with a full width at half maximum of about 1 mm when it is focussed on the target. The beam divergence should be kept as small as possible. The beam position immediately upstream of the target will be monitored with two 0.5 mm wire pitch SWIC's separated by 2 m. This arrangement determines the targeting angle to better than 0.5 mrad. For particles produced with a momentum of 150 GeV/c, the resolution in the transverse momentum due to the uncertainty in the targeting angle is only 75 MeV/c. Although we plan to take most of the data at 0 mrad production angle, it is important that the primary proton beam can be targeted at a production angle up to approximately ± 5 mrad in the vertical and horizontal planes for systematic studies as well as Ξ^- and $\overline{\Xi}^+$ yield measurements.

5.2 Target

Two targets, one for Ξ^- and the other for $\overline{\Xi}^+$ production, will be mounted on a target holder that can be moved remotely in the vertical as well as the horizontal direction. This allows fine tuning of the target position with respect to the spectrometer so that the secondary beam is symmetrically produced with respect to the nominal production direction. The targets, identical in size, will be short to minimize potential target size

effects, and will have different interaction lengths in order to produce the same charged particle flux in the spectrometer. A high-A target will be used because: 1) the physical length of the target can be made shorter, 2) fewer primary protons are needed to produce the required number of Ξ's, and 3) the relative yield of hyperons at low x_F is higher with heavy target material [32].

5.3 Hyperon Channel

After the primary protons interact in the target, a secondary charged beam is defined by a curved channel embedded in a dipole magnet with a uniform vertical field. The channel consists of brass and tungsten blocks as shown in Fig. 7. The 90 cm-long upstream tungsten block serves as a dump for the beam protons which strike the upstream face of the defining collimator at 7.5 mm to the left of the central orbit. The defining aperture is 5 mm wide in the bend view and 1 cm high in the vertical direction, giving a solid angle acceptance of 4.88 μsr.

The design of the magnetic channel has been optimized to maximize the Ξ to charged particle ratio and to select a narrow momentum bite. The central orbit of the channel has a radius of 270.27 m and a bend angle, defined by the tangents to the central orbit at the entrance and exit of the channel, of 22.56 mrad. With a field of 1.85 T, the central orbit corresponds to the trajectory of a 150 GeV/c charged particle. The channel acceptance — defined as the fraction of particles within the solid angle that emerge from the exit of the channel — is shown in Fig. 8 as a function of the secondary beam momentum.

At 0 mrad production angle, positively charged secondaries are mainly protons with momenta greater than 200 GeV/c. Because of the narrow and lower momentum bite of the channel, these high energy protons are not transported to the spectrometer, effectively increasing the fraction of $\overline{\Xi}^+$'s in the beam.

When the magnetic field of the sweeping magnet is reversed, a negatively charged beam is selected. With an NMR probe permanently installed in the collimator, it is possible to reproduce the field to high precision. In E756, even without an NMR, the momentum acceptance of the channel between the two charge modes agreed to 0.25 GeV/c, or better than one part in 10^3.

5.3.1 Decay Region

To minimize the number of interactions in the spectrometer, the 25 m long decay region will be evacuated using a 60 cm diameter vacuum pipe with thin windows at the ends. Space between the chambers will be filled with helium bags.

5.4 Spectrometer

Measuring the asymmetry to the 10^{-4} level requires a large flux of Ξ's which are accompanied by a much larger flux of charged pions (and protons). The limiting factor in

the number of Ξ's that can be accumulated is not the production cross section of the Ξ, which is quite large, but the maximum charged fluence the wire chambers can tolerate. In order to collect 1,400 reconstructed $\bar{\Xi}^+$ decays per second the spectrometer must be able to tolerate the passage of 4.3×10^7 Hz of protons and pions when a positively charged beam is selected (the fraction of Ξ^-'s in the negative beam is larger with the same fluence).

5.4.1 Wire Chambers

The wire chambers must have low mass and high-rate capability. There will be four wire chambers upstream of the analysis magnet and four behind. Table 6 is a summary of the geometry of the wire chambers that has been used in the Monte Carlo studies. Each chamber will contain three views, one having vertically strung wires and the other two having wires inclined at a stereo angle. The stereo angle will be chosen so that the resolutions in the bend and non–bend views are comparable. Since there are multiple planes in each view, there is sufficient redundancy to allow the chamber efficiencies to be measured accurately and the tracking efficiency is thus a weak function of the individual plane efficiency.

Table 6: Geometry of the wire chambers.

Z (m)[a]	Width (cm)	Height (cm)	Pitch (cm)	No. of Channels
26.0	76.8	45	0.1	3 × 768
30.0	76.8	45	0.1	3 × 768
34.0	76.8	45	0.1	3 × 768
38.0	76.8	45	0.1	3 × 768
44.0	76.8	45	0.1	3 × 768
46.0	198.4	60	0.2	3 × 992
49.0	198.4	60	0.2	3 × 992
52.0	198.4	60	0.2	3 × 992
Total channels:				20,448

[a]From the exit of the collimator

The chambers upstream of the analysis magnet will have small diameter ($12-15\,\mu$m) anode wires spaced at 1 mm and an anode-cathode gap of 3 mm or less. Since the particle density after the analysis magnet is reduced, it is possible to use chambers having a more conventional wire spacing of 2 mm at that location. All chambers will use either a fast gas such as $CF_4(80\%)/i-C_4H_{10}(20\%)$ or a traditional magic gas $Ar/i-C_4H_{10}/CF_3Br+$ Methylal at a gain of less than 10^5. The latter mixture may

be preferred in the higher flux chambers since only ionization within ~1 mm of the anode would undergo avalanche multiplication.

The rate limitation is given by the flux in the most upstream chamber which is 26 m downstream of the exit of the collimator. From the Monte Carlo simulation, the beam size at the first chamber is about 10 cm high and 25 cm wide. The rate is approximately 4×10^5 $s^{-1}cm^{-2}$ in the busiest region. If a 1 mm wire spacing MWPC is used, the highest rate per wire will be about 0.4 MHz. This is a high intensity, but not above that encountered in other high-rate experiments. Wire chambers operating at rates of several times 10^7 $s^{-1}cm^{-2}$ have successfully been built [37].

Another concern is radiation damage over the course of a 10^7 second run. Assuming that all of the ionization in a 6 mm path length is amplified at a maximal gain of 10^5, we estimate a deposited charge of ~ 0.08 C/cm on the hottest wires. This is within the accepted limit of ~ 1C/cm for 25 μm wires in traditional chamber gases.

Chamber Electronics

A low input impedance preamplifier will be mounted close to the wire followed by an Amplifier/Discriminator incorporating shaping circuitry to reduce the ion tail. Experience in E771 has shown that separating these two stages with approximately 30 feet of cable suppresses parasitic feedback sufficiently well to have stable operation at an anode threshold of $\sim 12,000e$. The discriminators will have a delayed output going to the data aquisition system as well as an optional prompt output for trigger purposes.

5.4.2 Analysis Magnet

The momentum analyzing magnet will be made up of two standard BM109 dipoles, each with an aperture of 61 cm wide by 30 cm high and an effective length of 2 m. The total transverse momentum kick is 1.8 GeV/c. The field is known to be uniform and can be easily mapped with the Fermilab ziptrack. From the experience gained in E756, the relative field values can be determined to better than 1×10^{-3}. As shown in Figs. 9 and 10, the agreement in the Ξ^- and $\overline{\Xi}^+$ as well as the Λ and $\overline{\Lambda}$ masses measured in E756 is excellent.

5.4.3 Hadronic Calorimeter

A simple hadronic calorimeter, used only to distinguish protons (antiprotons) (from Ξ decays) from background muons, is situated 70 meters downstream of the exit of the collimator, far enough downstream that the charged beam exiting the collimator is well separated from it. A schematic of the calorimeter is shown in Fig. 11. Its lateral size is 105×90 cm^2, and it is $6\lambda_I$ deep. It is a sampling calorimeter with scintillator as the active medium and lead as the absorber. There are a total of 50 layers of 0.5 cm scintillator and 2.0 cm lead, giving an interaction length of 20.3 cm and a radiation

length of 0.70 cm. Lead was chosen rather than iron as the absorber material because it gives a better energy resolution [38] and has a shorter radiation length, which confines electromagnetic showers from muon radiative processes to a smaller volume, allowing them to be discriminated against in the trigger rather easily.

The calorimeter is segmented laterally into seven horizontal and two vertical sections, and longitudinally into two sections, for a total of 28 channels. Each module is 62.5 × 45 × 15 cm^3. Essentially all of the protons from Λ decay which clear the spectrometer magnet enter a fiducial region which is at least one interaction length from the edge of the calorimeter. Protons entering at the edge of the calorimeter fiducial region have over 90% of their energy contained within the lateral extent of the calorimeter [39]. The longitudinal containment is better: only 2.5% of the shower energy will leak out the back [40].

The light is read out using photomultipliers coupled to wavelength shifter light guides on the top and the bottom of the calorimeter. We anticipate using Bicron BC-408 scintillator and Bicron BC-482A wavelength shifter (WLS) [41], which has a long attenuation length, good light output, and shows little degradation in light output when exposed to air for long periods of time. The wavelength shifter absorption spectrum is well matched to the emission spectrum of the BC-408, and the emission spectrum is well matched to the sensitivity of bialkali photomultipliers. Photomultipliers with a transistor base design [42] will be used to provide good gain stability with rate. We currently favor using the R-580 photomultiplier manufactured by Hamamatsu because of its excellent high rate characteristics [43]. The calorimeter response will be fast, with a FWHM of approximately 25 ns.

In the design shown in Fig. 11 the light is only read out on one end of the module in order that the calorimeter be hermetic. Because the light output at the WLS side of the scintillator tiles depends on the distance of the shower from the WLS, a special wrapping will be used to recover lateral uniformity of response. This will be done using Tyvek (Q173D) wrapping paper, from Du Pont [44], with a uniformity correction pattern, applied using a silk screen printing technique as has been done with the Zeus calorimeter [45]. A test rig will be constructed to determine the required pattern and test scintillator uniformity.

Calorimeter Energy Resolution

The hadronic energy resolution will be approximately $\sigma/\mathrm{E} = 60\%/\sqrt{E}$ [46], independent of energy as the calorimeter is compensating [47]. (If an iron absorber is used, with the same ratio of scintillator to absorber, the energy resolution would be worse: $\sigma/\mathrm{E} = 80\%/\sqrt{E}$ at 100 GeV. [38]) The electromagnetic resolution should be approximately $\sigma/\mathrm{E} = 30\%/\sqrt{E}$ [48]. The uncertainty in the muon energy loss is dominated by sampling fluctuations and hence should be similar to the electromagnetic energy resolution.

Calorimeter Muon Discrimination

The minimum proton (antiproton) momentum from Λ ($\overline{\Lambda}$) decay is 70 GeV (see Fig. 12). The resolution of the calorimeter at that energy is $\sigma = 5$ GeV. We wish to have very good efficiency for these protons, so the energy threshold will be set at approximately 20 GeV or 20σ away. (Note that the real-time energy resolution of the calorimeter will be worse than $60\%/\sqrt{E}$ and there will be some uncertainty in the trigger energy threshold due to drifts in the phototube gains.)

Muons deposit an energy of 1.9 GeV in the calorimeter due to ionization (assuming an *e/mip* ratio of 0.70, which is true for low momentum muons [49]). The uncertainty in the measurement of this energy is approximately $\sigma = 0.5$ GeV, assuming a Gaussian distribution. The distribution is better described by a Landau distribution, particularly at higher energies, where radiative processes are no longer rare. Note that the critical energy for muons in lead is approximately 250 GeV, well above our Monte Carlo estimate of 25 GeV for the mean muon momentum. Hence the tail of the Landau should not be pronounced. Experimental data taken with a similar calorimeter show that less than one out of a thousand muons of 20 GeV momentum deposit more than 8 GeV energy in the calorimeter [49].

To further discriminate against radiating high energy muons, the calorimeter trigger can be set to require a minimum energy in either adjacent calorimeter modules or in both the front and the back of the calorimeter. Electromagnetic showers induced by muon radiative processes are well localized, as is the ionization itself, whereas hadronic showers have a much longer and wider shower.

Calorimeter Radiation Damage

Radiation damage is not a problem. A hadron flux of approximately 10^5 per second over the period of a year gives a total flux of 6×10^{11} over an area of approximately 40×40 cm^2, or a dose of 10 Gy [50]. BC-408 scintillator has been measured to suffer little light reduction after a dose of 10 kGy [51].

Calorimeter Calibration

The calibration of the calorimeter will be easy. Every spill second over a thousand protons (or antiprotons) from Λ decays will be incident on the calorimeter. These have a momentum which is very well measured and will be used to calibrate the calorimeter and track its time dependence. An elaborate calibration system is not needed.

5.4.4 Hodoscope

A simple hodoscope, situated on the beam side of the spectrometer 60 meters from the exit of the collimator is used to trigger on pions from Ξ and Λ decay (see Fig 14). It

consists of 21 scintillation counters, each of 14×60 cm^2 area and 2 cm thickness. Each counter overlaps its neighbor by 2 cm giving a total width of 252 cm. The light is read out with phototubes placed at both ends. With these short, thick counters we expect a very high efficiency. We anticipate using Bicron BC-404 for the scintillator because of its fast response, and fast phototubes, such as the EMI 9814B [52] which has a FWHM of 3 ns. The hodoscope provides the timing for the experiment.

5.5 Trigger

The trigger has been kept simple in order to minimize potential biases. It relies on the fact that the decay of a Ξ^- ($\overline{\Xi}^+$) produces two pions with the same sign charge, but less momentum, than the beam exiting the hyperon channel, and a proton (antiproton) with the *opposite* sign charge. Because the polarity of the analysis magnet will be set equal to that of the hyperon magnet, the pions from the Ξ decay will be bent in the same direction (beam side) as the charged beam exiting the collimator, and the proton (antiproton) will be bent in the opposite direction to the charged beam. At the rear of the spectrometer both of the pions from the Ξ decay are well separated from the proton (antiproton), and both the pions and the proton (antiproton) are well separated from the charged beam exiting the collimator (see Fig. 13).

The trigger requires: 1) the presence, at the rear of the spectrometer, of a charged hadron in a hadronic calorimeter on the side opposite to the beam side of the spectrometer; and 2) the presence, again at the rear of the spectrometer, of at least one charged particle in a scintillator hodoscope on the beam side of the spectrometer. These two requirements — respectively called the proton and pion triggers — together are called the left-right trigger.

Because of the possibility of a large muon flux at the rear of the spectrometer — up to 2 MHz at the last MWPC (based on E756 studies) — either the proton trigger or the pion trigger must be made "muon blind". This is best done using a hadronic calorimeter. Because the protons have a higher momentum and are more tightly bunched together, the proton trigger rather than the pion trigger is implemented with the calorimeter. The pion trigger uses a simple scintillation counter hodoscope. Both of these trigger elements are placed outside of the intense charged particle beam exiting the collimator which has a flux of: 1.6×10^7 (4.3×10^7) per second in Ξ^- ($\overline{\Xi}^+$) mode with a nominal 10^{10} protons per second on target (see Table 3). This beam corresponds to an average bucket occupancy of 0.30 and 0.81, respectively for Ξ^- and $\overline{\Xi}^+$ running, of charged particles exiting the collimator. (The bucket spacing at Fermilab is 18.9 ns).

5.5.1 Trigger Rate

The trigger rate is summarized in Table 7. The trigger rate will be dominated by interactions of the charged beam exiting the collimator with material in the spectrometer,

as has been found in E756 using a similar trigger. The trigger rate must be kept below 100 kHz, the bandwidth to tape of the data acquisition system, a factor of 160 (430) less than the charged particle flux exiting the collimator in the Ξ^- ($\overline{\Xi}^+$) mode.

With 1.4% of an interaction length of material in the spectrometer, a rate of approximately 220 kHz (600 kHz) interactions per 10^{10} protons/s is expected for Ξ^- ($\overline{\Xi}^+$) running. Less than 5% of these interactions satisfy the left-right trigger, giving a trigger rate of 8 kHz (22 kHz) for Ξ^- ($\overline{\Xi}^+$) running. This is based on a sophisticated Monte Carlo simulation that reproduces the E756 trigger rate to better than 50%.

The spectrometer acceptance for Ξ's is given in Table 5. The trigger acceptance for Ξ's is well matched to the geometric acceptance: 99% of all the Ξ's that have both Ξ and Λ decay vertices in the vacuum decay region and whose decay products make it through the spectrometer magnet are accepted by the trigger. A total of 4,100 (2,300) Ξ^- ($\overline{\Xi}^+$) events are triggered on per 10^{10} protons/s on target. Of these 2,540 and 1,440 respectively for the Ξ^- and $\overline{\Xi}^+$ modes pass all software selection cuts.

Table 7: Trigger rate (per 10^{10} protons/s on target).

	Negative Running	Positive Running
Background trigger rate	8,300 Hz	22,200 Hz
$\Xi^\pm \rightarrow \Lambda\pi^\pm$ trigger rate	4,100 Hz	2,300 Hz
$K^\pm \rightarrow \pi^\pm\pi^\pm\pi^\mp$ trigger rate	900 Hz	2,000 Hz
Total:	13,300 Hz	26,500 Hz

5.5.2 Proton Trigger

Because of the large muon rate, a hadronic calorimeter is used, rather than a hodoscope (as was used in E756), to detect the presence of a proton (antiproton) from the Λ ($\overline{\Lambda}$) decay. The muon rejection of the calorimeter has to be approximately two orders of magnitude in order that the data acquisition system not saturate. To be safe, an order of magnitude more rejection is desirable because of the large uncertainty in the estimate of the muon rates.

The calorimeter must be fast, have good energy resolution, and be large enough to insure a good efficiency over its entire fiducial area. It does not have to be particularly radiation hard, or well segmented, and calibration is easy due to the large flux of well-measured protons incident on it.

Although the muon rejection factor seems easy to attain, measuring an asymmetry to 1×10^{-4} makes a high trigger efficiency for both protons and antiprotons extremely desirable. Hence the energy threshold on the proton trigger must be set low enough

for good efficiency. Although the amount of energy a muon deposits in dense matter is small, at large enough energies, radiative processes become important [53]. These processes, unlike ionization, are characterized by large energy fluctuations, and produce electromagnetic showers.

We estimate that the average muon momentum at the calorimeter will be about 25 GeV. (The exact value depends somewhat on the details of the siting of the experiment.) As discussed in the section describing the hadronic calorimeter, this is well below the critical energy of lead and experimental data taken with a similar calorimeter indicates that a rejection factor of one in 10^3 should be easy to obtain which retaining a very high proton (antiproton) efficiency.

5.5.3 Pion Trigger

The pion trigger is implemented with a simple scintillator hodoscope situated on the beam side of the spectrometer, 60 meters from the exit of the collimator (see Fig. 5). The hodoscope intercepts all but the unwanted low momentum pions clearing the magnet aperture. It does not intercept any of the charged particle beam exiting the collimator.

5.5.4 Trigger Electronics

The trigger electronics will be simple. The hodoscope trigger will employ standard NIM electronics. Fast phototubes are used to provide good single bucket timing.

Signals from the calorimeter phototubes will be split in two, with part going to flash ADC's (or perhaps the fast ADC's being developed for the KTeV experiment [54]) and then to the data acquisition system. The digitization of the signals should take less than 5 microseconds. The dynamic range of the ADC's should be sufficient to allow the muon energy to be well measured. The other part of the phototube output will be used to form the trigger, which will be done with the analog sum of the total energy in the calorimeter, and perhaps, front and rear sums, or separate lateral sums as well. This needs to be done in about half a microsecond.

5.6 Data Acquisition

The design goal of the DAQ system is to read 20,000 channels with a maximum trigger rate of 100,000 per spill second, build events, and write them to tape. We assume a maximum event size of 416 bytes (a factor of 2 larger than that of E756), resulting in a sustained data logging requirement of about 14 Mbyte/s — a high rate, but no larger than has been previously logged at Fermilab. The overall system deadtime should not exceed 10%, meaning that we should be able to log comfortably at least 90,000 triggers per second, *a factor of three greater than the estimated $\bar{\Xi}^+$ trigger rate and a factor of seven greater than the estimated Ξ^- trigger rate.*

The maximum event size is calculated as follows. There are 8 chambers, each with 3 wire planes (X, U and V plane). The ideal hit multiplicity for an event of interest is 3 per plane. If we take double hits and noise hits into account, a maximum of 8 hits per plane is a reasonable estimate. To be even more conservative, we always consider this worst case in our throughput calculations. Since each wire channel needs 2 bytes for encoding, a maximum of 384 bytes will be read out from all the chambers. Furthermore, we assume that a total of 20 bytes are generated by scintillators and calorimeter. The run and event number, event length and end of event marker will take up another 12 bytes. Therefore a maximum event size of 416 Bytes presents a very conservative estimate.

The design of the acquisition system is driven by the requirements of modularity (new technologies should be implementable as they become available without affecting the overall system), and scalability (it should be possible to accommodate an increase in performance).

The layout of the acquisition system is given in Fig. 15. The centerpiece is a standard 6U VME crate (DAQ-crate) that holds one or more Front-End Interfaces (FEI) that communicate with Front-End Crates (FEC), Event Builders (EB), Interfaces to Tape units (TI), and a State Machine (StM) which controls and monitors the activities of the readout sequences. A group of FEC's form a read-out branch. Several such branches can be accessed in parallel. Auxiliary readout of scalars, magnetic field monitors and other slow control devices will be done separately but will be embedded into the standard data stream.

The FEC contains the Front-End Modules (FEM) that read and latch the signals from the MWPC's and counters. The FEI communicates with the DAQ-crate and a Front-End Processor (FEP) which executes a real time kernel (e.g. VxWorks) for time-critical operations. The main functions of the FEP are data collection from all FEM's in the FEC, data reduction through reformatting of the event fragment, and temporary storage of data until the EB pulls a new block of events into its local memory.

There are six system components:

1. Front-End Module: In Fig. 16 the 256 differential ECL detector signals are received by the FEM and converted to TTL logic. The data are latched into a FIFO array. The FIFO's are deep enough to derandomize the intensity fluctuations of the incoming beam. The hit is then encoded as absolute wire address by an address encoder such as a digital signal processor and stored in one of two VME accessible on-board buffers. At the end of encoding, the address encoder will put out a word to signal the End of Event (EOE), e.g. FFFF, and append it to the event fragment. Data are written into the same buffer until the FEP decides to read out the FEM. The FEP broadcasts a SWITCH_BUFFER signal on the VME bus to all FEM's in the FEC and subsequently performs a block-read of the full buffer. In summary, the FEM's act as VME slaves to the FEP and have a double buffer scheme implemented. A "busy" signal will be generated to disable the trigger when the readout sequence cannot keep up with the trigger rate. Also a minimum

deadtime will be imposed once a trigger is accepted. In the current design we set the deadtime to 100 ns, limiting the FIFO speed to 10 MHz.

2. Front-End Processor (FEP): The FEP retrieves data with chained VME block-reads from all FEM's. After the FEP has fetched all these packets it assembles the data belonging to the same trigger and forms a new event fragment containing event number and fragment length. The FEP has large on-board memory (maximum 128 MByte) to hold event fragments over one full spill. This enables the FEI to transfer data during the spill and in between spills.

3. Event Builder (EB): The EB fetches all the event fragments from all FEC's to the local memory. Then it builds the final event from the event fragments belonging to the same trigger before writing it out to the permanent storage.

4. State Machine (StM): This module will synchronize and arbitrate the related DAQ processes. For example, it coordinates the trigger signals and the data transport through the DAQ.

5. Front-End-Interface (FEI): One FEC has to communicate with the DAQ-crate at a sustained rate of almost 2 MByte/s. The total throughput from all FEC's to the EB is expected to be around 18 MByte/s. Thus we will employ a fast link that enables us to daisy-chain several or all FEC's with the DAQ-crate. In case the setup latency for transfers is substantial we will use the State Machine to control the data flow.

6. Data Logging: We expect to log up to 14 MByte of data per second to the permanent storage. An array of five Exabyte Mammoth tape drives [55], which will be available at the end of 1994, and which write (in non-compressed mode) 3 MByte/s and pack 20 GByte per tape will be used.

5.7 Total Ξ Yields

The total Ξ^- and $\overline{\Xi}^+$ yield is limited by the bandwidth of the data acquisition system and by the requirement that we run on positives and negatives with the same fluence through the wire chambers. In order to saturate the bandwidth of the DAQ (10% dead time) a trigger rate per spill second of 90,000 is needed. In Ξ^- running this corresponds to a total flux of 108 MHz exiting the collimator and a *reconstructed* Ξ^- yield of 17,100 per spill second. To keep the charged particle fluence through the wire chambers the same in $\overline{\Xi}^+$ running, a corresponding trigger rate is 67,000 per spill second is needed giving a *reconstructed* $\overline{\Xi}^+$ yield of 3,600 per spill second.

At these rates the total Ξ^- and $\overline{\Xi}^+$ yield in a 200 day run with 50% duty factor is 9×10^9 each (assuming 80% of the running is on $\overline{\Xi}^+$). This corresponds to an error in the asymmetry $\mathcal{A} = (\alpha_\Lambda \alpha_\Xi - \alpha_{\overline{\Lambda}} \alpha_{\overline{\Xi}})/(\alpha_\Lambda \alpha_\Xi + \alpha_{\overline{\Lambda}} \alpha_{\overline{\Xi}})$ of 0.5×10^{-4}.

Because of uncertainties in our yield estimates, and because of the uneven spill structure in fixed target running, we are being more conservative and claim a maximum trigger rate of only 30 kHz per spill second. In Ξ^- running this corresponds to 36 MHz of charged particles exiting the collimator and a *reconstructed* Ξ^- yield of 5,700 per spill second. The corresponding reconstructed $\overline{\Xi}^+$ yield per spill second is 1,200. The total yield at this trigger rate, again assuming that 80% of the running is on $\overline{\Xi}^+$, is 2.9×10^9 for both Ξ^- and $\overline{\Xi}^+$. This corresponds to an error in the asymmetry $\mathcal{A} = (\alpha_\Lambda \alpha_\Xi - \alpha_{\overline{\Lambda}} \alpha_{\overline{\Xi}})/(\alpha_\Lambda \alpha_\Xi + \alpha_{\overline{\Lambda}} \alpha_{\overline{\Xi}})$ of 0.8×10^{-4}.

6 Offline Computing Needs

A sustained rate of 10,000 events per second will be written to tape assuming a 30,000 Hz trigger rate. In 200 days of running with a duty factor of 50% the total number of events will be 86×10^9 on 1,800 8mm–20 GB tapes (assuming an event size twice that of E756). This is a data sample on the order of that taken by E791 in the 1991 fixed target run [56].

Our estimate of the offline computing requirements is summarized in Table 8. In the first pass analysis, which reconstructs events, the CPU time required to process the E756 data on a HP 9000/735 workstation (rated 81 SPEC_int92) is 3 ms/event (including I/O time). We expect it will take comparable time to analyze an event in this experiment. A total of 2,100 SPEC_int92 are needed if the entire data set is to be reconstructed in 10^7 seconds.

The data throughput required for event reconstruction in 10^7 seconds is 3.6 MB/s. We expect to acquire 15 of the Exabyte Mammoth tape drives which will leave us with a nominal bandwidth of 45 MB/s.

For the final analysis, again based on our experience gained in E756, it will take approximately 1 ms to process a DST event on a HP-735. Assuming 4×10^9 Ξ events, a total of 3.2×10^8 SPEC_int92-seconds are needed for the final analysis. This could be done in 70 hours on the University of Virginia Digital alpha cluster.

Note that the total amount of DST data is 2,400 GB, or 120 tapes, assuming a 600 byte event size. (The E756 DST event size is 68 bytes!) In order to read all of these events from tape in 70 hours requires a sustained rate of 9.5 MB/s, well within the 45 MB/s bandwidth of our 15 Mammoth drives.

For Monte Carlo studies two types of events are generated: complete events and hybrid events. In a complete Monte Carlo event the parent particle is generated at the target, tracked through the collimator and the spectrometer, and digitized. The sophisticated E756 Monte Carlo takes about 45 ms to generate such an event on a HP-735. Hybrid Monte Carlo events use the decay vertex and momentum of the real Ξ's. Only the decay products are generated by the Monte Carlo. This minimizes errors due to poor simulation of the parent particle kinematic parameters. This technique has been extensively used in many high statistics hyperon polarization experiments [57]. With 10 ms needed to generate a hybrid event (on a HP-735), it also reduces the amount of computer time needed to generate an event. To generate a number of Monte Carlo events that is equal to the amount of data requires a processor power of 810 SPEC_int92 in 10^7 seconds.

The total amount of processor power needed to reconstruct, analyze, and generate an equivalent number of Monte Carlo events is approximately 3,000 SPEC_int92 in 10^7 seconds. Available computer resources among the collaborating institutions is over 1,200 SPEC_int92 (see Table 9). (We have omitted the lower end platforms available to the collaboration in Table 9.) We expect that by the time we begin the data analysis —

Table 8: Estimate of offline computing requirements.

Event Reconstruction	
Total triggers:	86×10^9
Total bytes:	36,000 GB
Total tapes (20 GB):	1,800
Reconstruction time per event:	0.24 SPEC_int92-second[a]
Total CPU needed:	2.1×10^{10} SPEC_int92-second
CPU per 10^7 seconds:	2,100 SPEC_int92
Final Analysis	
Total Ξ events:	4×10^9
Analysis time per event:	0.081 SPEC_int92-second[b]
Total CPU needed:	3.2×10^8 SPEC_int92-second
CPU per 10^7 seconds:	32 SPEC_int92
Monte Carlo Studies	
Events needed:	1.0×10^{10}
Analysis time per event:	0.81 SPEC_int92-second[c]
Total CPU needed:	8.1×10^9 SPEC_int92-second
CPU per 10^7 seconds:	810 SPEC_int92
Total CPU per 10^7 seconds needed:	2,942 SPEC_int92

[a]Based on the E756 reconstruction time using an HP-735 (81 SPEC_int92).
[b]Based on the E756 DST analysis time using an HP-735 (81 SPEC_int92).
[c]Based on the E756 Monte Carlo using an HP-735 (81 SPEC_int92).

1997, assuming a long fixed target run — the available processor power will have at least doubled by planned upgrades to the existing hardware to 3,000 SPEC_int92. Additional computer acquisitions will further augment this. *Hence we expect to be able to analyze all of the data in approximately half a year without recourse to the Fermilab farm.* We would like, however, to have several hundred SPEC_int92 of offline Fermilab processor power available during the running of the experiment and a fraction of the Fermilab processor farm for the data analysis.

Table 9: Presently available computing resources.

			Performance (SPEC_int92)	
Institution	Model	Number	Unit	Total
Univ. Virginia	Digital Alpha 3000/400	12	75	900
Berkeley	HP 9000/735	3	81	243
	HP 9000/730	2	37	74
Total:				1,217

7 Systematics

The experimental apparatus is designed to minimize systematic biases that produce false *CP* asymmetries. Because the Ξ^- and Λ alpha parameters both change sign under the *CP* transformation, the distribution of the proton in the Λ rest frame should be identical to that of the antiproton in the $\overline{\Lambda}$ rest frame. (The Λ and $\overline{\Lambda}$ distributions in the Ξ^- and $\overline{\Xi}^+$ rest frames should also be identical because the Ξ's are produced with no polarization.) ***Hence, in principle, the proton and antiproton distributions can be directly compared with no acceptance corrections to search for CP violation.*** In practice, acceptance corrections with have to be made, but they will be very small.

Systematic effects which have the potential to cause false asymmetries are of great concern in light of the fact that we wish to measure an asymmetry to the 10^{-4} level. Sources of biases which can cause false *CP* asymmetries fall into three classes: 1) differences in acceptance between the Ξ^- and $\overline{\Xi}^+$ decay products, 2) nonzero polarization of the Ξ^- or $\overline{\Xi}^+$, and 3) differences between the p and $\bar{p}$ cross sections.

7.1 Effect of Differences in the Acceptance

There are many possible causes of differences in the Ξ^- and $\overline{\Xi}^+$ acceptance. For example, targeting differences, magnetic field differences, and differences in the chamber efficiencies. Every effort will be made to minimize such differences.

Targeting differences can result in differences in the secondary production of Ξ's in the collimator. Such events are eliminated by requiring that the Ξ's point back to the target. To compensate for slight differences in the positive and negative magnetic fields of the hyperon channel and spectrometer magnets we intend to measure the differences in the field values to a part in 10^4 or better. The earth's magnetic field, which won't be flipped, produces slight changes in the acceptance between Ξ^- and $\overline{\Xi}^+$. The effect is small: an added 25 μrad deflection to a 15 GeV/c particle (amounting to 1 part in 10^3), the lowest momentum accepted by the spectrometer. This effect can be compensated for or corrected for in the Monte Carlo.

Because the Ξ^- and $\overline{\Xi}^+$ data samples will not be taken simultaneously, temporal changes in the apparatus could give rise to false asymmetries. To minimize rate dependent efficiencies in the chambers, we will be careful to run both positive and negative beams such that the charged particle flux at the exit of the collimator is always the same. Nevertheless, at the high charged particle fluences anticipated for the experiment, chamber efficiencies are not expected to be extremely high and localized inefficiencies producing false asymmetries at the 10^{-4} level are conceivable. In order to minimize such effects we have added redundant chamber planes at every measurement station. This allows the individual plane efficiencies to be measured to the desired accuracy and reduces the dependence of the tracking efficiency on the individual plane efficiency.

7.1.1 How the Analysis Method Minimizes Potential Biases

Despite efforts taken to minimize acceptance differences, some small differences will remain. Our method of analyzing the Λ polarization — which is different than that used previously by the hyperon group at Fermilab — greatly reduces the effect of these differences. Recall that to measure the product of the Ξ and Λ alpha parameters one needs to measure the distribution of polar angles that the protons makes with respect to the Λ polarization. This distribution is given by:

$$\frac{dP}{d\Omega} = \frac{1}{4\pi}(1 + \alpha_\Lambda \vec{P}_\Lambda \cdot \hat{p}_p), \tag{22}$$

where $\vec{P}_\Lambda$ is the Λ polarization and $\hat{p}_p$ is the proton momentum direction in the Λ rest frame. In previous hyperon polarization experiments measuring the Λ polarization and magnetic moment, the projection of this distribution on rest frame axes parallel to the lab frame x, y, and z axes has been measured. This was done because the Λ polarization in those experiments was fixed in space.

The situation in P871 is quite different. The Λ polarization is not fixed: its direction differs from event to event, and is given by the direction of the Λ momentum in the Ξ rest frame (see Fig. 17). The magnitude is always the same and is given by α_Ξ. The slope of the proton $\cos\theta$ distribution is equal to $\alpha_\Xi \alpha_\Lambda$,

$$\frac{dP}{d\cos\theta} = \frac{1}{2}(1 + \alpha_\Xi \alpha_\Lambda \cos\theta), \tag{23}$$

only in that frame in which the polar axis is determined by the direction of the Λ polarization. Hence we do not analyze the Λ polarization along axes fixed with respect to the lab axes, but in a coordinate frame in which the Λ polarization defines the polar axis.

Because the Λ direction changes from event to event over the 4π solid angle in the Ξ^- rest frame and because the acceptance along the helicity axis in the Λ rest frame is very uniform, acceptance differences localized in a particular part of the apparatus do not map onto any particular part of the $\cos\theta$ distribution of the proton. This will become evident in the following discussion.

7.1.2 Estimating Biases from E756 Data

In order to get a quantitative estimate of the effect of acceptance differences on the asymmetry measurement, we have chosen pairs of Ξ^- data sets from E756 with large acceptance differences and compared their proton distributions in the Λ rest frame. Since all of the events are Ξ^-'s, any difference between the proton distributions is solely due to acceptance differences between the two samples and not due to *CP* violation. *No attempt was made to correct for acceptance differences between the data sets.* Over 10 million Ξ^- events were analyzed.

We have chosen to investigate systematic effects using real rather than Monte Carlo data for several reasons. First, real data, unlike Monte Carlo data, has *all* effects which might cause biases — those known as well as those we have not yet thought of. Second, generating millions of Monte Carlo events is very time consuming. And finally, one can always correct for any biases put into the Monte Carlo since their source is exactly known. We have used all Ξ^- events rather than both Ξ^- and $\overline{\Xi}^+$ events from E756 because there are more of them, and because they have precisely the same $\cos\theta$ slope: $\alpha_\Lambda\alpha_\Xi$. *Any differences are due to biases and not CP violation!*

The data samples we have compared were taken at different hyperon magnet settings, producing different momentum distributions, and at different targeting angles, producing different values of the Ξ^- polarization. Samples with non-zero production angles are known to be polarized with a magnitude of about 12%.

The difference in the proton cosine distributions of any two samples is determined by taking the ratio:

$$R(\cos\theta) = \frac{A_1(\cos\theta)(1+a\cos\theta)}{A_2(\cos\theta)(1+a\cos\theta)}, \tag{24}$$

$$= \frac{A_1(\cos\theta)}{A_2(\cos\theta)}, \tag{25}$$

where $A_1(\cos\theta)$ and $A_2(\cos\theta)$ are the acceptances as a function of $\cos\theta$ of the two samples, $a = \alpha_\Xi\alpha_\Lambda$, and $\cos\theta$ is the polar angle the proton makes relative to the Λ polarization direction (which is the Λ momentum direction in the Ξ rest frame). Since $R(\cos\theta)$ is very uniform in $\cos\theta$, we parameterize it as

$$R(\cos\theta) = a + b\cos\theta \tag{26}$$

where the slope b is a measure of how well the acceptances of the two samples agree with each other. The intercept a is unity when the samples are properly normalized and the slope b is zero if the acceptances are identical *and* the fit is good.

Table 10 and Fig. 18 summarize the difference in $\cos\theta$ acceptance for data samples with comparable Ξ^- polarization but different average Ξ^- momentum. The acceptance mismatch strongly depends on the difference in momentum of the samples down to a momentum difference of $\Delta p = 20$ GeV/c, below which there is no statistically significant difference. It is important to note that in the insensitive region the proton $\cos\theta$ distributions in the Λ rest frame already agree to better than a few parts per thousand although the samples have significant acceptance differences in the laboratory frame and were taken at different times.

In P871 we will control the acceptance differences to well over an order of magnitude better than the differences shown above and we will correct any known acceptance differences. In order to minimize the bias due to a difference between the Ξ^- and $\overline{\Xi}^+$ momentum distributions we have a small collimator aperture which selects a narrow

Table 10: Acceptance difference as a function of momentum mismatch.

$< p_1 >^a$	$< p_2 >^b$	Δp^c	$\Delta P_\Xi{}^d$	$\lvert b \rvert$	χ^2/DOF
318.74	458.83	140.1	0.04	0.1442 ± 0.0041	3.76
318.74	427.34	108.6	0.03	0.1271 ± 0.0027	6.54
318.74	385.48	66.8	0.01	0.0923 ± 0.0024	4.10
385.48	427.34	41.9	0.02	0.0355 ± 0.0022	1.47
427.34	458.83	31.5	0.01	0.0183 ± 0.0039	0.74
458.83	478.98	20.2	0.04	0.0032 ± 0.0048	0.74
467.13	462.41	4.7	0.00	0.0029 ± 0.0051	1.54

[a]Mean Ξ^- momentum of sample 1 (GeV/c).
[b]Mean Ξ^- momentum of sample 2 (GeV/c).
[c]Difference in Ξ^- momentum (GeV/c).
[d]Difference in the Ξ^- polarization.

momentum bite. As a result, the Ξ^- and $\overline{\Xi}^+$ momenta are determined largely by the collimator acceptance rather than by their production properties (which are different). To get an idea of how well the Ξ^- and $\overline{\Xi}^+$ acceptances match we have normalized the momentum spectra of the E756 Ξ^- and $\overline{\Xi}^+$ data to each other and then compared various Ξ^- and $\overline{\Xi}^+$ kinematic quantities. (The normalization is necessary because the momentum bite of the E756 magnetic channel was much broader than the P871 design and hence the Ξ^- and $\overline{\Xi}^+$ momentum spectra were different.) As shown in Figs. 19–21, the comparison is almost perfect — chi-squares per degree of freedom indicate no difference — even though the two data samples were taken at widely different times. In particular, in the comparison between the $\cos\theta$ distributions of the proton polar angle with respect to the Λ momentum in the Λ rest frame — the asymmetry we need to measure to search for *CP* violation — the slope b is -0.001 ± 0.009 with a χ^2/DOF of 0.67, indicating no statistically significant difference (see Fig. 22).

By extrapolation from the studies of the E756 data, we expect that the acceptance contribution in P871 to the measurement of the $\cos\theta$ slope will be considerably less than 10^{-4}.

7.2 Effect of Non-zero Ξ Polarization

Another potential source of bias is from non-zero Ξ^- and $\overline{\Xi}^+$ polarizations. The most probable source of such polarization would be a slight mistargetting. The resultant polarization would be extremely small due to the low p_T and small x_f of the Ξ. Any source of Ξ polarization can be measured to the 10^{-3} level and can be corrected for. A non-zero Ξ polarization results in a small fixed component to the Λ polarization in

addition to its helicity. Unlike the helicity, which changes from event to event, this new component is fixed in space. The effect of any fixed component of Ξ polarization on the measurement of the Λ helicity is diluted by our method of analysis — where the analysis polar axis changes from event to event. Because of the near uniform acceptance along the Λ momentum in the Λ rest frame, sources of polarization that are fixed in space average to almost identically zero.

The best evidence for this comes from another analysis of the E756 data. Samples of Ξ^-'s with equal and opposite production angles (± 2.5 mrad) were analyzed for differences in their proton $\cos\theta$ distributions. The data samples were chosen to have widely different polarizations: on average +12% and −12%, and widely different acceptances. This is partially due to the different polarizations, but mainly due to the tendency of the Ξ^- to follow the direction of the incident beam. The +2.5 mrad Ξ^- decay products tend to inhabit the upper part of the apparatus whereas the −2.5 mrad Ξ^- decay products inhabit the lower part. The magnitude of the difference is illustrated in Fig. 24 showing the vertical position of the proton at the spectrometer magnet center. The difference is huge.

How do these large differences in acceptance in the laboratory affect the measurement of the slope of the $\cos\theta$ distribution? Fig. 25 shows the proton $\cos\theta$ distributions from two samples. Fitting the ratio of the two to the form given by Eq. 26 shows no significant difference: the slope b of this comparison is $(2.3 \pm 2.9) \times 10^{-3}$ with a χ^2/DOF = 16.3/18. In Table 11 we show the same comparison for several similar samples of different Ξ polarization. There are no statistically significant differences in the proton $\cos\theta$ distributions between the two samples in each case despite the large differences in acceptance.

Table 11: Acceptance difference for samples of opposite polarization.

$< p_{+\theta} >^a$	$< p_{-\theta} >^b$	Δp^c	$\Delta P_\Xi{}^d$	b	χ^2/DOF
317.67	319.07	−1.40	0.23	-0.0017 ± 0.0027	1.02
318.74	319.34	−0.60	0.25	$+0.0023 \pm 0.0029$	0.90
385.48	383.45	2.03	0.26	-0.0016 ± 0.0017	1.20
427.34	425.85	1.49	0.28	-0.0030 ± 0.0024	0.74
458.83	454.32	4.51	0.29	-0.0063 ± 0.0047	0.93
478.98	478.42	0.56	0.25	-0.0125 ± 0.0044	1.03

[a] Mean momentum of positive production angle sample (GeV/c).
[b] Mean momentum of negative production angle sample (GeV/c).
[c] Difference in momentum (GeV/c).
[d] Difference in the Ξ^- polarisation.

Combining all the above samples we find $b = (2.5 \pm 10.4) \times 10^{-4}$, i.e. there is no

significant difference between the two $\cos\theta$ slopes of interest at the 10^{-3} level. Hence the dilution of the effect of the Ξ polarization is large and we expect that even smaller polarizations — on the order of a few tenths of a percent — will contribute less than 10^{-4} to the measured asymmetry.

In any case, we do not intend to only hope for a small Ξ polarization, but to actually measure it. Measuring it to the required 10^{-3} level is possible and would require only a fraction of the total data sample. We expect to find no polarization, but in fact could extract the *CP* asymmetry even in the presence of a Ξ polarization greater than 10^{-3}.

7.3 Differences in the p and $\bar{p}$ Cross Sections

Secondary interactions of the Ξ^- and $\overline{\Xi}^+$ decay products in the spectrometer can cause differences in the Ξ^- and $\overline{\Xi}^+$ reconstruction efficiencies. If such differences favor on part of the proton $\cos\theta$ distribution over another then false *CP* asymmetries can result.

In order to study this effect we have generated 5 million Ξ^- and $\overline{\Xi}^+$ Monte Carlo events in the P871 apparatus (using a modified version of the well-tested E756 Monte Carlo). Each proton or antiproton from a Ξ decay was forced to interact in the spectrometer with a distribution according to the amount of material at each location. PYTHIA was used to generate the number, type, and momentum of the resulting secondaries which were tracked through the spectrometer by the P871 Monte Carlo. The events were then reconstructed and the $\cos\theta$ distributions of the proton and antiproton were compared for those events that were successfully reconstructed. Only 120,000 events survived. The difference in the slopes of the $\cos\theta$ distributions ($\alpha_\Xi\alpha_\Lambda$ for both the Ξ^- and $\overline{\Xi}^+$ samples) was found to be -0.017 ± 0.010. Because P871 will have approximately 1.4% of an interaction length of material, this translates to a sensitivity of about $(2.9 \pm 1.7) \times 10^{-4}$ in the asymmetry A. Again, no attempt was made to correct for acceptance differences between the two data sets.

7.4 Other Potential Biases and Checks

There are other potential sources of biases. The radiative decays $\Lambda \to p\pi^-\gamma$ or $\overline{\Lambda} \to p\pi^+\gamma$ occur with a branching ratio of only 10^{-3} and don't contribute to the asymmetry A at the 10^{-4} level. Backgrounds from other sources are very small, as is evident in Fig. 23 which shows the $p\pi^-$and $\bar{p}\pi^+$ invariant masses. Most of the continuum in the invariant mass distribution is due to poorly reconstructed Ξ events. This kind of background is reproduced in the Monte Carlo simulation in E756. With better position resolution and more redundant tracking measurements in this experiment, we expect this background to be highly suppressed.

To test the level of the systematics we intend to compare the Ξ^- and $\overline{\Xi}^+$ as well as Λ and $\overline{\Lambda}$ masses as well as their lifetimes as a function of the hyperon momentum. They should be identical if *CPT* is conserved. We will also have a sample of $K^- \to \pi^-\pi^-\pi^+$

and $K^+ \to \pi^+\pi^+\pi^-$ decays on the order of the Ξ sample. These can be analyzed as if they are $\Xi^\pm$ decays to search for false asymmetries.

8 Future Improvements

The *CP* sensitivity of this proposal, assuming systematic errors are not a problem, is not limited by the number of Ξ^- and $\overline{\Xi}^+$ hyperons that can be produced, but by the rates that the wire chambers can handle, the trigger selectivity, and the bandwidth of the data acquisition system. New technologies are being developed that are pushing these limits to higher levels. Wire chambers have been built that can take an order of magnitude more flux than we anticipate with no untoward effects [37]. The development of gas microstrip chambers [58] promises an even higher rate capability. Recently an experiment, NA12, has run at high intensities for 100 days with 8 microstrip gas chambers at CERN [59]. The chambers have a rate capability higher than 5×10^7 cm^{-2}s^{-1}. Vigorous R&D efforts are underway to increase the size and lower the mass of these chambers. If these efforts are successful, fluxes of two orders of magnitude higher than we anticipate in this proposal could be tolerated.

Similar improvements are being made in the data acquisition systems and triggers. Hence we expect in the future that large increases in the yield will be possible and the *CP* sensitivity of the experiment can be pushed beyond 10^{-4}.

9 Other Physics

9.1 CP Violation in Charged Kaon Decays

Direct *CP* violation can also show up in differences between K^+ and K^- decays. Two observables sensitive to *CP* asymmetries are:

$$\Delta\Gamma(\tau) = \frac{[\Gamma(K^+ \to \pi^+\pi^+\pi^-) - \Gamma(K^- \to \pi^-\pi^-\pi^+)]}{[\Gamma(K^+ \to \pi^+\pi^+\pi^-) + \Gamma(K^- \to \pi^-\pi^-\pi^+)]}, \tag{27}$$

and the asymmetry Δg in the slope parameter of the Dalitz plot which measures the energy dependence of the odd pion. The Dalitz plot of $K_{3\pi}$ decay is conventionally parameterized [7] with the form:

$$|M^2| \propto 1 + g\frac{(s_3 - s_0)}{m_\pi^2} + h\frac{(s_3 - s_0)^2}{m_\pi^2} + j\frac{(s_2 - s_1)}{m_\pi^2} + k\frac{(s_2 - s_1)^2}{m_\pi^2} + \ldots, \tag{28}$$

with

$$s_i = (m_K - m_i)^2 - 2m_K T_i, \; i = 1,2,3, \tag{29}$$

$$s_0 = \frac{1}{3}({m_K}^2 + {m_1}^2 + {m_2}^2 + {m_3}^2), \tag{30}$$

where m_i and T_i are the mass and the kinetic energy of the i^{th} pion, and the index 3 is used for the opposite sign pion in the decay. The coefficient j is zero if *CP* is conserved. Furthermore, if any of the other slope parameters, g, h, and k for $K^+ \to \pi^+\pi^+\pi^-$ is not the same as that for $K^- \to \pi^-\pi^-\pi^+$ decay, then *CP* symmetry is violated.

Because standard model estimates of $\Delta\Gamma(\tau)$ are very small ($< 10^{-6}$) [60], it seems unlikely that *CP* violating asymmetries will be observed there. The situation is more favorable for the slope parameters. Experimentally, the values of h and k are found to be very small [7]. Hence it will be very difficult to observe *CP*-odd effect by determining the difference in either h or k between $K^+ \to 3\pi$ and $K^- \to 3\pi$ decays. The slope parameter g is large (-0.2154 ± 0.0035 [7]) and hence interest in searching for direct *CP* violation in $K_{3\pi}$ decay has focused on it. The asymmetry of the slope parameter g is defined by

$$\Delta g = \frac{g(K^+) - g(K^-)}{g(K^+) + g(K^-)}. \tag{31}$$

Theoretical predictions of Δg vary from 1.4×10^{-3} to the order of 10^{-6} [61,62,63]. The best measurement of Δg is from a BNL experiment done in the late 60's which, with about 3.2 million $K^\pm \to 3\pi$ decays, determined Δg to be -0.0070 ± 0.0053 [64].

Our anticipated charged Kaon yields are given in Table 12. Despite the small acceptance due to the long $K^\pm$ lifetime — on average 2.2% of the $K^\pm$'s will decay in the decay region with the π's inside the spectrometer active area — the yields are very high; comparable to the Ξ yields. (About 50% of the $K_{3\pi}$ events pass reconstruction and

selection cuts.) In a 200 day run (assuming a 50% duty factor) we will collect 1.5×10^9 $K^+ \to \pi^+\pi^+\pi^-$ and 0.7×10^9 $K^- \to \pi^-\pi^-\pi^+$ decays. This implies a sensitivity for CP violation of about 1×10^{-4}.

There are several competing proposals. The NA48 collaboration has entertained using their apparatus to investigate charged-K decays. In a one-year run they would accumulate approximately 2×10^8 $K^+ \to \pi^+\pi^+\pi^-$ and $K^- \to \pi^-\pi^-\pi^+$ decays to get an error of 5×10^{-4} in Δg [65]. The E865 collaboration at Brookhaven is also considering measuring Δg [66]. They hope to collect 10^{10} decays in a few weeks of running. Finally, the Φ factory hopes to collect about 10^9 K^+K^- decays to allow a measurement of $\Delta g = 5 \times 10^{-4}$ [67].

Table 12: Charged Kaon yields (per 10^{10} protons).

	$K^+ \to \pi^+\pi^+\pi^-$	$K^- \to \pi^-\pi^-\pi^+$
Yield at target[a] (Hz)	6.5×10^6	2.9×10^6
Yield at collimator exit[b] (Hz)	2.7×10^6	1.2×10^6
Branching ratio	0.0559	
Lifetime acceptance	0.022	
Trigger acceptance	0.61	
Reconstruction efficiency	0.64	
Event selection cut efficiency	0.80	
Total (per spill second)	1,040	460
Total (200 day run)[c]	1.5×10^9	0.66×10^9

[a]Inside a cone with a solid angle of 4.88 μsr centered along the incident beam direction.
[b]Decay loss and channel acceptance have been taken into account.
[c]Assuming a 30% spill duty factor and a 50% experimental duty factor.

9.2 Other Physics

There are other physics topics that can be addressed by P871. We list some of them here.

- Precision measurements of the decay parameter α of Ξ and Ω^- decays.
- Tests of CPT in the differences in masses and lifetimes of particle and antiparticle in the $\Xi^\pm$, $\Omega^\pm$, Λ, and kaon systems.
- Search for the $\Delta S = 2$ decay: $\Xi^- \to p\,\pi^-\pi^-$.
- Search for the $\Delta S = 2$ decay: $\Omega^- \to \Lambda\pi^-$.

- Search for the $\Delta S = 3$ decay: $\Omega^- \to p\,\pi^-\pi^-$.
- Precise measurements of the polarization of the Ξ^- and $\overline{\Xi}^+$ at very small production angles and low x_F.
- Measurements of the Ξ^- and $\overline{\Xi}^+$ production cross sections.

If we were to add a muon station to the spectrometer then other interesting physics topics would become available including:

- Search for $K^\pm \to \pi^\pm\mu^+\mu^-$.
- Search for $K^- \to \pi^+\mu^-\mu^-$. (This mode is probably limited by the π/μ rejection that is possible.)
- Search for $\Xi^- \to p\mu^-\mu^-$.

With silicon strip detectors, or gas microstrip chambers at the exit of the collimator, at least two more rare decays can be searched for:

- Search for $\Sigma^- \to p\mu^-\mu^-$.
- Search for $\Sigma^+ \to p\mu^+\mu^-$.

Some of the above decays can also be searched for in the charged conjugate modes.

10 Costs

In this section we give our best estimates of the costs of the experiment. We expect these costs to be accrued over a period of two years. A detailed breakdown of the cost of constructing the spectrometer — wire chambers, calorimeter, hodoscope, readout electronics, and data acquisition system — is given in Table 18. The total cost is \$1,246K excluding \$146K needed for electronics from PREP. (Note that the cost per channel of the wire chamber electronics is \$37 excluding the cost of the data acquisition system.) The costs of the spectrometer are to be born by the collaborating institutions according to the breakdown given in Table 14. As of this writing we are somewhat short what is needed, but are confident that once approved new collaborators will make up the difference.

The total cost of constructing and mounting the experiment depends on the beam line used. An investigation by the beam group at Fermilab [68] found three beam lines that are well matched to the needs of the experiment: P-Center, P-West, and M-Center. Costs estimates for mounting the experiment in each of these beam lines are given in Tables 15, 16, and 17 [69]. Note that some of the rigging costs in the tables for P-West and M-Center must be done irrespective of P871. The total cost of mounting the experiment, for each of the three beam lines, is given in Table 13. Note that the Fermilab contribution in each case includes \$146K of existing PREP electronics.

We have omitted costs of running the experiment, which would be accrued in 1996 and 1997, and would be relatively minor (\$20K for tapes, for example). We have also omitted costs associated with analyzing the experiment, which would be accrued following 1997. Both LBL and the University of Virginia have substantial existing computer resources, so we expect these costs to be less than \$100K.

Table 13: P-871 Cost Summary.

Component	P-Center		P-West		M-Center	
	Fermilab	Collaboration	Fermilab	Collaboration	Fermilab	Collaboration
Beam line equipment	250,000		520,000		320,000	
Wire chamber fabrication		115,000		115,000		115,000
Chamber readout electronics	3,000	792,000	3,000	792,000	3,000	792,000
Hadronic calorimeter	12,000	73,000	12,000	73,000	12,000	73,000
Pion hodoscope	41,000	24,000	41,000	24,000	41,000	41,000
Trigger logic	90,000		90,000		90,000	
DAQ System		242,000		242,000		242,000
Total:	396,000	1,246,000	666,000	1,246,000	466,000	1,246,000

Table 14: Collaborating institution cost breakdown [$].

Institution	Funding Source	Year 1	Year 2
LBL	DOE University	250,000	250,000
Academia Sinica	Taiwan Research Council	?	100,000
University of Virginia	DOE University	100,000	100,000
University of Wisconsin	DOE University	50,000	50,000
Illinois Inst. of Tech.	DOE University	75,000	75,000
University of S. Alabama	DOE University	10,000	10,000
University of Houston	DOE University	?	?
Total:		485,000 + ?	585,000 + ?

Table 15: P-Center cost estimate [$].

Beam, Target, and Hyperon Channel	
Hyperon channel (fab. and install.)	50,000
Vacuum decay pipe (fab. and install.)	20,000
Fab. and install. muon spoilers	20,000
Cost of rapid removal of all E781 detectors	30,000
Interlock modifications	5,000
Experiment	
Move existing BM109's	10,000
Move E781 calorimeter	10,000
Install cable trays	10,000
Miscellaneous electrical	5,000
Provide counting rooms	90,000
Total:	$250,000

Table 16: P-West cost estimate [$].

Beam, Target, and Hyperon Channel	
Primary beamline: remove spoilers and install angle varying bends	40,000
Target and shielding	
Target mechanism	10,000
Reconfigure existing shielding	40,000
Hyperon channel (fab. and install.)	50,000
Install hyperon channel B2	20,000
Extra transerexes and busswork for AVB and hyperon	100,000?
Move toroids 1' east	20,000
Vacuum decay pipe inside existing toroids	20,000
Move SELMA 10 m downstream, remove polepiece	50,000
Remove E705/E771 (labourers, carpenters, etc.)	40,000
Remove Rosie	25,000
Remove E705/E771 muon wall	50,000
Interlock modifications	5,000
Experiment	
Install calorimeter	20,000
Modify cable trays	10,000
Modify existing counting rooms	20,000
Total:	$520,000 + ?

Table 17: M-Center cost estimate [$].

Beam, Target, and Hyperon Channel	
Primary beamline	
Add vertical AVB bend magnet (10')	20,000
Target and shielding	
Target mechanism	10,000
Remove Eartly magnets and dump	40,000
Hyperon channel (fab. and install.)	50,000
Install B2 hyperon magnet	20,000
Reshield hyperon cave	20,000
Reuse E799 vacuum decay pipe (fab. and install.)	10,000
Move existing MC7 experimental shielding	20,000
Remove existing MC7 experimental equipment	20,000
Modify existing MC7 muon spoilers	10,000
Construct secondary beam stop	5,000
Interlock modifications	5,000
Experiment	
Install 2 BM109 magnets	40,000
Install calorimeter	10,000
Install cable trays	10,000
Small upstream (MC7) counting room	30,000
Total:	$320,000

Table 18: Detector costs.

Hadronic Calorimeter							
Component	Unit	Unit Cost [$]	Ref.	# of units	Fermilab	Collab.	Total Cost [$]
Scintillator	$0.5 \times 45.0 \times 62.5$ cm^3	54	1	560		30,240	30,240
Waveshifter	$1.0 \times 15.0 \times 62.5$ cm^3	84	2	28		2,352	2,352
Lead	lb	0.47	3	24,000		11,280	11,280
Photomultiplier	channel	350	4	28		9,800	9,800
Bases	channel	100	5	28		2,800	2,800
Linear fan-In	16 channels	860	6	2	1,720		1,720
Discriminator	16 channels	1,650	7	3	4,950		4,950
Camac crate	each	5,000	8	1	5,000		5,000
Flash ADC	channel	50	9	28		1,400	1,400
Miscellaneous			10			15,000	15,000
Subtotal:					11,670	72,872	84,542

Pion Hodoscope							
Component	Unit	Unit Cost [$]	Ref.	# of units	Fermilab	Collab.	Total Cost [$]
Scintillator	$2.0 \times 14.0 \times 60.0$ cm^3	259	11	21		5,439	5,439
Photomultiplier	channel	350	12	42		14,700	14,700
Bases	channel	100	13	42		4,200	4,200
High voltage	80 channels	11,067	14	1	11,067		11,067
Discriminator	16 channels	1,650	15	4	6,600		6,600
Delay	16 channels	2,720	16	3	8,160		8,160
Coincidence unit	16 channels	1,869	17	2	3,738		3,738
Logic unit	32 channels	2,321	18	1	2,321		2,321
Camac crate	each	5,000	19	1	5,000		5,000
Miscellaneous			20		4,000		4,000
Subtotal:					40,886	24,339	65,225

Wire Chambers							
Component	Unit	Unit Cost [$]	Ref.	# of units	Fermilab	Collab.	Total Cost [$]
PWC	45×77 cm^2	10,000	21	5		50,000	50,000
PWC	60×200 cm^2	15,000	21	3		45,000	45,000
Amplifier	4 channels	44	22	5,250		231,000	231,000
Discriminator	32 channels	352	23	656		230,912	230,912
Latch	256 channels	2,200	24	82		180,400	180,400
Cable	16 channels/200 ft	100	25	1,300		130,000	130,000
High voltage	per pair	800	26	4	3,200		3,200
Low voltage	each	1,000	27	20		20,000	20,000
Gas system	system	20,000	28	1		20,000	20,000
Subtotal:					3,200	907,000	910,200

Data Acquisition System							
Component	Unit	Unit Cost [$]	Ref.	# of units	Fermilab	Collab.	Total Cost [$]
F.E. VME Crate	each	5,000	29	9		45,000	45,000
F.E. Interface	card	2,200	30	10		22,000	22,000
F.E. Processor	card	5,000	31	9		45,000	45,000
Memory Module	128 MB	6,500	32	9		58,500	58,500
DAQ VME Crate	each	2,500	33	1		2,500	2,500
State Machine	card	3,000	34	1		3,000	3,000
Event Builder	card	15,000	35	2		30,000	30,000
Tape Interface	card	2,500	36	4		10,000	10,000
Software License	each	600	37	10		6,000	6,000
Exabyte drive	each	4,000	38	5		20,000	20,000
Subtotal:						242,000	242,000

Trigger							
Component	Unit	Unit Cost [$]	Ref.	# of units	Fermilab	Collab.	Total Cost [$]
NIM electronics	module	1,500	—	40	60,000		60,000
CAMAC Crate	crate	5,000	—	2	10,000		10,000
NIM Bin	crate	2,000	—	10	20,000		20,000
Subtotal:					90,000		90,000

References

1. Bicron BC-408 scintillator; Bicron, 12345 Kinsman Rd., Newbury OH 44065.
2. Bicron BC-482A wavelength shifter; Bicron, 12345 Kinsman Rd., Newbury OH 44065.
3. Calcium Lead; Vulcan Lead Resources, Inc., 1400 W. Pierce St., Milwaukee, WI 53204.
4. Hamamatsu R-590; Hamamatsu Corp., 360 Foothill Rd., Bridgewater, NJ 08807-0910.
5. To be home built.
6. LeCroy 428F; LeCroy Corp., 700 Chestnut Ridge Rd., Chestnut Ridge, NJ 10977-6499.
7. LeCroy 4413; LeCroy Corp., 700 Chestnut Ridge Rd., Chestnut Ridge, NJ 10977-6499.
8. CAMAC crate and controller. Vendor not specified.
9. Type not yet selected.
10. Fabrication jig and prototype plus miscellaneous supplies.
11. Bicron BC-404 scintillator; Bicron, 12345 Kinsman Rd., Newbury OH 44065.
12. EMI 9814B; THORN EMI Gencom Inc., 23 Madison Rd., Fairfield, NJ 07006.
13. To be home built.
14. The high voltage supply will be used for both the hodoscope and calorimeter. LeCroy 1449, 1442N high voltage supply; LeCroy Corp., 700 Chestnut Ridge Rd., Chestnut Ridge, NJ 10977-6499.
15. LeCroy 4413; LeCroy Corp., 700 Chestnut Ridge Rd., Chestnut Ridge, NJ 10977-6499.

16. LeCroy 4518; LeCroy Corp., 700 Chestnut Ridge Rd., Chestnut Ridge, NJ 10977-6499.
17. LeCroy 4516; LeCroy Corp., 700 Chestnut Ridge Rd., Chestnut Ridge, NJ 10977-6499.
18. LeCroy 4532; LeCroy Corp., 700 Chestnut Ridge Rd., Chestnut Ridge, NJ 10977-6499.
19. CAMAC crate and controller. Vendor not specified.
20. Cables, etc.
21. Based on the KTeV estimates, *Conceptual Design Report: Kaons at the Main Injector*, FN-568.
22. This is based on a quote from LeCroy on the price of their PCOS IV preamp. It includes a tail cancelling shaper.
23. Design similar to E789 silicon strip detector readout system with the addition of a one-shot pulse stretcher. See B. Turko et al., IEEE Trans. Nucl. Sci. **39** (1992) 758.
24. To be home built. The estimate includes the costs of design, parts and fabrication.
25. Three sections of 34 conductor twist-n-flat having total length 200'.
26. Fermilab standard chamber high voltage power supply.
27. 100 amp Lambda power supply.
28. To be home built.
29. 9U VME crate (1.5kW); Dawn VME Products, 47073 Warm Springs Blvd., Fremont, CA 94539.
30. PTI 940; Performance Technologies, 315 Science Parkway, Rochester, NY 14620.
31. MVME 167.
32. Micro Memory Inc., 9540 Vassar Avenue, Chatsworth, CA 91311.
33. Standard 6U VME crate; Dawn VME Products, 47073 Warm Springs Blvd., Fremont, CA 94539.
34. MVME 162.
35. SPARC CPU-10; Themis Computer, 6681 Owens Drive, Pleasanton, CA 94588.
36. Performance Technologies, 315 Science Parkway, Rochester, NY 14620.
37. LBL sitewide licence.
38. Estimated cost of the new Exabyte Mammoth tape drive due out in the fall of 1994.

Appendix 1: What do we Actually Measure?

The angular distribution of the proton in the decay chain: $\Xi^- \to \Lambda\pi^-$, $\Lambda \to p\,\pi^-$, where the Ξ^- is produced unpolarized, is given by:

$$\frac{dP}{d\cos\theta} = \frac{1}{2}(1 + a\cos\theta), \tag{1}$$

where $a = \alpha_\Lambda\alpha_\Xi$ and θ is the polar angle of the proton in the Λ rest frame relative to the Λ momentum direction in the Ξ rest frame. Similarly, the angular distribution of the antiproton in the antiprocess: $\overline{\Xi}^+ \to \overline{\Lambda}\pi^+$, $\overline{\Lambda} \to \overline{p}\,\pi^+$, where the $\overline{\Xi}^+$ is produced unpolarized, is given by:

$$\frac{dP}{d\cos\theta} = \frac{1}{2}(1 + \overline{a}\cos\theta), \tag{2}$$

where $\overline{a} = \alpha_{\overline{\Lambda}}\alpha_{\overline{\Xi}}$. We write the expressions for the alpha parameters of the antiparticles as:

$$\begin{aligned} \alpha_{\overline{\Lambda}} &= -\alpha_\Lambda + \Delta\alpha_\Lambda, \\ \alpha_{\overline{\Xi}} &= -\alpha_\Xi + \Delta\alpha_\Xi. \end{aligned}$$

It is $\Delta\alpha_\Lambda$ and $\Delta\alpha_\Xi$ that we wish to measure: if *CP* is violated they must be nonzero. Measuring the angular distributions of Eq. (1) and Eq. (2) gives:

$$\begin{aligned} a &= \alpha_\Lambda\alpha_\Xi, \\ \overline{a} &= (-\alpha_\Lambda + \Delta\alpha_\Lambda)(-\alpha_\Xi + \Delta\alpha_\Xi). \end{aligned}$$

The difference between the two asymmetries is:

$$\begin{aligned} \mathcal{A} = \frac{a - \overline{a}}{a + \overline{a}} &= \frac{\alpha_\Lambda\alpha_\Xi - (-\alpha_\Lambda + \Delta\alpha_\Lambda)(-\alpha_\Xi + \Delta\alpha_\Xi)}{\alpha_\Lambda\alpha_\Xi + (-\alpha_\Lambda + \Delta\alpha_\Lambda)(-\alpha_\Xi + \Delta\alpha_\Xi)}, \\ &= \frac{+\alpha_\Lambda\Delta\alpha_\Xi + \alpha_\Xi\Delta\alpha_\Lambda - \Delta\alpha_\Lambda\Delta\alpha_\Xi}{2\alpha_\Lambda\alpha_\Xi - \alpha_\Lambda\Delta\alpha_\Xi - \alpha_\Xi\Delta\alpha_\Lambda + \Delta\alpha_\Lambda\Delta\alpha_\Xi}. \end{aligned}$$

Leaving out terms which are second order in $\Delta\alpha_\Lambda$ and $\Delta\alpha_\Xi$ in the numerator and first order in the denominator gives:

$$\begin{aligned} \mathcal{A} &\cong \frac{\alpha_\Lambda\Delta\alpha_\Xi + \alpha_\Xi\Delta\alpha_\Lambda}{2\alpha_\Lambda\alpha_\Xi}, \\ &\cong \frac{\Delta\alpha_\Xi + \Delta\alpha_\Lambda(\alpha_\Xi/\alpha_\Lambda)}{2\alpha_\Xi}. \end{aligned}$$

We wish to relate this to the individual asymmetries in the Ξ and Λ alpha parameters:

$$A_\Lambda = \frac{\alpha_\Lambda + \alpha_{\overline{\Lambda}}}{\alpha_\Lambda - \alpha_{\overline{\Lambda}}} = \frac{\Delta\alpha_\Lambda}{2\alpha_\Lambda},$$

$$A_\Xi = \frac{\alpha_\Xi + \alpha_{\overline{\Xi}}}{\alpha_\Xi - \alpha_{\overline{\Xi}}} = \frac{\Delta\alpha_\Xi}{2\alpha_\Xi}.$$

Plugging these in gives:

$$\frac{a - \overline{a}}{a + \overline{a}} = A_\Xi + A_\Lambda. \tag{3}$$

We have gone through this simple derivation in some detail in order to emphasize that what we are sensitive to is the *CP* asymmetry in both the Ξ and the Λ alpha parameters. In fact there is no way the two alpha parameters can be deconvoluted if one measures the Λ polarization through its self-analyzing weak decay. Although in theory $\Delta\alpha_\Lambda$ and $\Delta\alpha_\Xi$ could be equal and opposite in sign, the chances of such a conspiracy are remote: most calculations predict that A_Λ and A_Ξ have equal sign, and in fact the standard model prediction of [9] shows them to be roughly equal in magnitude as well, doubling the size of the measured asymmetry.

Appendix 2: Error in the Asymmetry Measurement

We wish to measure the difference between the the product of the Λ and Ξ^- alpha parameters and the $\overline{\Lambda}$ and $\overline{\Xi}^+$ alpha parameters:

$$\mathcal{A} = \frac{\alpha_\Lambda \alpha_\Xi - \alpha_{\overline{\Lambda}} \alpha_{\overline{\Xi}}}{\alpha_\Lambda \alpha_\Xi + \alpha_{\overline{\Lambda}} \alpha_{\overline{\Xi}}} = \frac{a - \overline{a}}{a + \overline{a}} = A_\Lambda + A_\Xi.$$

The error in this measurement is given by:

$$\begin{aligned} \delta\mathcal{A} &= \sqrt{\left(\frac{d\mathcal{A}}{da}\Delta a\right)^2 + \left(\frac{d\mathcal{A}}{d\overline{a}}\Delta\overline{a}\right)^2}, \\ &= \frac{2}{(a+\overline{a})^2}\sqrt{(\overline{a}\Delta a)^2 + (a\Delta\overline{a})^2}, \\ &= \frac{1}{2a}\sqrt{\Delta a^2 + \Delta\overline{a}^2}, \end{aligned}$$

where we have set $a = \overline{a}$. The product of the two alpha parameters is measured by measuring the asymmetry a in the proton (antiproton) decay distribution:

$$\frac{dP}{d\cos\theta} = \frac{1}{2}(1 + a\cos\theta).$$

The error in a is estimated using [70]:

$$\begin{aligned} \Delta a &= \frac{1}{\sqrt{N}}\sqrt{2a^3/(\log(1+a) - \log(1-a) - 2a)}, \\ &\cong \sqrt{\frac{3}{N}}, \end{aligned}$$

where the expression strictly applies only when the acceptance is uniform. We find:

$$\delta\mathcal{A} = \frac{1}{2a}\sqrt{\frac{3}{N_{\Xi^-}} + \frac{3}{N_{\overline{\Xi}^+}}},$$

where N_{Ξ^-} and $N_{\overline{\Xi}^+}$ are respectively the number of Ξ^- and $\overline{\Xi}^+$. If the two data samples are equal then:

$$\delta\mathcal{A} = \frac{1}{a}\sqrt{\frac{3}{2N}}.$$

The number of events needed to measure $\mathcal{A}$ to $\delta\mathcal{A}$ precision is:

$$\begin{aligned} N &= \frac{3}{2a^2}\frac{1}{(\delta\mathcal{A})^2}, \\ &= \frac{17.5}{(\delta\mathcal{A})^2}, \end{aligned}$$

where we have substituted $a = \alpha_\Lambda\alpha_\Xi = (-0.456)(0.642) = -0.293$. To measure an asymmetry with an error of $\delta\mathcal{A} = 1 \times 10^{-4}$ requires 1.8×10^9 Ξ^- events and the same number of $\overline{\Xi}^+$ events.

References

[1] J.H. Christenson, J.W. Cronin, V.L. Fitch and R. Turlay, Phys. Rev. Lett. **13** (1964) 138.

[2] L. Wolfenstein, Phys. Rev. Lett. **13** (1964) 562.

[3] L.K. Gibbons et al. (E731), Phys. Rev. Lett. **70** (1993) 1203.

[4] H. Burkhardt et al. (NA31), Phys. Lett **B206** (1988) 169.

[5] A. Pais, Phys. Rev. Lett. **3** (1959) 242.
O.E. Overseth and S. Pakvasa, Phys. Rev. **184**, (1969) 1663.

[6] P.M. Ho et al., Phys. Rev. **D44** (1991) 3402.

[7] Review of Particle Properties, Phys. Rev. **D45** 1992) 1.

[8] T.D. Lee and C.N. Yang, Phys. Rev. **108** (1957) 1645.

[9] John F. Donoghue, Xiao-Gang He and Sandip Pakvasa, Phys. Rev. **D34** (1986) 833.

[10] Tim Brown, S.F. Tuan and Sandip Pakvasa, Phys. Rev. Lett. **51** (1983) 1823.

[11] Ling-Lie Chau and Hai-Yang Cheng, Phys. Lett. **B131** (1983) 202.

[12] John F. Donoghue and Sandip Pakvasa, Phys. Rev. Lett. **55** (1985) 162.

[13] John F. Donoghue, Barry R. Holstein and German Valencia, Phys. Lett. **B178** (1986) 319.

[14] John F. Donoghue, Third Conf. on the Intersections between Particle and Nuclear Physics, Rockport ME, 14–19 May, 1988.

[15] M.J. Iqbal and G.A. Miller, Phys. Rev. **D41** (1990) 2817.

[16] X.G. He, H. Steger and G. Valencia, Phys. Lett. **B272** (1991) 411.

[17] E.A. Paschos and Y.L. Wu, Mod. Phys. Lett. **A6** (1991) 93.

[18] S. Weinberg, Phys. Rev. Lett. **37** (1976) 657.
T.D. Lee, Phys. Rev. **D8** (1973) 1226; Phys. Rep. **96** (1974) 143.

[19] M. Kobayashi and T. Maskawa, Prog. Theor. Phys. **49** (1973) 652.

[20] M. Shifman, A. Vainshtein, and V. Zakharov, Nucl. Phys. **B120** (1977) 316.
F. Gilman and M. Wise, Phys. Lett. **B93** (1980) 129.

[21] G. Valencia, private communication.

[22] J.M. Flynn and L. Randall, Phys. Lett. **B224** (1989) 221.

[23] G. Buchalla, A. Buras and M. Harlander, Nucl. Phys. **B337** (1990) 313.

[24] P. Chauvat et al., Phys. Lett. **163B** (1985) 273.

[25] M.H. Tixier et al., Phys. Lett. **B212** (1988) 523.

[26] P.D. Barnes et al., Phys. Lett. **B199** (1987) 147.

[27] N. Hamann et al., CERN/SPSLC 92–19, 30 March 1992.

[28] S.Y. Hsueh, "Search for direct *CP* violation in $\bar{p} + p \to \bar{\Lambda} + \Lambda \to \bar{p}\pi^+ + p\pi^-$", Proposal to Fermilab, January 2, 1992.

[29] E.M. Gonzalez, Proceedings of the Meeting on the Tau-charm Factory Detector and Machine, University of Seville, Andalucia, Spain, 29 April – 2 May 1991, Ed. by J. Kirkby and J.M. Quesada.

[30] T.R.Cardello et al., Phys. Rev. **D32** (1985) 1.

[31] A.J. Malensek, Fermilab note FN-341 (1981), unpublished.

[32] A. Beretvas et al., Phys. Rev. **D34** (1986) 53.

[33] M. Bourquin et al., Z. Phys. **C5** (1980) 275.

[34] B. Lundberg et al., Phys. Rev. **D40** (1989) 3557.

[35] J. Lach and Y. Li, Fermilab note TM-1555 (1989), unpublished.

[36] G. Guglielmo, private communication.

[37] J. Fischer, A. Hrisoho, V. Radeka and P. Rehak, Nucl. Instr. and Meth. **A238** (1985) 249.

[38] R. Wigmans, Nucl. Instr. and Meth. **A259** (1987) 389.

[39] D. Acosta et al., Nucl. Instr. and Meth. **A316** (1992) 184.

[40] H. Abramowicz et al., Nucl. Instr. and Meth. **180** (1981) 429.

[41] Bicron, 12345 Kinsman Rd., Newbury OH 44065.

[42] C.R. Kerns, IEEE Trans. on Nucl. Science, *NS-24* (1973) 353.

[43] Hamamatsu Corp., 360 Foothill Rd. Bridgewater, NJ 08807-0910.

[44] DuPont, P.O. Box 80016, Wilmington, DE 19880-0016.

[45] The Zeus Detector, Status Report, March 1989.

[46] G. Drews et al., Nucl. Instr. and Meth. **A290** (1990) 335.

[47] P.K. Job et al., Nucl. Instr. and Meth. **A316** (1992) 174.

[48] J. Del Peso and E. Ros, Nucl.. Instr. and Meth. **A276** (1989) 456.

[49] D. Acosta et al., Nucl. Instr. and Meth. **A320** (1992) 128.

[50] D.E. Groom, "Radiation Levels in the SSC Interaction Regions", SSC-SR-1033, June 10, 1988.

[51] C. Zorn et al., Nucl. Instr. and Meth. **A276** (1989) 58.

[52] THORN EMI Gencom Inc., 23 Madison Rd., Fairfield, NJ 07006.

[53] W. Lohmann, R. Kopp, and R. Voss, "Energy Loss of Muons in the Energy Range 1–10,000 GeV," CERN Report 85–03 (1985).

[54] KTeV Design Report, FN-580, Fermilab, January 22, 1992.

[55] Exabyte Corp., 1685 38th Street, Boulder CO 80301.

[56] S. Amato et al., Nucl. Instr. and Meth. **A324** (1993) 535.

[57] G. Bunce, Nucl. Instr. Meth. **172** (1980) 553.

[58] A. Oed, Nucl. Instr. and Meth. **A263** (1988) 351.
F. Angelini et al., Nucl. Instr. and Meth. **A283** (1989) 755.

[59] F. Angelini et al., Nucl. Instr. and Meth. **A315** (1992) 21.

[60] B. Grinstein, S.J. Reg, and M.B. Wise, Phys. Rev. **D33** (1986) 1495.

[61] A.A. Bel'kov et al., Phys. Lett. **B300** (1993) 283.

[62] G. D'Ambrosio, G. Isidori, and N. Puver, Phys. Lett. **B273** (1991) 497.

[63] Hai–Yang Cheng Phys. Rev. **D44** (1991) 919.

[64] W.T. Ford et al., Phys. Rev. Lett. **25** (1970) 1370.

[65] G.D. Barr *et al.*, Proposal for NA48, CERN/SPSC/90-22.

[66] M. Zeller *et al.*, BNL proposal E865 (1991).

[67] P. Franzini, INFN preprint LNF-92/024 (P) (1992).

[68] A. Malensek and R. Tokarek, *Possible Beam Locations for P-871*, March 4, 1994.

[69] C.N. Brown, *P871: Preliminary Cost Guesstimate*, March 24, 1994.

[70] A.G. Frodesen, O. Skjeggestad and H. Tofte, "Probability and Statistics in Particle Physics" (Universitetsforlaget, Oslo, 1979) p. 219.

List of Figures

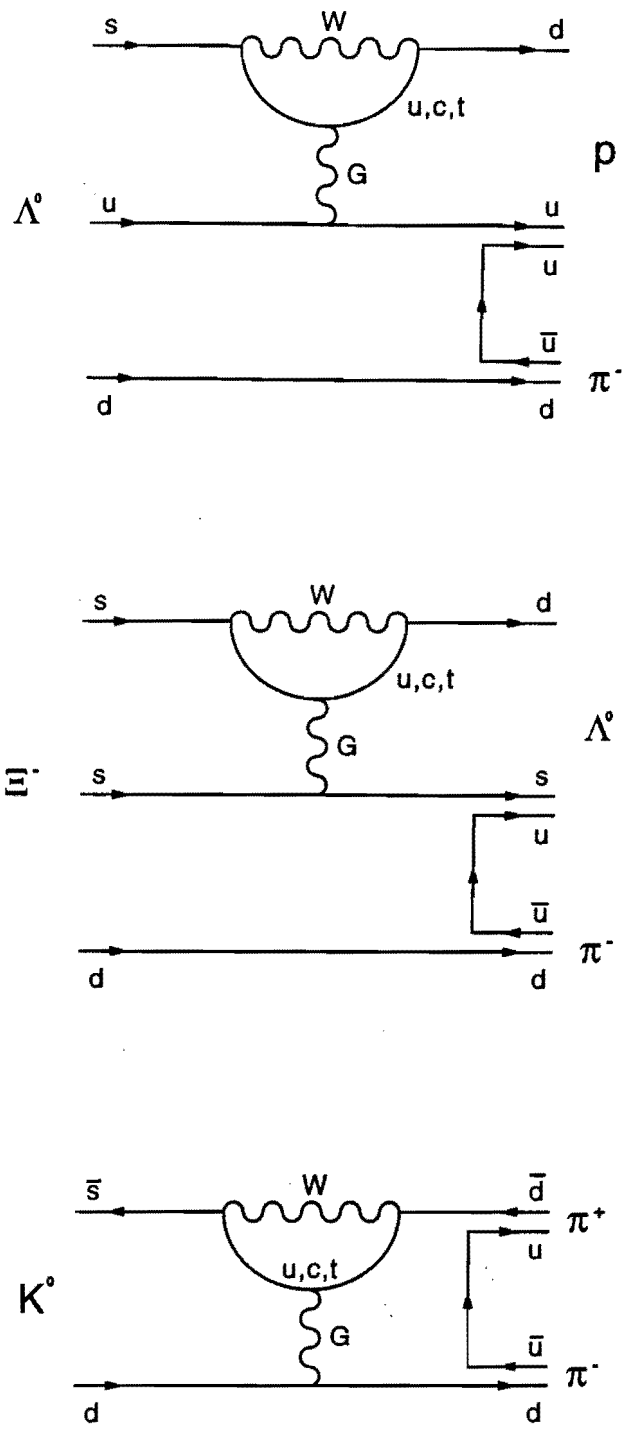

Figure 1: Penguin diagrams responsible for $|\Delta S| = 1$ direct CP violation in $\Lambda \to p\pi^-$, $\Xi^- \to \Lambda\pi^-$ and $K \to \pi^+\pi^-$ decays according to the standard model.

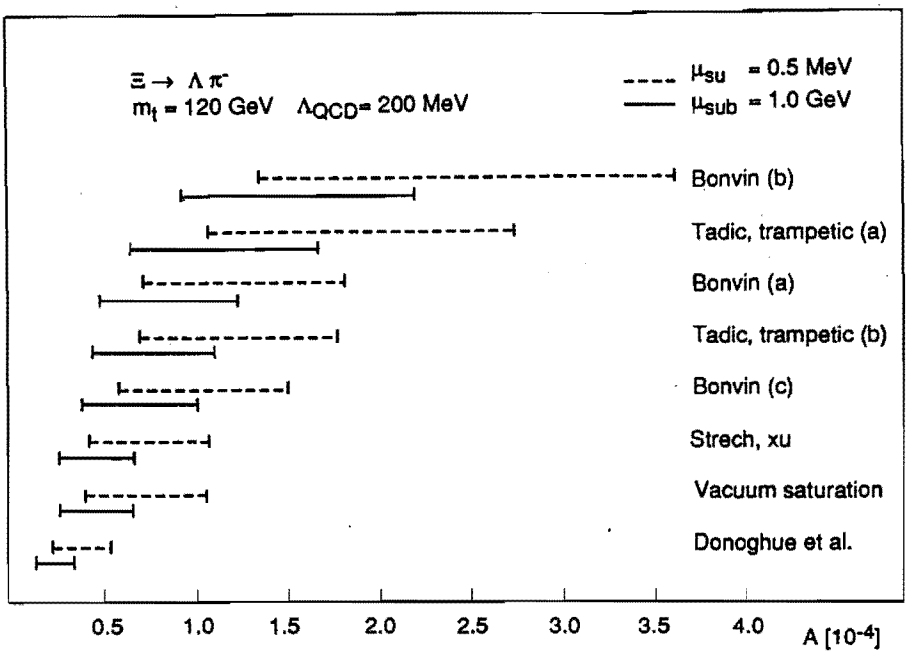

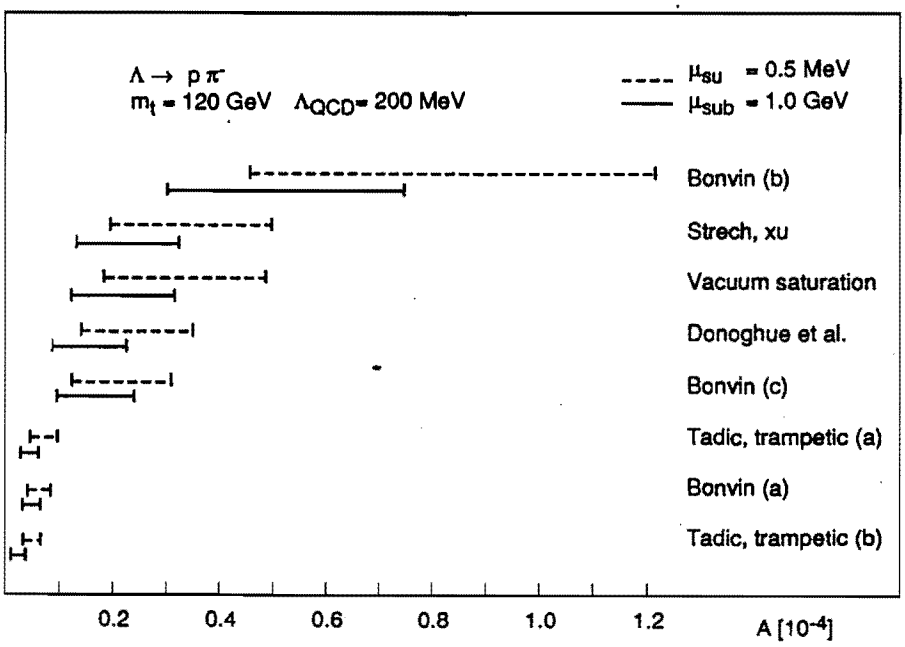

Figure 2: Range of standard model predictions of (a) $(\alpha_\Xi + \alpha_{\overline{\Xi}})/(\alpha_\Xi - \alpha_{\overline{\Xi}})$ and (b) $(\alpha_\Lambda + \alpha_{\overline{\Lambda}})/(\alpha_\Lambda - \alpha_{\overline{\Lambda}})$ from the model of Xe, Steger, and Valencia [21] using matrix elements calculated from various models.

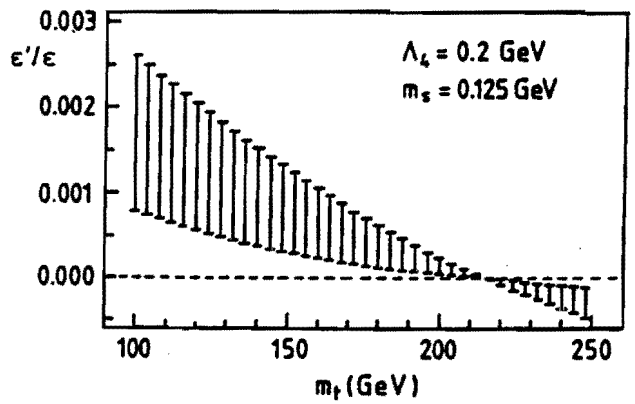

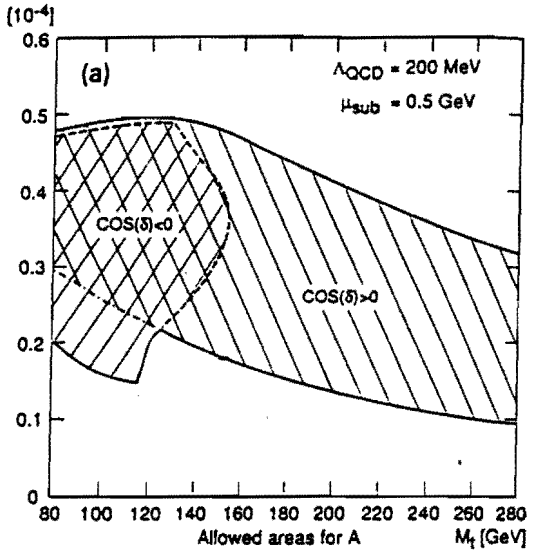

Figure 3: Standard model predictions for (a) ϵ'/ϵ [17] and (b) $(\alpha_\Lambda + \alpha_{\overline{\Lambda}})/(\alpha_\Lambda - \alpha_{\overline{\Lambda}})$ [16] showing the dependence on the top quark mass.

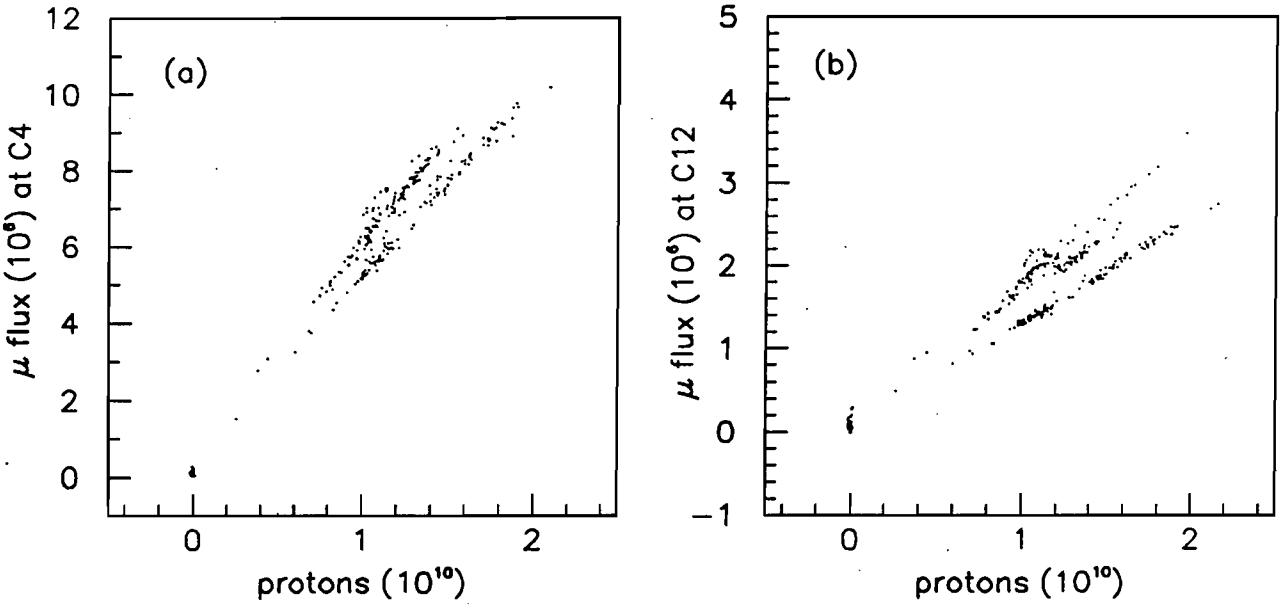

Figure 4: Muon fluence measured in E756 at (a) an upstream chamber (*C4*: 26 m from the collimator exit), and (b) a downstream chamber (*C12*: 49 m from exit).

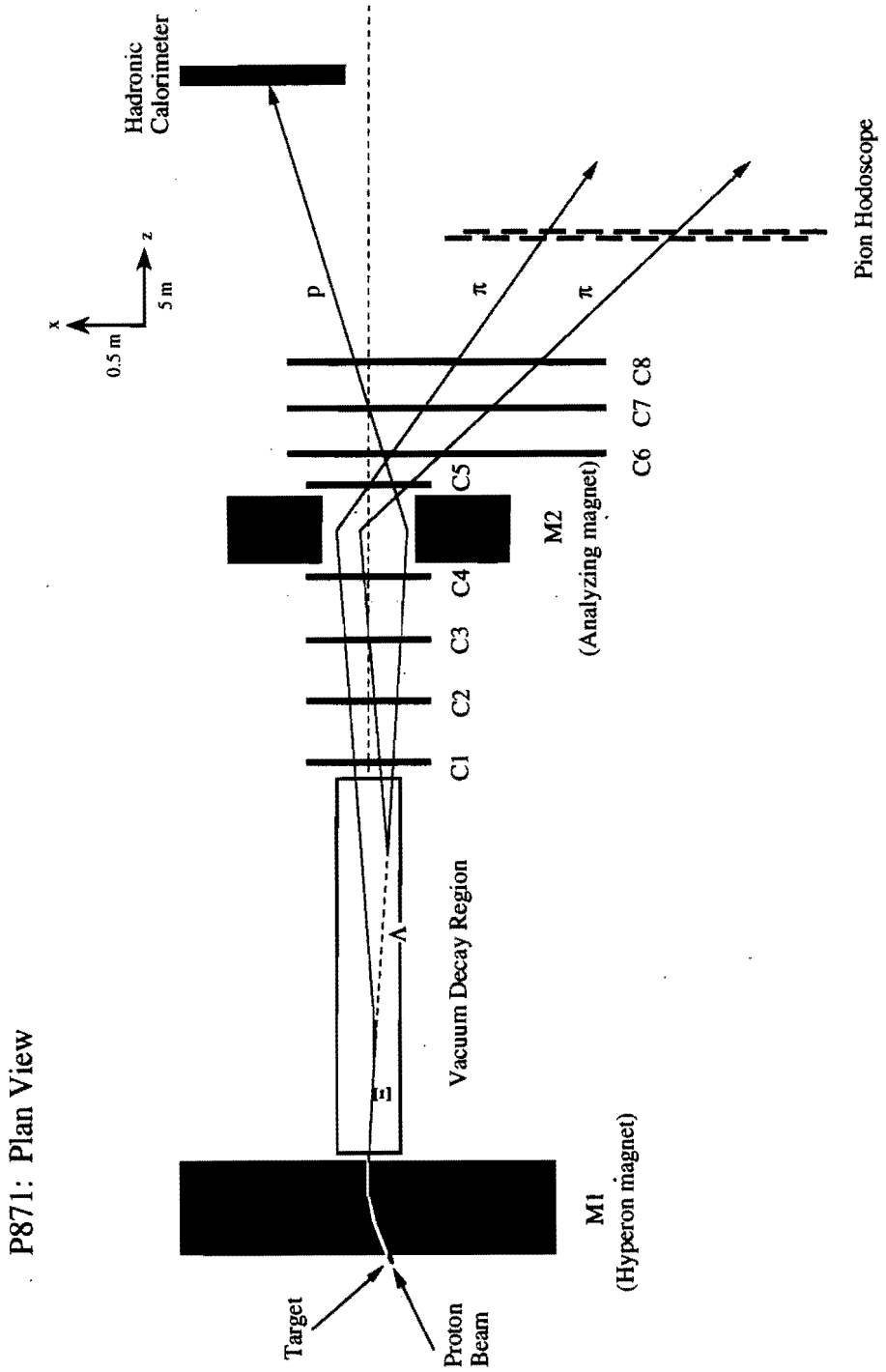

Figure 5: Plan view of the P871 spectrometer.

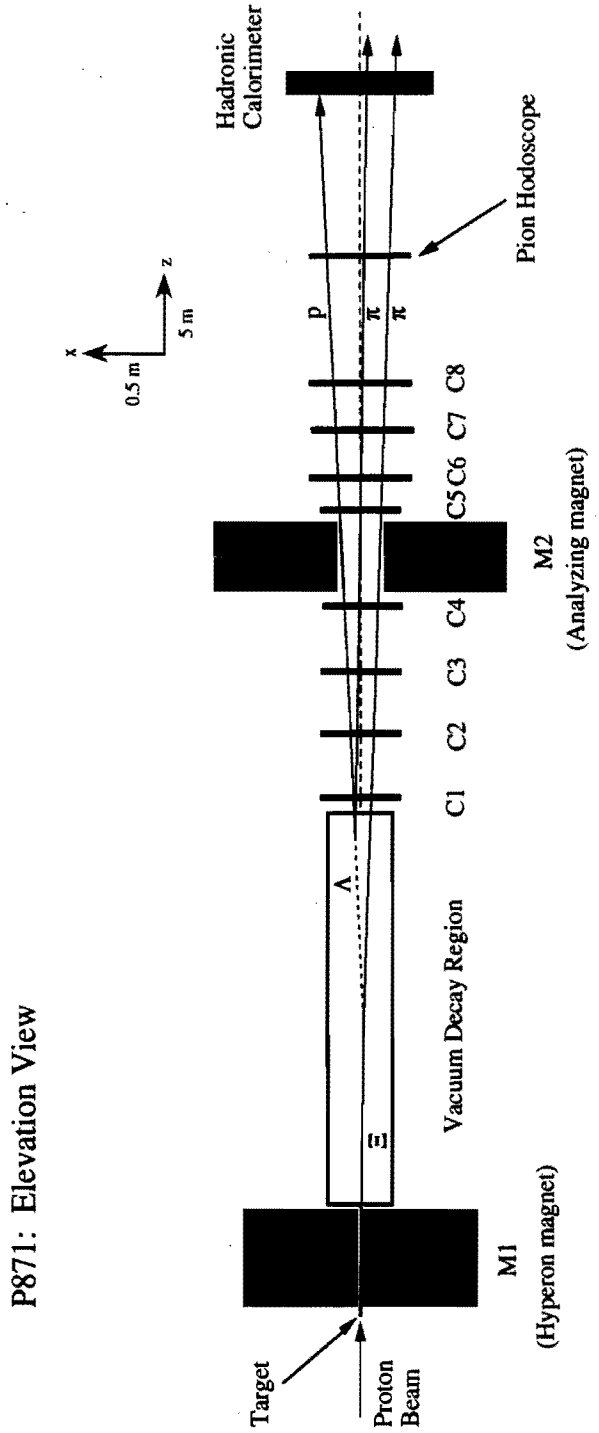

Figure 6: Elevation view of the P871 spectrometer.

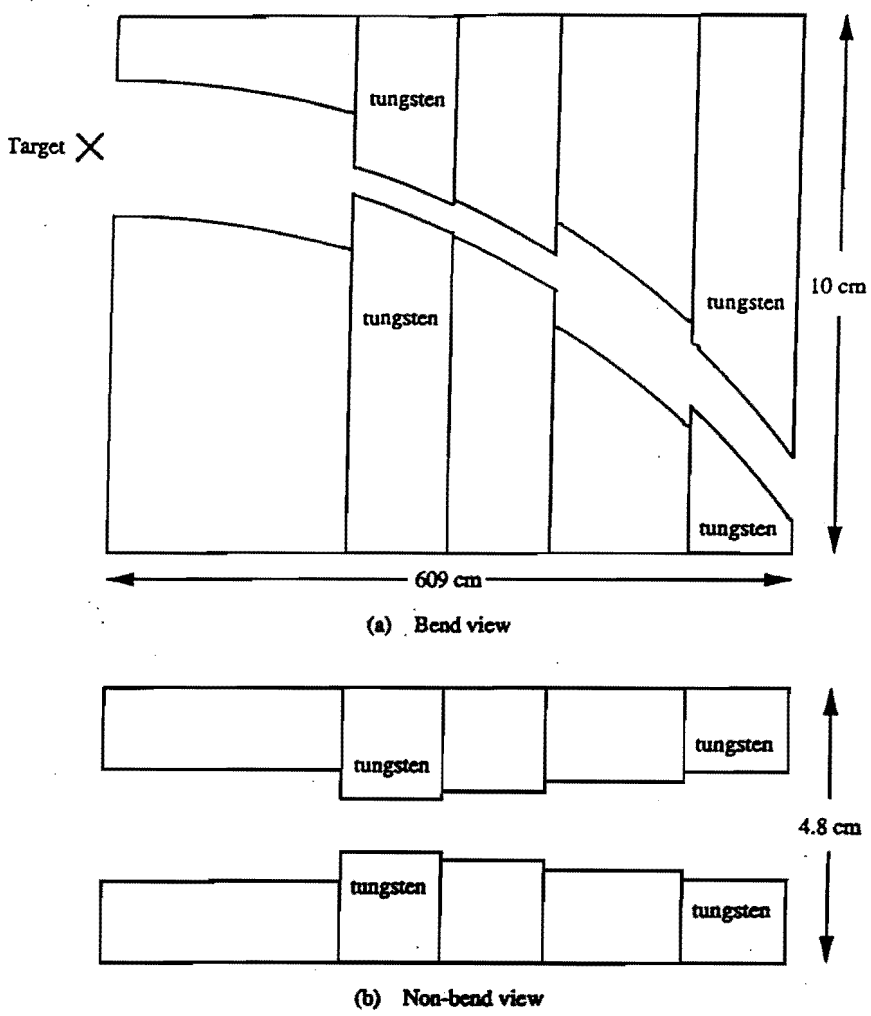

Figure 7: The P871 hyperon channel.

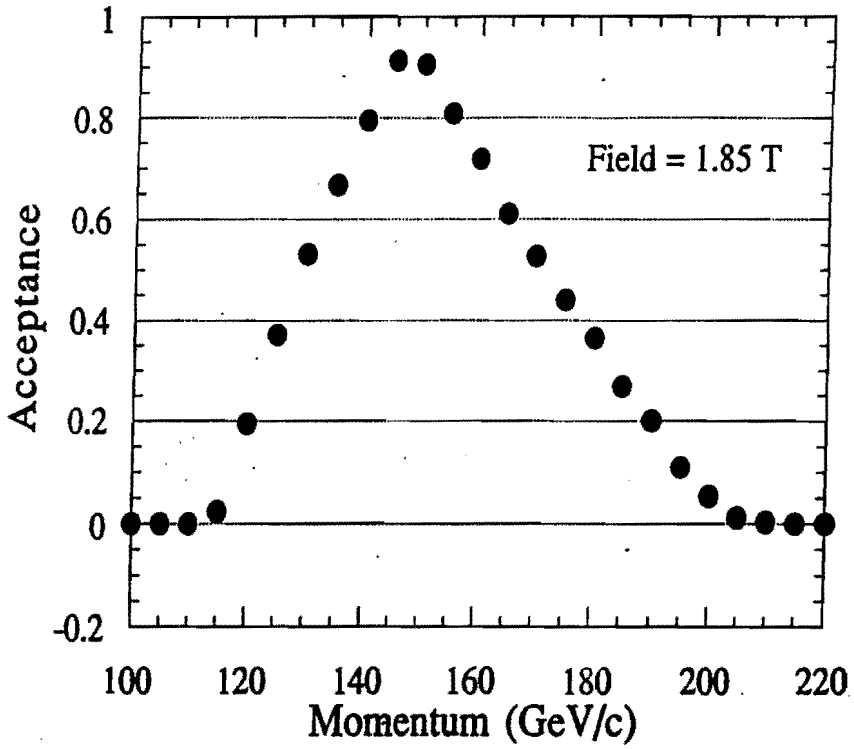

Figure 8: The hyperon channel acceptance.

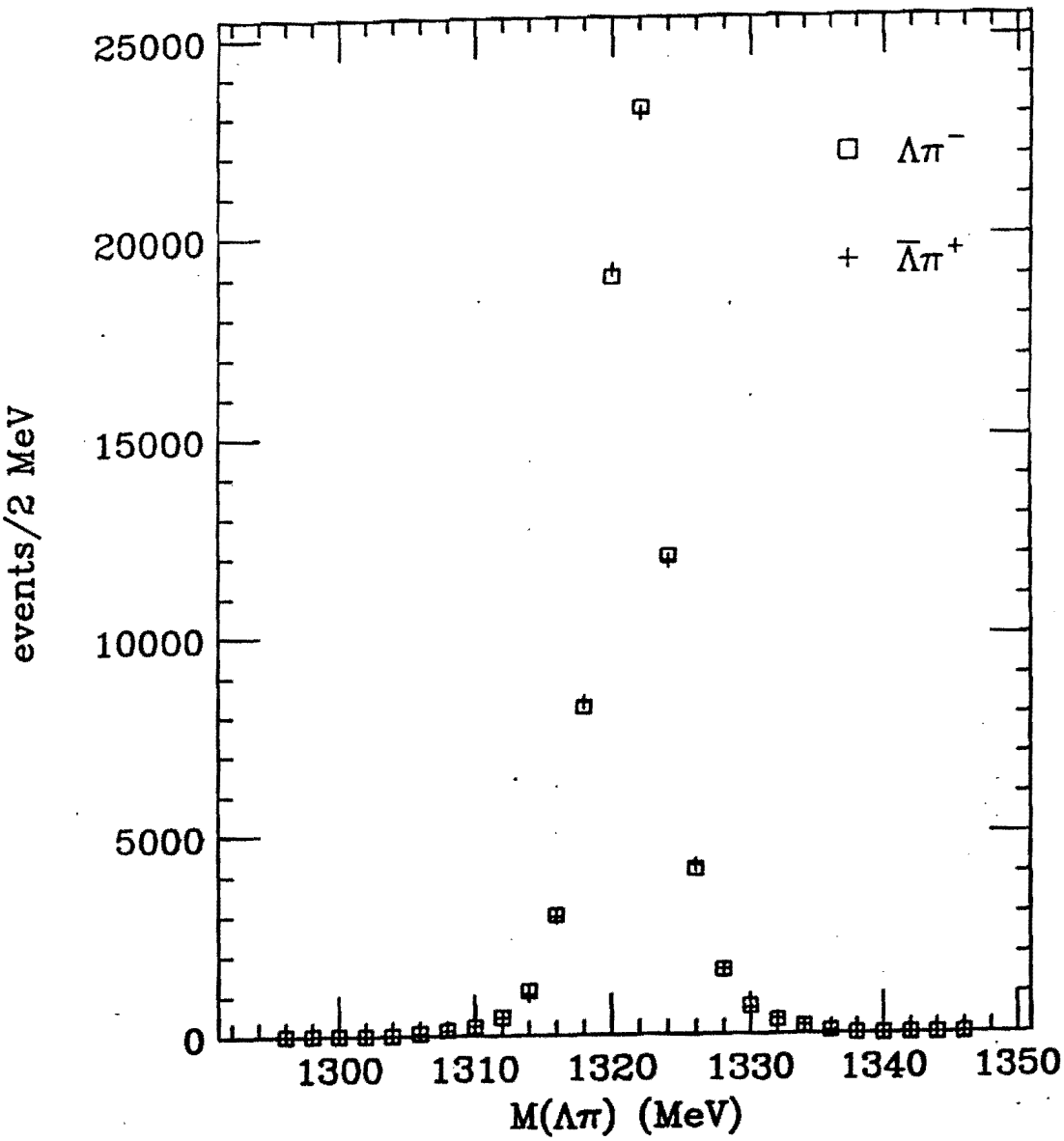

Figure 9: Comparison between the $\Lambda\pi^-$ and $\overline{\Lambda}\pi^+$ invariant masses from E756.

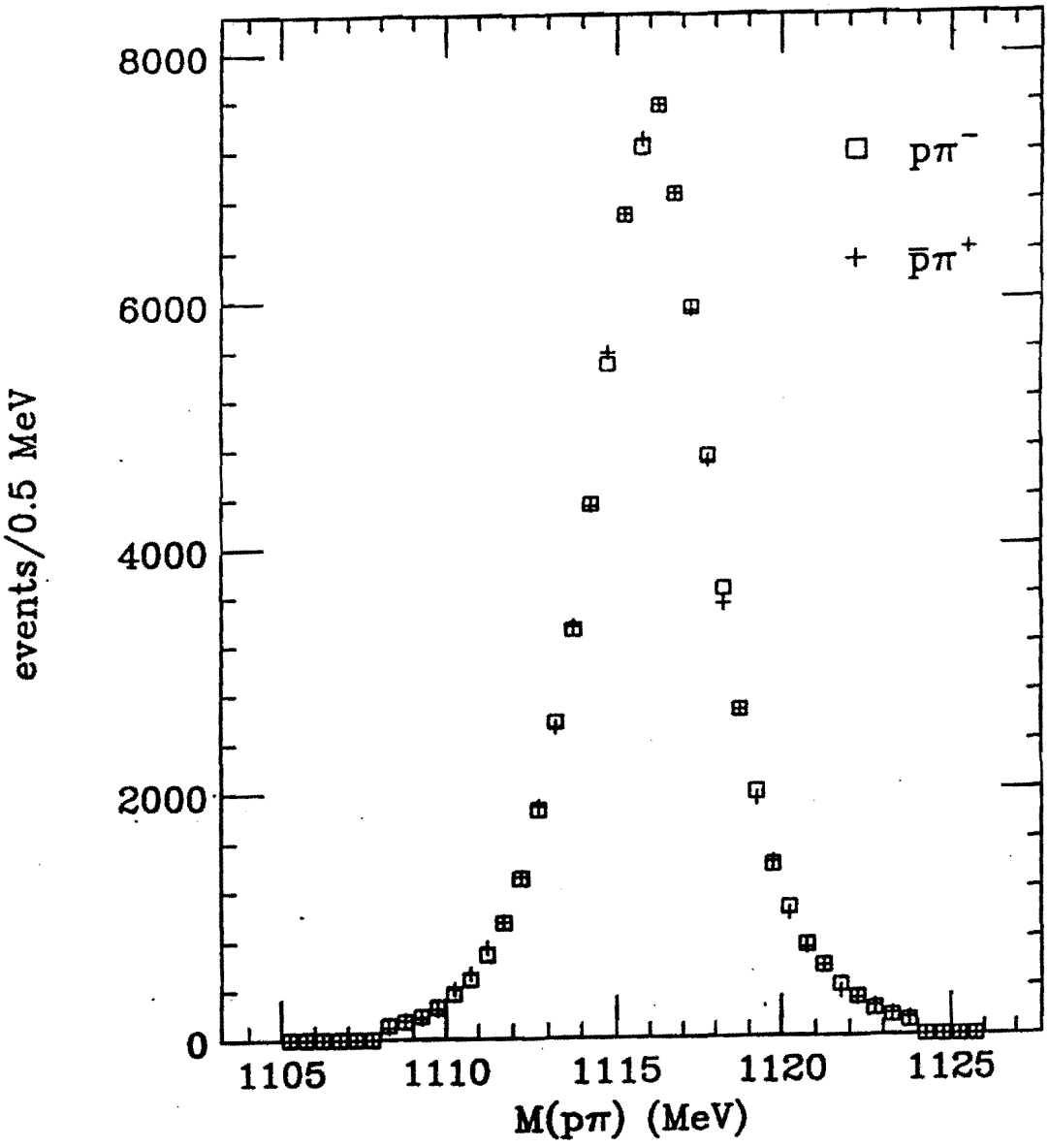

Figure 10: Comparison between the $p\pi^-$ and $\bar{p}\pi^+$ invariant masses from E756.

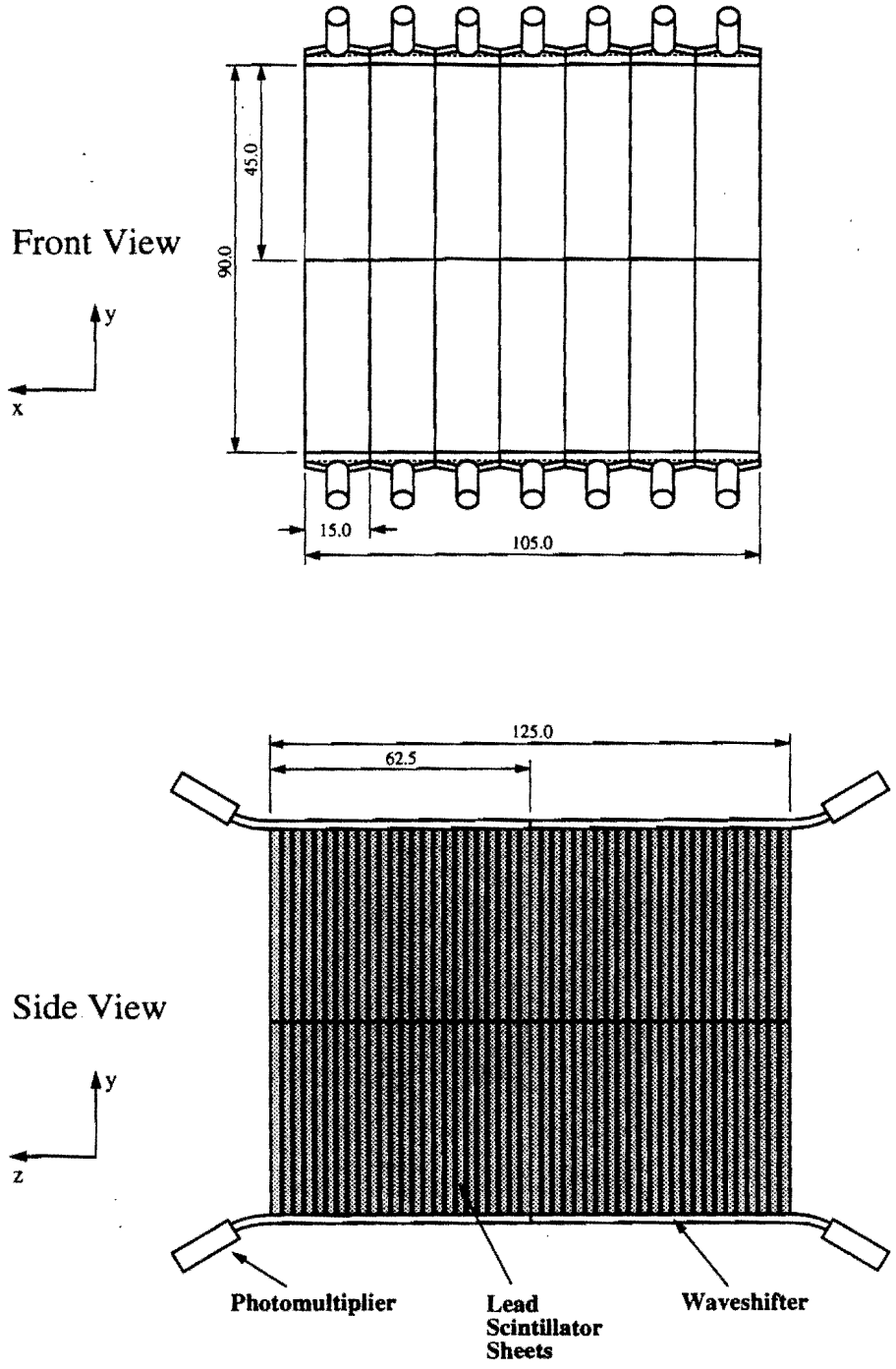

Figure 11: Front and side views of the hadronic calorimeter. Units are cm.

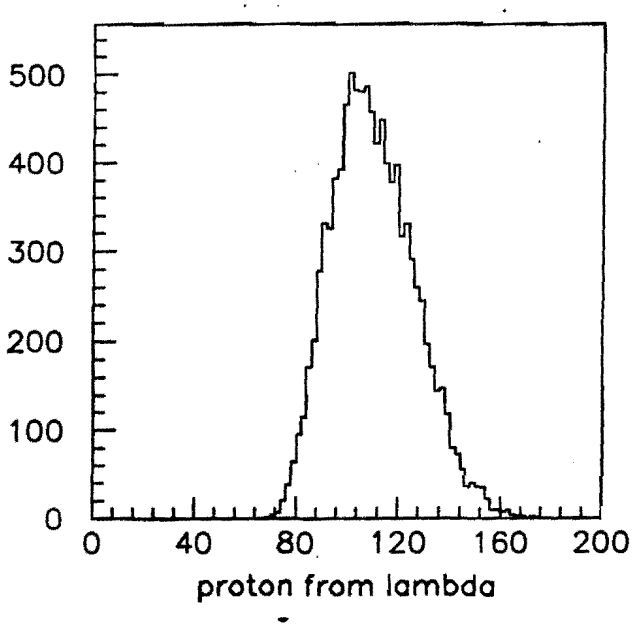

Figure 12: The proton momentum (in GeV/c) from Λ decays.

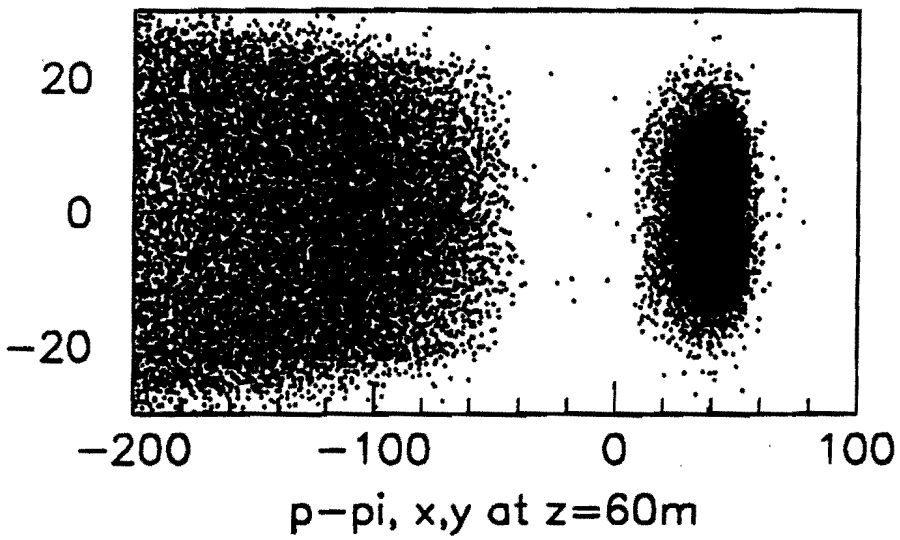

Figure 13: The x and y distributions of the charged particles from $\Xi \rightarrow \Lambda\ \pi$, and $\Lambda \rightarrow p\pi$ decays at the rear of the spectrometer (position of the pion hodoscope). The proton inhabits the right side and the the pions the left. Units are cm.

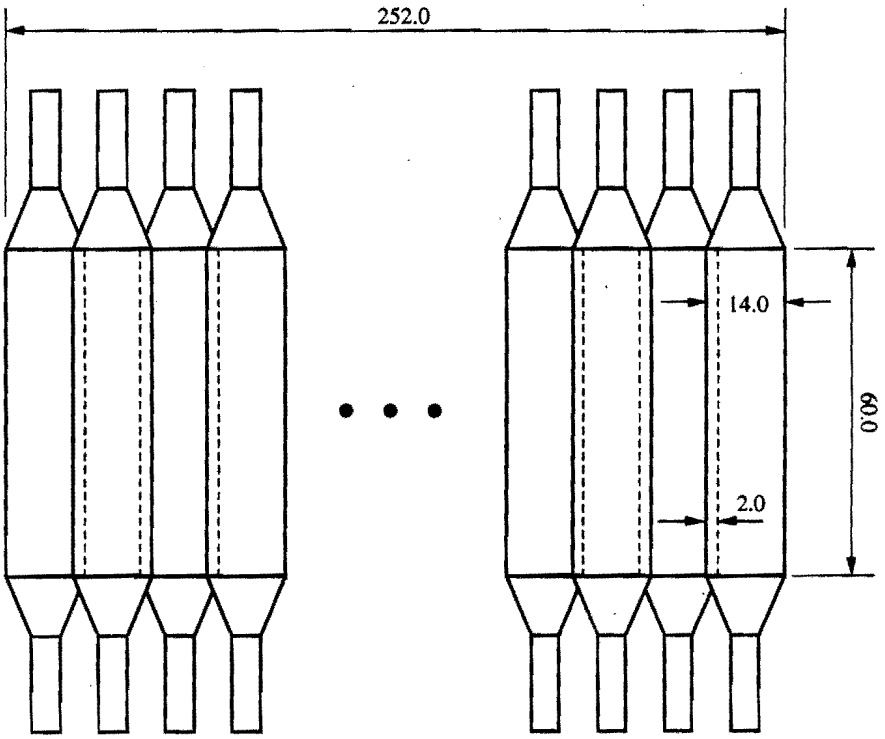

Figure 14: The pion hodoscope. Units are cm.

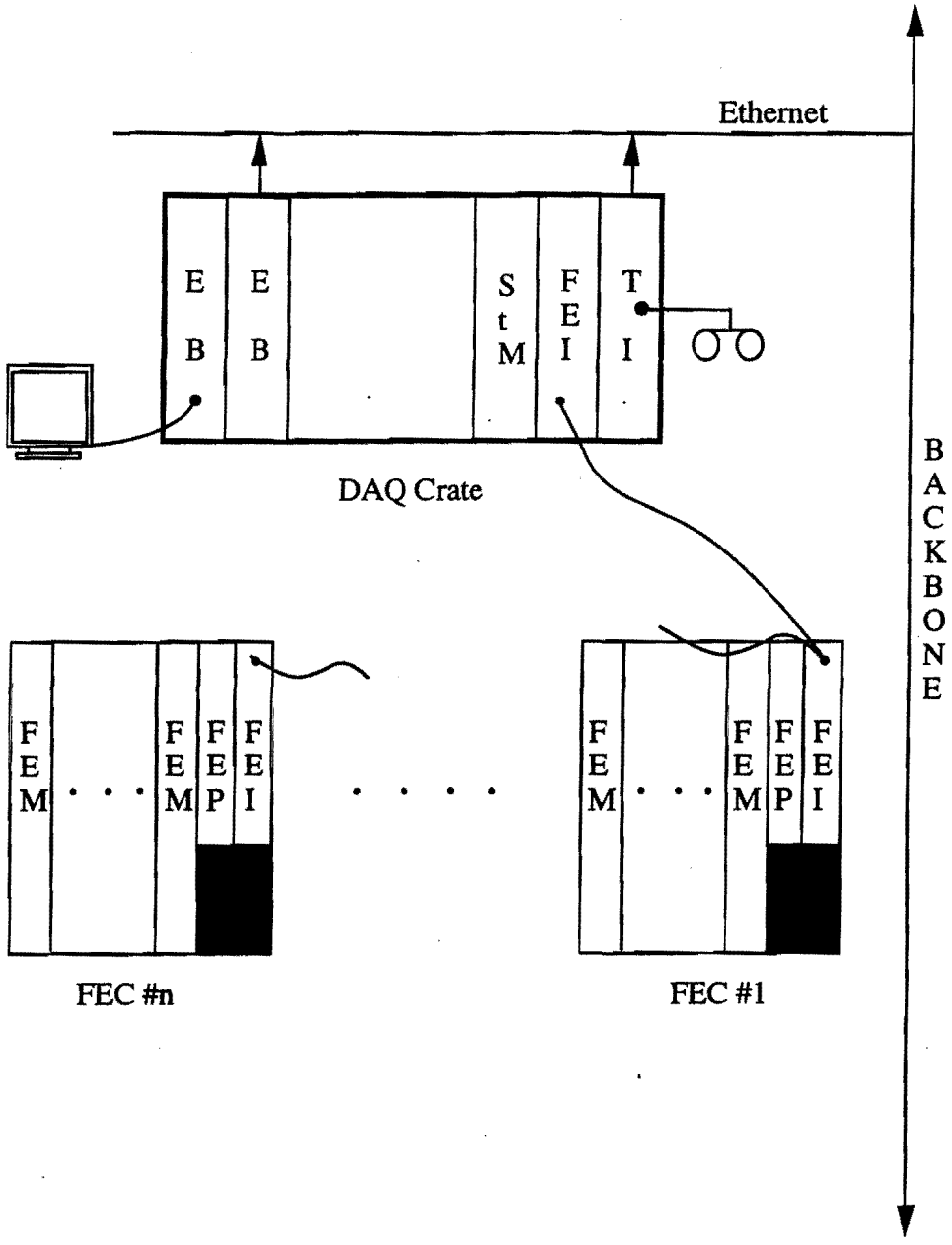

Figure 15: Layout of the data acquisition system.

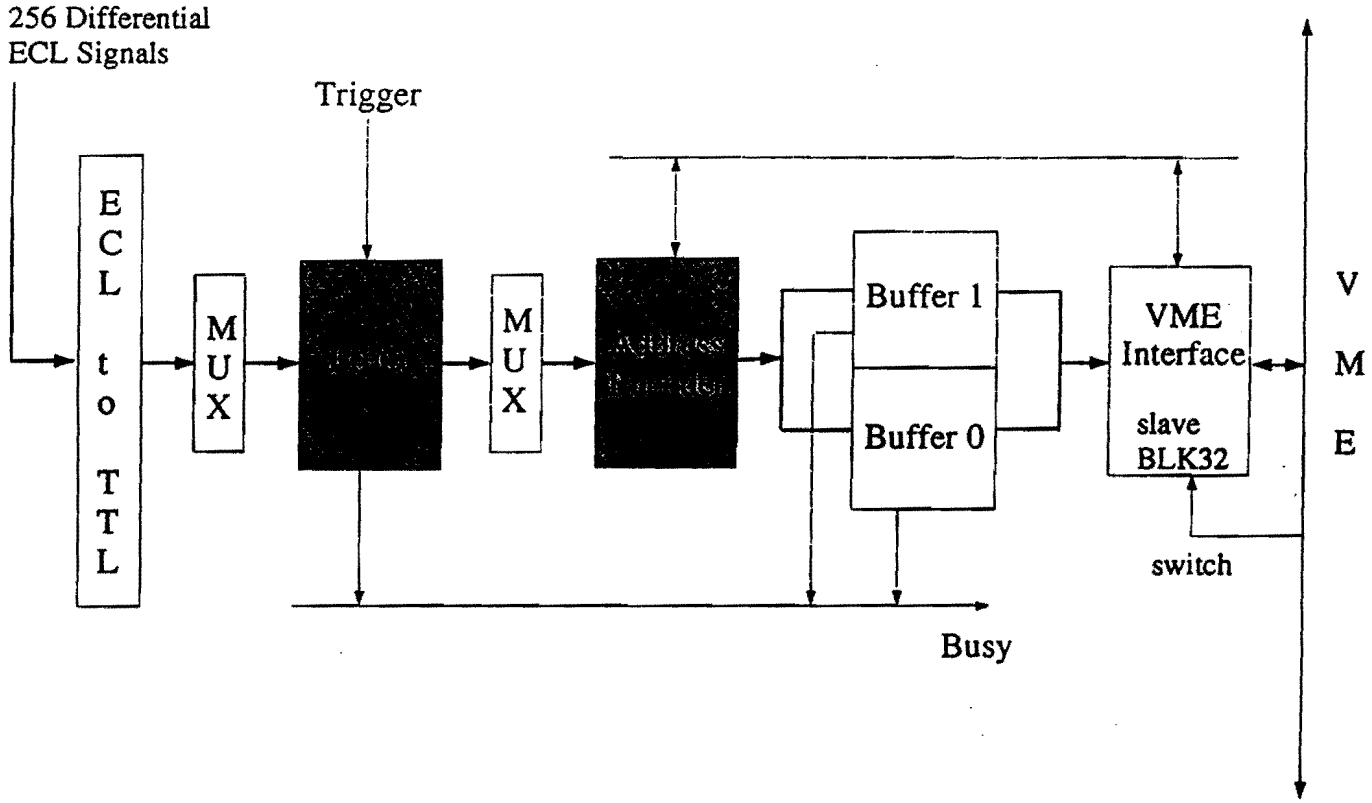

Figure 16: Block diagram of a front-end module.

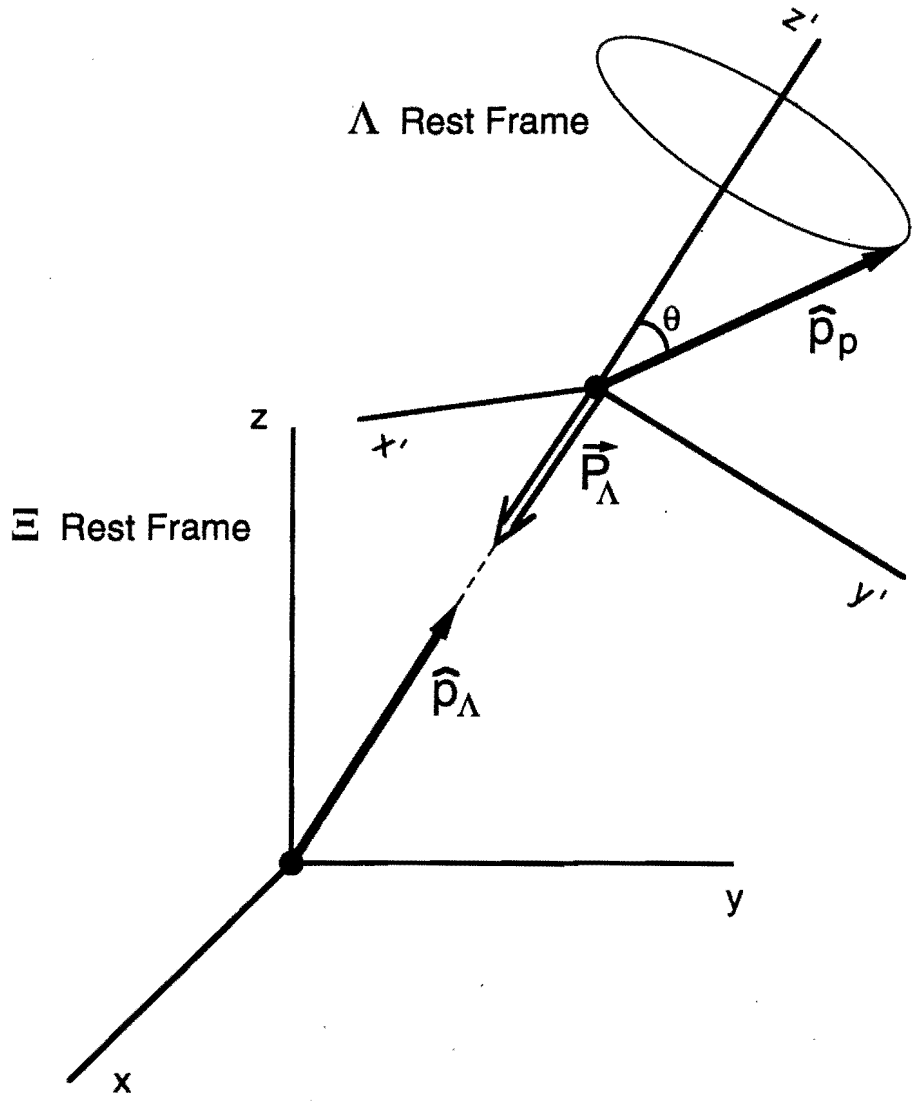

Figure 17: Analysis frames used in the Λ polarization analysis. The Λ polarization ($\vec{P}_\Lambda$) is antiparallel to the Λ momentum in the Ξ rest frame (α_Ξ is negative). The Λ momentum defines the polar (z') axis in the frame in which the proton $\cos\theta$ distribution is measured.

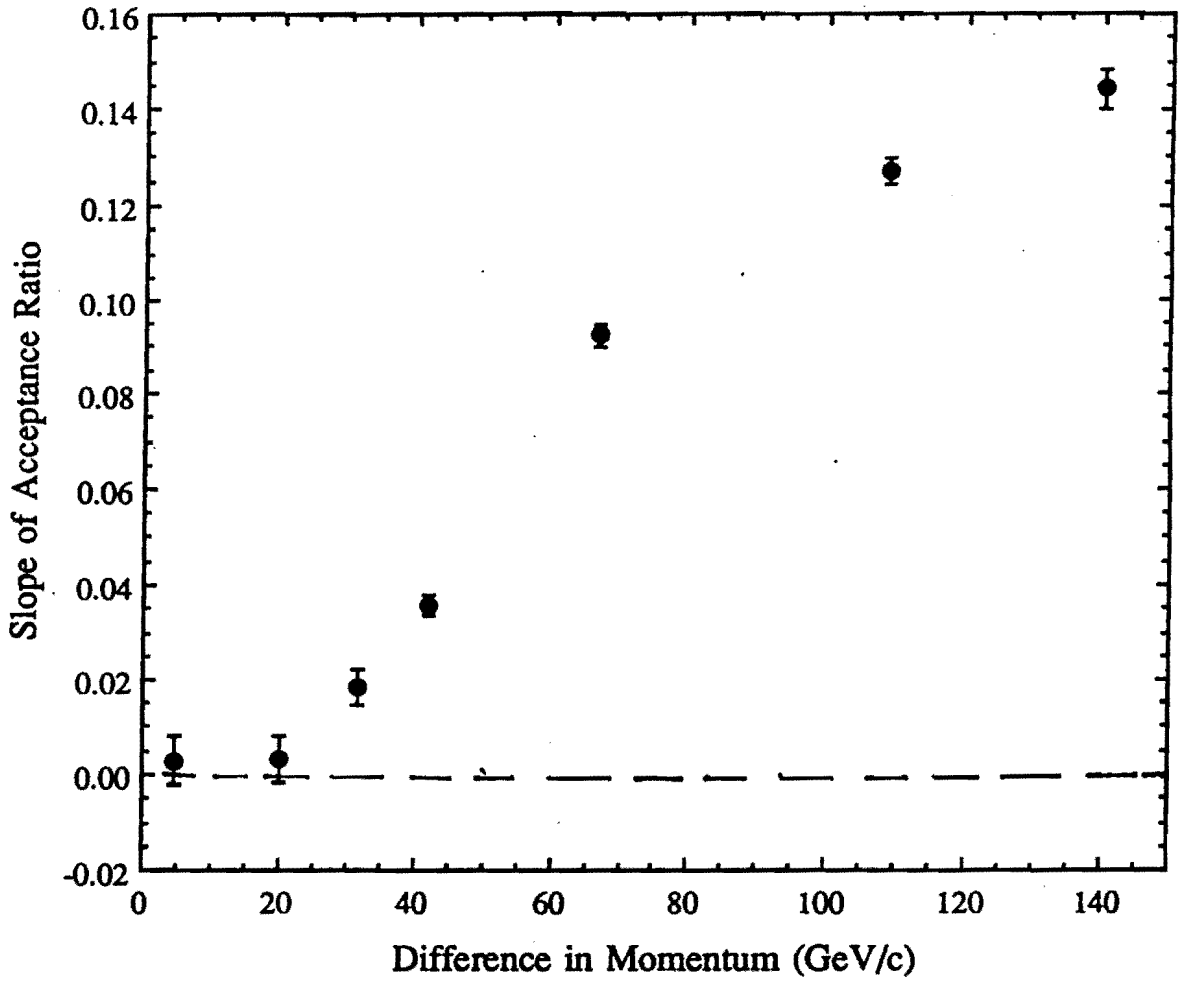

Figure 18: Difference in the proton $\cos\theta$ distributions for pairs of E756 Ξ^- data samples with different average momentum. The slope b of the ratio, $R = a + b\cos\theta$, of the two $\cos\theta$ distributions is given as a function of the momentum difference.

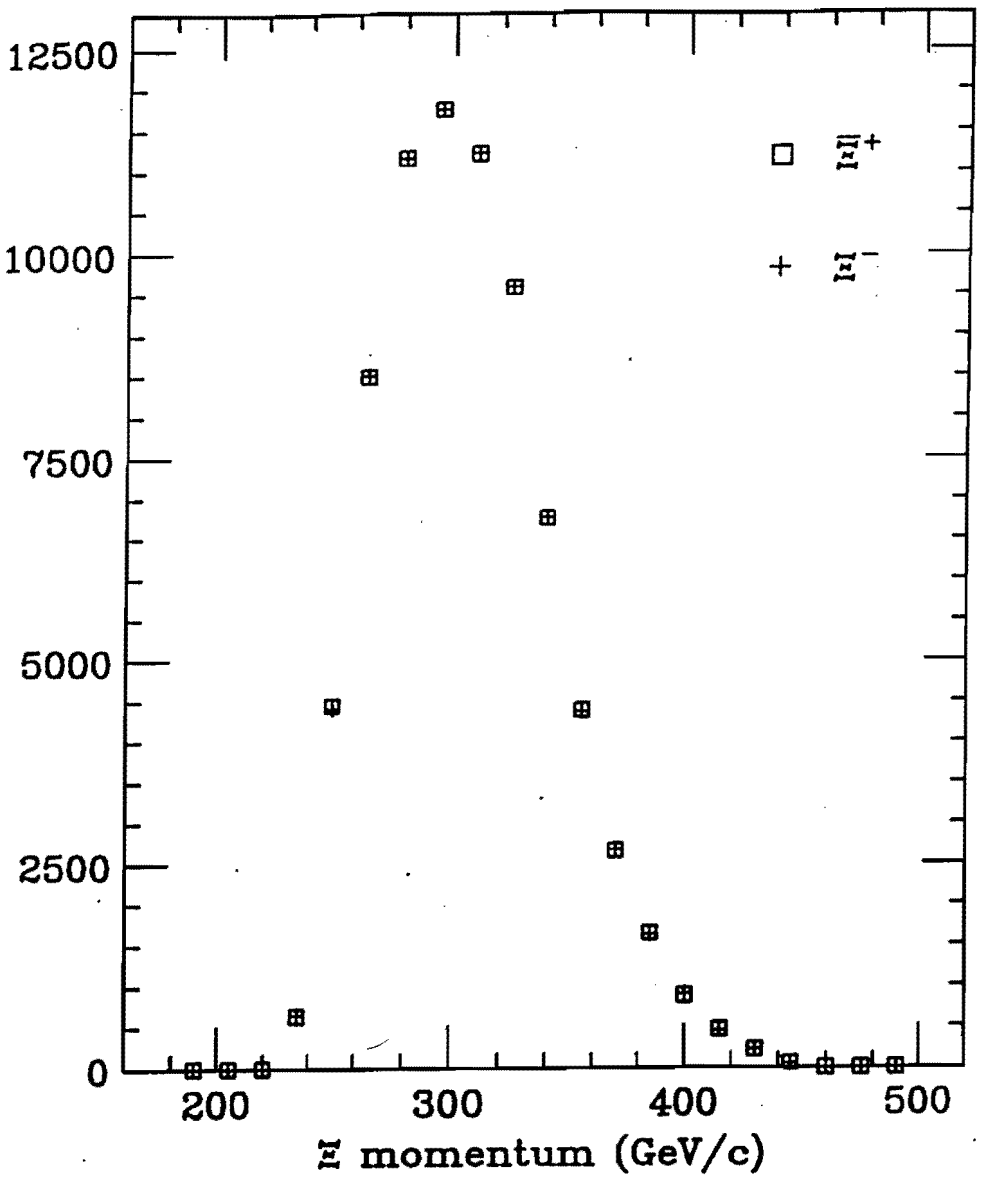

Figure 19: Comparison between the Ξ^- and $\bar{\Xi}^+$ momenta from E756, after normalization.

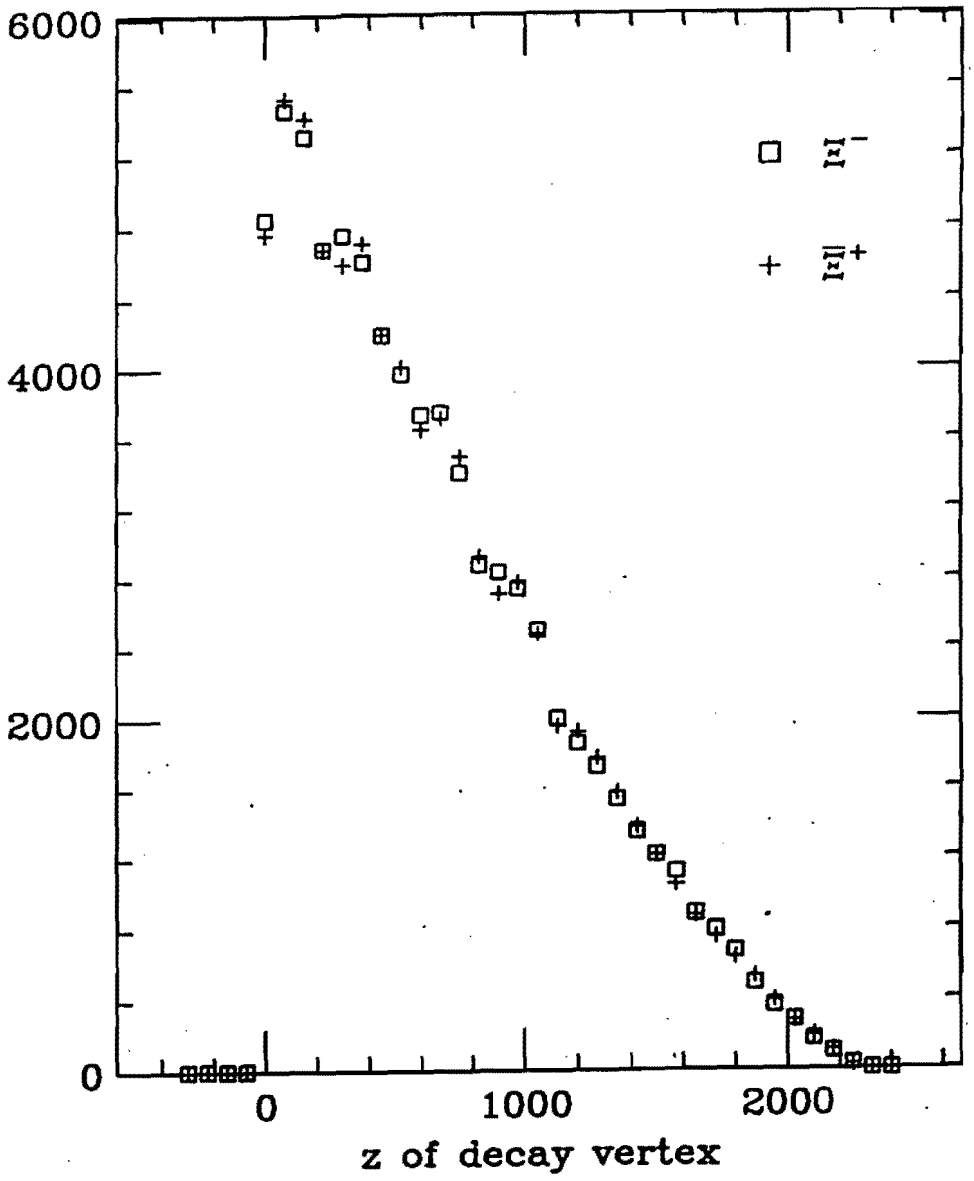

Figure 20: Comparison between the Ξ^- and $\overline{\Xi}^+$ z decay vertices for E756.

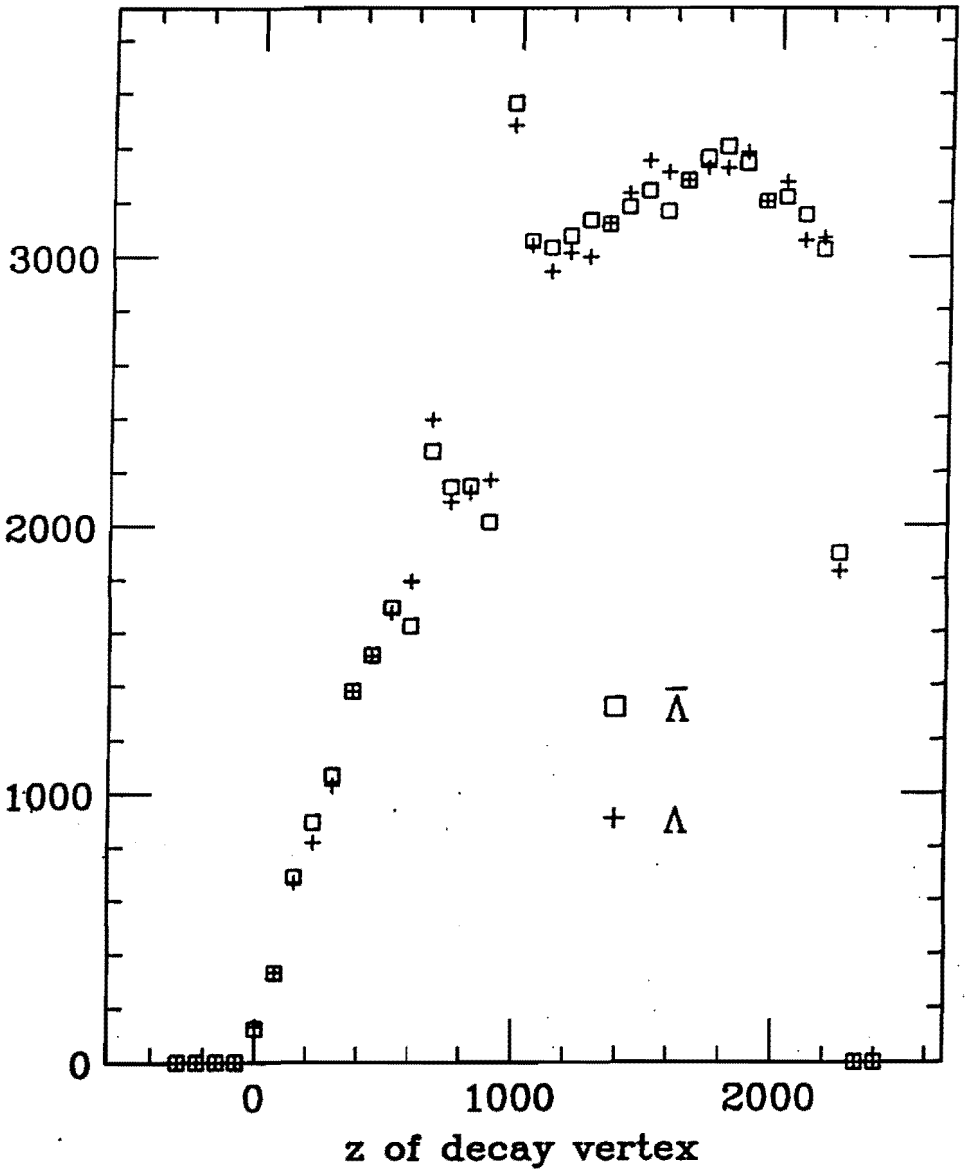

Figure 21: Comparison between the Λ and $\overline{\Lambda}$ z decay vertices from E756.

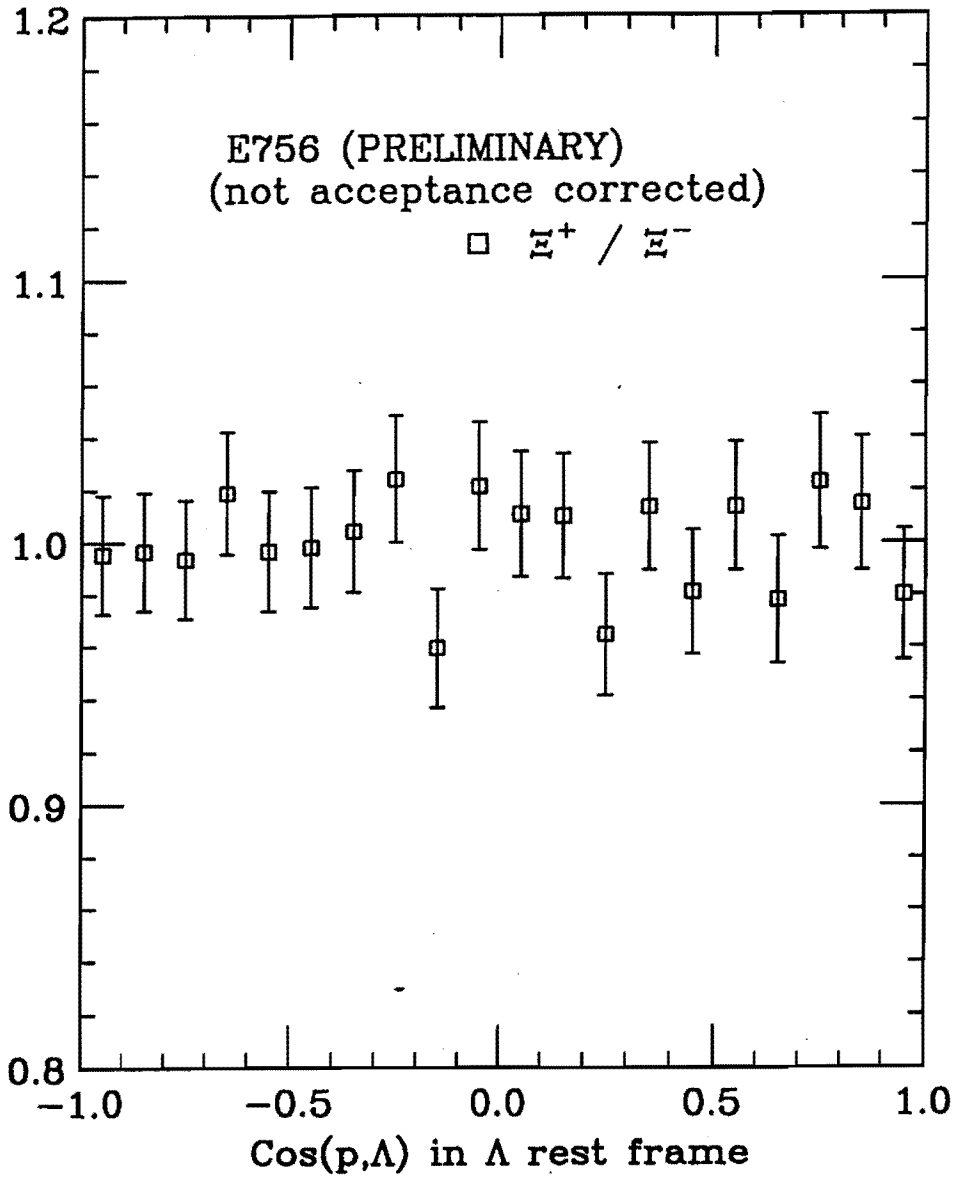

Figure 22: The ratio of the proton and antiproton $\cos\theta$ distributions from the E756 Ξ^- and $\bar{\Xi}^+$ data samples. No significant difference is evident despite the fact that no acceptance corrections have been made. (The sign of the cosine has been reversed.)

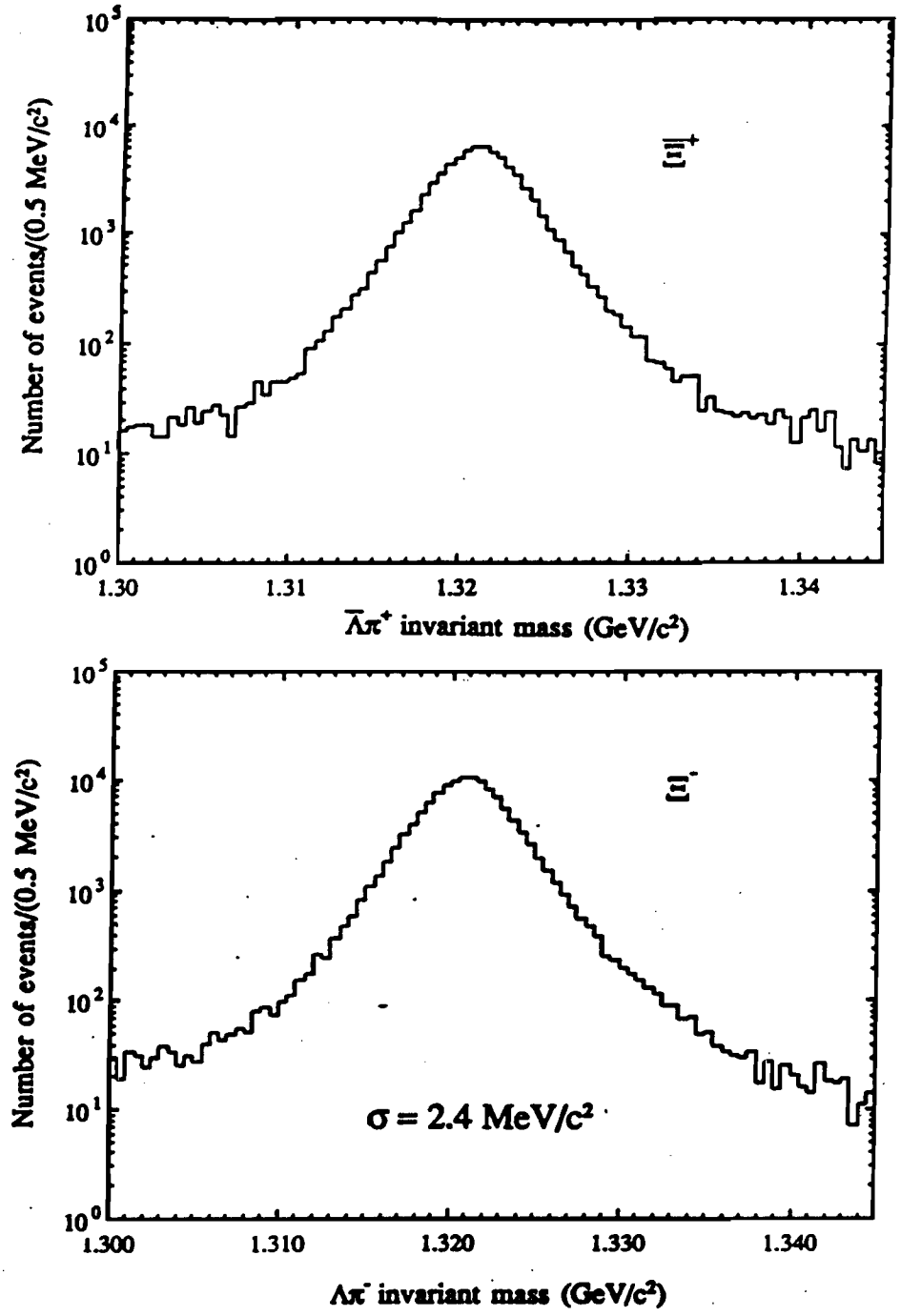

Figure 23: The $\Lambda\pi^-$ and $\bar{\Lambda}\pi^+$ invariant masses from E756, showing the level of the background.

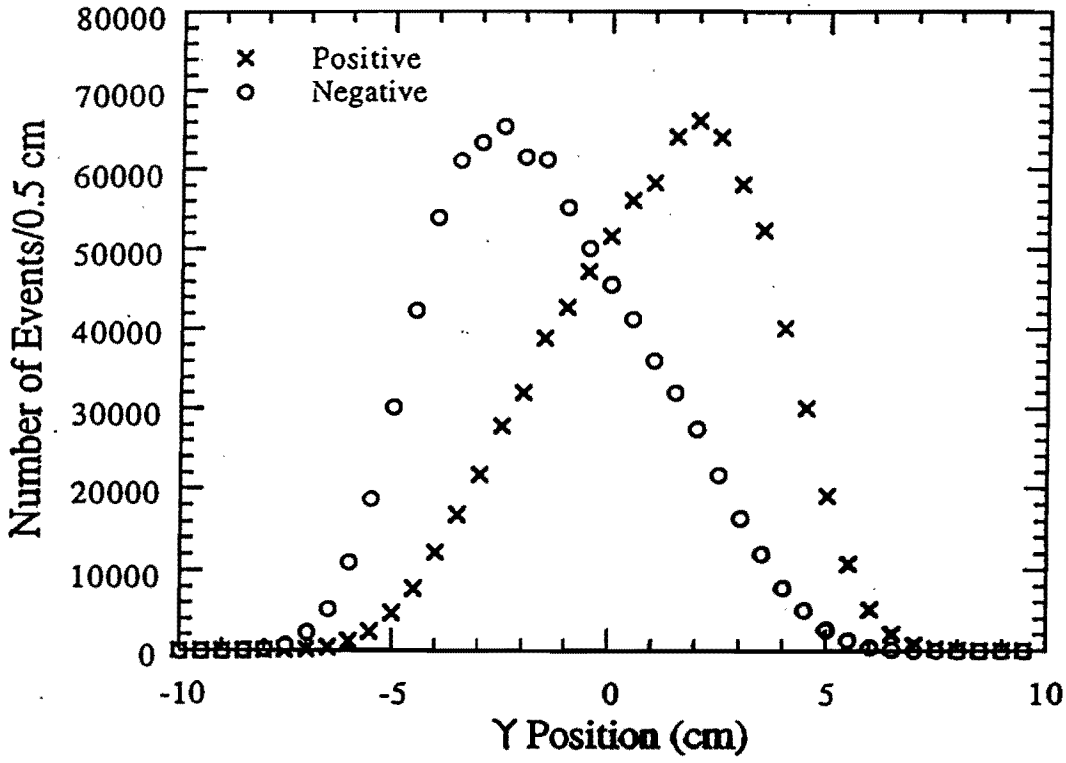

Figure 24: The y position of the proton at the analyzing magnet for +2.5 mrad and −2.5 mrad production angles in E756.

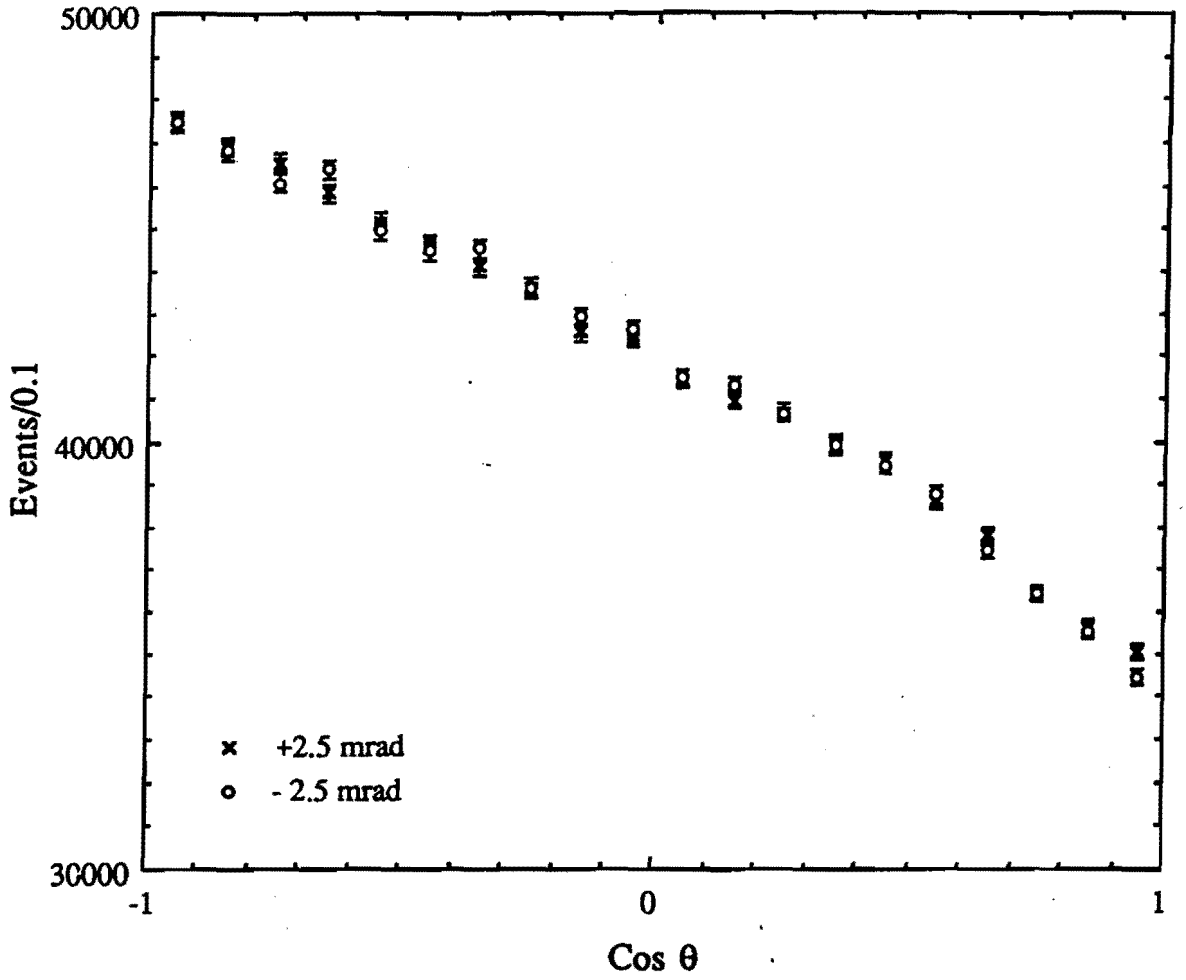

Figure 25: The proton $\cos\theta$ distribution from $\Xi^- \rightarrow \Lambda\pi^-$, $\Lambda \rightarrow p\pi^-$ decays in E756. The X's (O's) are protons from Ξ^-'s that were produced from protons targeted at +2.5 mrad (–2.5 mrad). No acceptance corrections have been made.